THÈSE

En vue de l'obtention du

DOCTORAT DE L'UNIVERSITÉ DE TOULOUSE

Délivré par :

Institut National Polytechnique de Toulouse (INP Toulouse)

Discipline ou spécialité :

Réseaux, Télécommunications, Systèmes et Architecture

Présentée et soutenue par :

Mme BOUCHRA BENAMMAR

le vendredi 5 décembre 2014

Titre :

FORMES D'ONDES AVANCEES ET TRAITEMENTS ITERATIFS POUR LES CANAUX NON LINEAIRES SATELLITES

Ecole doctorale :

Mathématiques, Informatique, Télécommunications de Toulouse (MITT)

Unité de recherche :

Institut de Recherche en Informatique de Toulouse (I.R.I.T.)

Directeur(s) de Thèse :

MME MARIE LAURE BOUCHERET

MME NATHALIE THOMAS

Rapporteurs :

M. CHRISTOPHE LAOT, TELECOM BRETAGNE CAMPUS DE BREST

M. PIERRE DUHAMEL, SUPELEC

Membre(s) du jury :

M. PHILIPPE CIBLAT, TELECOM PARISTECH, Président

M. CHARLY POULLIAT, INP TOULOUSE, Membre

M. MARCO LOPS, UNIVERSITA DEGLI STUDI DI CASSINO, Membre

M. MATHIEU DERVIN, THALES ALENIA SPACE, Membre

Mme MARIE LAURE BOUCHERET, INP TOULOUSE, Membre

Mme NATHALIE THOMAS, INP TOULOUSE, Membre

Remerciements

Je tiens tout d'abord à remercier mes encadrants de thèse pour m'avoir fait confiance, et soutenu durant ma thèse. Plus spécialement, je remercie Marie-Laure Boucheret pour ses éclairages salutaires au sujet des modulations en mono et multi-porteuse, et que personne ne s'avise de dire que le SC-FDMA est une modulation mutli-porteuse au risque de s'attirer les foudres de Marie-Laure. Je remercie aussi Nathalie Thomas, pour ses nombreuses relectures et pour sa gentillesse en toute circonstance qui ont eu un effet ô combien réconfortant (*merci pour les bonbons*). Mes remerciements vont aussi à Charly Poulliat pour m'avoir guidé tout au long de ma thèse et avoir été présent à toute heure afin de me relire, qu'il trouve en mes mots toute ma gratitude.

Durant ces trois années de thèse, j'ai aussi eu des échanges avec Mathieu Dervin ingénieur de recherche à Thalès. Je souhaiterai le remercier pour sa disponibilité. Il a sû répondre de manière très pédagogique à mes innombrables questions aux sujets des enjeux des systèmes actuels.

Je remercie aussi Pierre Duhamel Directeur de recherche CNRS au sein du Laboratoire Signaux et Systèmes de Paris ainsi que Christophe Laot Professeur à TELECOM Bretagne qui m'ont fait l'honneur de rapporter ma thèse. Que soient aussi remerciés Philippe Ciblat professeur à TELECOM ParisTech et Marco Lops professeur à l'université de Cassino en Italie pour avoir accepté d'examiner ma thèse.

Ensuite, parce que la vie du laboratoire n'aurait pas été aussi agréable sans eux, je souhaite remercier de tout coeur tous mes amis et collègues de laboratoire. Plus spécialement je remercie, Abdé, Cécilé, Yoann, Qi, Ningning, Sébastien, Olivier (dit Jack-Sparrow), Sokchenda (agent SS), Romain, Bilel, Farouk, Ahmad, Mohammad, Mohamed, Aziz, Nesrine, JB (the hat man), Farouk,

Facundo, Emilie, Jean-Gabriel (dit le corse) et Hermine. N'oublions pas les TeSA-people (les gens de l'au-delà ... du canal) Raoul, Victor, Jorge (dit Georges), Jean-Adrien (l'acteur), Tarik (le penseur) et Fabio. Comment oublier ces parties de Hanabi, de contact, de bowling ou de speed-cubing ? Que cela soit sur le terrain de foot, perchés au sommet du Montségur, en pique-nique à Pech David ou mieux encore, affalés sur la piste de la patinoire, vous avez su rendre inoubliable mon séjour parmi vous. Je vous souhaite à tous tout le bonheur et la réussite que l'on peut espérer.

Mes derniers remerciements vont à ceux sans qui rien de tout cela n'aurait été possible. Je remercie très chaleureusement mes parents pour leur sacrifices afin de me permettre de venir étudier en France, mon frère et enfin ma moitié pour m'avoir soutenue durant ma thèse et avoir partagé mes joies et mes peines. Je souhaite que vous trouviez dans mes mots l'expression de mon sincère respect et amour.

Bouchra

Résumé

L'augmentation de l'efficacité spectrale des transmissions mono-porteuses sur un lien de diffusion par satellite est devenu un défi d'envergure afin de pallier la demande croissante en débits de transmission. Si des techniques émergentes de transmissions encouragent l'utilisation de modulations à ordre élevé telles que les modulations de phase et d'amplitude (APSK), certaines dégradations sont encourues lors du traitement à bord du satellite. En effet, en raison de l'utilisation d'amplificateurs de puissance ainsi que de filtres à mémoires, les modulations d'ordre élevé subissent des distorsions non-linéaires dues à la fluctuation de leur enveloppe, ce qui nécessite des traitements au sein de l'émetteur ou bien au sein du récepteur. Dans cette thèse, nous nous intéressons au traitement de l'interférence non-linéaire au sein du récepteur, avec une attention particulière aux égaliseurs itératifs qui améliorent les performances du système au prix d'une complexité élevée. A partir du modèle temporel des interférences non-linéaires induites par l'amplificateur de puissance, des algorithmes de réception optimaux et sous optimaux sont dérivés, et leurs performances comparées. Des égaliseurs à complexité réduite sont aussi étudiés dans le but d'atteindre un compromis performances-complexité satisfaisant. Ensuite, un modèle des non-linéarités est dérivé dans le domaine fréquentiel, et les égaliseurs correspondants sont présentés. Dans un second temps, nous analysons et dérivons des récepteurs itératifs pour l'interférence entre symboles non linéaire. L'objectif est d'optimiser les polynômes de distributions d'un code externe basé sur les codes de contrôle de parité à faible densité (LDPC) afin de coller au mieux à la sortie de l'égaliseur. Le récepteur ainsi optimisé atteint de meilleures performances comparé à un récepteur non optimisé pour le canal non-linéaire. Finalement, nous nous intéressons à une classe spécifique de techniques de transmissions mono-porteuse basée sur le multiplexage par division de fréquence

(SC-OFDM) pour les liens satellites. L'avantage de ces formes d'ondes réside dans l'efficacité de leur égaliseur dans le domaine fréquentiel. Des formules analytiques de la densité spectrale de puissance et du rapport signal sur bruit et interférence sont dérivées et utilisées afin de prédire les performances du système.

Publications

Journals in preparation

1. B.Benammar, N.Thomas, C.Poulliat, ML.Boucheret, M.Dervin, "Iterative Receivers For Non Linear Satellite Channels" to be submitted to IEEE trans. on Communications.
2. B.Benammar, N.Thomas, C.Poulliat, ML.Boucheret, M.Dervin, "Performance Analysis Of Block Circular Filter-Bank Modulations" to be submitted.

International conferences

Accepted

1. B.Benammar, N.Thomas, C.Poulliat, ML.Boucheret, M.Dervin, "Asymptotic Analysis and Design of Iterative Receivers for Non Linear ISI Channels" ISTC August 18-22, 2014, Bremen, Germany.
2. B.Benammar, N.Thomas, C.Poulliat, ML.Boucheret, M.Dervin, "On Linear Frequency Domain Turbo-Equalization of Non Linear Volterra Channels" ISTC August 18-22, 2014, Bremen, Germany.
3. H.Abdulkader, B.Benammar, C.Poulliat, ML.Boucheret, N.Thomas, "Analysis and Design of Radial Basis Function-Based Turbo Equalizers" ISTC August 18-22, 2014, Bremen, Germany.
4. H.Abdulkader, B.Benammar, C.Poulliat, ML.Boucheret, N.Thomas, "Neural Networks-Based Turbo Equalization of a Satellite Communication Channel" SPAWC June 22-25, 2014, Toronto, Canada.
5. B.Benammar, N.Thomas, C.Poulliat, ML.Boucheret, M.Dervin, "On linear MMSE Based Turbo-equalization of Nonlinear Satellite Channels" ICASSP May 26-31, 2013, Vancouver, Canada.
6. B.Benammar, N.Thomas, ML.Boucheret, C.Poulliat, M.Dervin, " Analytical expressions of Power Spectral Density for General Spectrally Shaped SC-FDMA Systems" EUSIPCO Sep. 9-13, 2013, Marrakech, Morocco.

National conferences

1. B.Benammar, N.Thomas, C.Poulliat, ML.Boucheret, M.Dervin, "Turbo- Egalisation MMSE Lineaire De Canaux Non Lineaires" GRETSI Sep. 3-6, 2013, Bretagne, France.

Abstract

Increasing both the data rate and power efficiency of single carrier transmissions over broadcast satellite links has become a challenging issue to comply with the urging demand of higher transmission rates. If emerging transmission techniques encourage the use of high order modulations such as Amplitude and Phase Shift Keying (APSK) and Quadrature Amplitude Modulation (QAM), some channel impairments arise due to on-board satellite processing. Indeed, due to satellite transponder Power Amplifiers (PA) as well as transmission filters, high order modulations incur non linear distortions due to their high envelope fluctuations which require specific processing either at the transmitter or at the receiver.

In this thesis, we investigate on non linear interference mitigation at the receiver with a special focus on iterative equalizers which dramatically enhance the performance at the cost of additional complexity. Based on the time domain model of the non linear interference induced by the PA, optimal and sub-optimal receiving algorithms are proposed and their performance compared. Low complexity implementations are also investigated for the sake of a better complexity-performance trade-off. Then, a non linear frequency domain model is derived and the corresponding frequency equalizers are investigated.

In the second part, we analyse and design an iterative receiver for the non linear Inter Symbol Interference (ISI) channel. The objective is to optimize an outer Low Density Parity Check (LDPC) code distribution polynomials so as to best fit the inner equalizer Extrinsic information. The optimized receiver is shown to achieve better performance compared to a code only optimized for linear ISI channel.

Finally, we investigate on a specific class of single carrier transmissions relying on Single Carrier Orthogonal Frequency Division Multiplexing (SCO-FDM) for satellite downlink. The advantage of such waveforms lies in their practical receiver implementation in the frequency domain. General analytical formulas of the power spectral density and signal to noise and interference ratio are derived and used to predict the bit error rate for frequency selective multiplexers.

Abreviations

AM-AM	Amplitude to Amplitude
AM-PM	Amplitude to Phase
BCH	Bose, Ray-Chaudhuri et Hocquenghem
BEC	Binary Erasure Channel
BICM	Bit Interleaved Coded Modulation
BP	Belief Propagation
BPSK	Binary Phase Shift Keying
CA	Complex Adds
CC	Convolutional Codes
CCDF	Cumulative Complementary Density Function
CM	Complex Multiplies
CN	Check Node
DFT	Discrete Fourier Transform
DVB-S	Digital Video Broadcasting Satellite
ENGINES	Enabling Next GeneratIon NEtworks for broadcast Services
ETSI	European Telecommunications Standards Institute
EW-SC-FDM	Extended Weighted Singe-Carrier Frequency Division Multiplexing
EXIT	EXtrinsic Information Transfer
FET	Field Effect Transistor

FIR	Finite Impulse Response
FSS	Fixed Services Satellite
GF	Galois Field
GFDM	Generalised Frequency Division Multiplexing
GM	Gaussian Mixture
IBO	Input Back-Off
IMUX	Input MUltipleXer
LDPC	Low Density Parity Check
MAP	Maximum A Posteriori
MLSE	Maximum Likelihood Sequence Equalizer
MMSE	Minimum Mean Square Error
MSE	Mean Square Error
MSS	Mobile Services Satellite
OFDM	Orthogonal Frequency Division Multiplexing.
OFDMA	Orthogonal Frequency Division Multiple Access.
OMUX	Output MUltipleXer
OBO	Output Back-Off
PAPR	Peak to Average Power Ratio
QAM	Quadrature and Amplitude modulations
QPSK	Quadrature Phase Shift Keying
RF	Radio Frequency
RS	Reed Solomon
SISO	Soft Input Soft Output
SP	Sum Product (SP)
SSPA	Solid State Power Amplifier
TT & C	Telemetric Tracking and Command
TWTA	Travelling Wave Tube Amplifier
UE	User Equipment
VN	Variable Node

Contents

List of Figures

List of Tables

Introduction (French)

Pendant plus d'un demi siècle, les systèmes satellites ont acheminé et transporté des données vers des contrées lointaines et sur des zones étendues. Que ce soit pour les télécommunications, le positionnement ou l'observation de la terre, l'augmentation des débits des communications par satellite revêt une importance majeure dans les évolutions futures de ces technologies.

Lorsqu'il s'agit de développer un système de communication, plusieurs paramètres entrent en jeu afin de dimensionner les capacités des liens. Plus précisément, en fonction de la nature du service rendu par le satellite (fixe, mobile, diffusion), du sens de la communication (liaison montante ou descendante), de la bande passante disponible ainsi que de la complexité permise, les solutions permettant d'augmenter le débit et l'efficacité en puissance peuvent différer.

L'efficacité en puissance mesure la robustesse face aux perturbations du bruit et est souvent liée à la distance minimale du code et de la modulation utilisés. L'efficacité spectrale quant à elle, caractérise le débit de la communication pour une bande donnée et est reliée à la cardinalité de la modulation ainsi qu'au rendement de codage. Il existe en général un compromis entre efficacité en puissance et efficacité spectrale. Cependant, de nouvelles avancées dans le domaine des traitements itératifs ont permis de réduire ce compromis en exploitant un degré de liberté supplémentaire qui est celui de la complexité.

Dans cette thèse, nous nous positionnons au niveau de la voie descendante d'un système de diffusion par satellite. Pour une telle application, l'élément dimensionnant est le transpondeur à bord du satellite qui comprend les filtres multiplexeurs ainsi que l'amplificateur de puissance. En effet, puisque le satellite est contraint en termes de consommation de puissance et d'interférence sur les canaux adjacents, le transpondeur est ainsi "le goulot" de l'optimisation du système. Nous étudions donc deux techniques permettant d'augmenter les débits du système et évaluons leur impact sur les éléments du transpondeur.

D'une part, l'utilisation de modulations d'ordre élevé permet d'augmenter le nombre de bits transmis par utilisation du canal, mais entraine pour les modulations d'amplitude et de phase une augmentation de la fluctuation

de l'enveloppe du signal. Ceci donne lieu à de l'interférence non linéaire quand ces signaux sont traités par un amplificateur de puissance opérant à saturation (ou proche de la saturation). Ce type d'interférence est aussi rencontré dans d'autres applications telles que les canaux à enregistrement magnétique ou les communications par fibre optique. D'autre part, augmenter les débits utiles peut aussi être réalisé, en augmentant le débit du signal. Cependant, si la bande du signal dépasse celle des filtres multiplexeurs, la sélectivité en fréquence du canal satellite est augmentée, générant une interférence additionnelle à la réception.
Pour les deux techniques d'augmentation de l'efficacité spectrale, une analyse de la nature et de la quantité d'interférence est nécessaire afin d'adopter les méthodes de réduction d'interférences adéquates. Les traitements peuvent ainsi être envisagés au niveau de l'émetteur au travers de techniques dites de pré-compensation ou de pré-distorsion, ou au niveau du récepteur par des techniques dites d'égalisation. Dans cette thèse nous nous intéressons plus particulièrement à l'analyse et l'optimisation des récepteurs itératifs pour le canal non linéaire, ainsi qu'aux formes d'ondes nouvelles permettant des algorithmes de réception plus efficaces.

Structure du manuscrit

Cette thèse s'articule en quatre chapitres principaux dont voici les descriptifs:

- **Chapitre 1:** Ce chapitre présente une description du système satellite surle quel notre étude portera. Il s'agit d'un système de diffusion par satellite et plus spécifiquement du standard de diffusion vidéo numérique (DVB). Nous présentons les nouvelles modulations proposées dans le standard DVB-S2 qui permettent d'atteindre un compromis intéressant entre efficacité en puissance et efficacité spectrale. Nous étudions ensuite les éléments constituants du transpondeur à bord du satellite, en évaluant l'impact de paramètres tels que le roll-off des filtres, la bande du signal, les reculs de l'amplificateur sur la quantité et la forme de l'interférence reçue. Ensuite, nous présentons un modèle de l'interférence non linéaire au rythme symbole en nous basant sur une décomposition en somme infinie dite de Volterra. Pour des raisons de complexité, ce modèle est tronqué aux *raisonnables* troisième et cinquième ordres, et l'impact de cette troncature sur la précision du modèle est évalué. Enfin, le modèle fréquentiel équivalent de la décomposition en séries de Volterra est décrit et sera utilisé ultérieurement pour les traitements fréquentiels.

- **Chapitre 2:** Ce chapitre traite des égaliseurs non itératifs pour le modèle non linéaire du canal satellite. Dans un premier temps, nous présentons une description sous forme de chaîne de Markov des non linéarités qui permet de dériver des égaliseurs optimaux au sens symbole et séquence. En raison

de la complexité exponentielle de ces égaliseurs, nous étudions des égaliseurs sous optimaux linéaires et non linéaires. Plus précisément, nous développons les expressions d'égaliseurs linéaires qui minimisent l'erreur quadratique moyenne ainsi que deux égaliseurs non linéaires à retours de décision. Ensuite, d'une manière similaire au domaine temporel, nous présentons des expressions d'égaliseurs linéaires et non linéaires fréquentiels. Nous dérivons ainsi de nouveaux résultats concernant l'égalisation hybride temps-fréquence pour le canal de Volterra. Enfin, ces différentes implémentations sont comparées en termes de taux d'erreurs binaires et de complexité.

- **Chapitre 3:** Ce chapitre présente des résultats sur la turbo égalisation du canal non linéaire satellite. Premièrement, nous rappelons des résultats sur l'égalisation itérative optimale pour des canaux décrits par un treillis, ce qui est le cas du canal nonlinéaire modélisé par une série de Volterra. Ensuite, nous dérivons des expressions pour les égaliseurs linéaires basés sur le modèle de Volterra, et étudions les approximations à faible complexité de ces égaliseurs. Par ailleurs, nous analysons l'égalisation itérative fréquentielle du canal de Volterra. Dans un second temps, nous concevons et optimisons le code canal qui permet de s'adapter au mieux aux messages issus de l'égaliseur en utilisant la méthode d'ajustement de la courbe (*curve fitting*) en utilisant l'outil EXIT. Pour ce faire, nous modélisons la sortie de l'égaliseur par un mélange de Gaussiennes qui est plus adéquat que l'approximation Gaussienne pour des modulations non binaires. Enfin, nous illustrons les gains en termes de taux d'erreurs binaires des codes ainsi optimisés en comparaison avec des codes non optimisés.

- **Chapitre 4:** Dans le chapitre 4, nous étudions la seconde méthode permettant d'améliorer les débits, et ce en élargissant la bande du signal aux dépens d'une augmentation de la sélectivité en fréquence des filtres à bord du satellite. Afin de réduire les interférences issus de cette augmentation de bande, nous présentons une forme d'onde permettant des traitements fréquentiels simplifiés. Cette forme d'onde a les avantages d'une modulation mono-porteuse en termes de fluctuations d'enveloppe, et les avantages d'une modulation multi-porteuses en termes d'égalisation fréquentielle simplifiée. Dans le cadre de notre étude, nous présentons un modèle fréquentiel et son équivalent en temporel pour cette forme d'onde, ce qui permet de dériver des formules analytiques de densité spectrale de puissance. De plus, nous étudions les interférences résiduelles après égalisation linéaire et dérivons des formules analytiques de rapport signal à bruit plus interférences qui nous permettent de prédire les performances du système.

Contributions principales

Les contributions principales de cette thèse sont résumées comme suit:

- Chapitre 1: Nous étudions l'impact des paramètres du système sur la représentation en série de Volterra de l'interférence non linéaire du canal satellite. Nous dérivons aussi un modèle, en nous basant sur des paramètres souhaités du système, qui constituera notre canal de test plus tard dans le manuscrit.
- Chapitre 2: Nous dérivons des égaliseurs temporels et fréquentiels linéaires et non linéaires du canal de Volterra et comparons les complexités. Nous présentons de nouveaux résultats sur l'égalisation hybride temps-fréquence appliquée au modèle de Volterra.
- Chapitre 3: Nous présentons l'égalisation itérative linéaire dans le domaine temporel [Benammar et al., 2013b] ainsi que dans le domaine fréquentiel [Benammar et al., 2014a]. Nous modélisons les sorties de l'égaliseur par un mélange de Gaussiennes dont nous dérivons les paramètres pour de la détection sur un canal Gaussien. Cette approximation est utilisée pour l'optimisation du code canal que nous appliquons à différentes classes d'égaliseurs optimaux [Benammar et al., 2014b] et sous-optimaux.
- Chapitre 4: Nous dérivons un modèle temporel généralisé de la forme d'onde mono porteuses par multiplexage à division orthogonale en fréquence (SC-OFDM). Nous proposons en outre des formules analytiques de la densité spectrale de puissance [Benammar et al., 2013a] et du rapport signal à bruit plus interférences pour ce type de forme d'ondes.

Introduction

For more than half a century, satellite systems have been conveying data over large and remote areas. Providing high throughput satellite communications is a challenging aspect in the evolutions of next generation satellite technologies be it for telecommunications, positioning or earth observation, .

When designing communication systems, many features interplay in dimensioning the link capacities. More specifically, depending on the nature of the satellite service (fixed, mobile, broadcast), the transmission link (up or down-link), the available bandwidth, and the acceptable complexity, solutions providing high spectral and power efficient satellite communications may differ.

The power efficiency measures the robustness to noise impairments and is usually related to the minimum distance of the code and modulation. The spectral efficiency characterises the communication throughput per occupied bandwidth and thus is related to the cardinality of the modulation and the rate of channel coding. There usually exists a trade-off between achieving a good power and spectral efficiency simultaneously. However, emerging advances in iterative processing have allowed reducing this trade-off by exploiting an additional degree of freedom which is the system complexity. In this thesis, we position ourselves in the forward link of a broadcast satellite system. For such a system, the key component is the satellite transponder which comprises multiplexing filters and the satellite amplifier. Indeed, since there are constraints on the available power and the maximum adjacent channel interference allowed, the transponder is usually the bottleneck in the design of broadcasting satellite systems. We thus investigate the impact of using two methods for increasing the throughput on the satellite transponder and thus on the overall system performance.

On the one hand, increasing the throughput by using high order modulations yields to higher signal fluctuations which give rise to non linear interference when the signals are amplified by a nearly saturated satellite amplifier. This kind of interference is also encountered in magnetic recording channels and fiber optical communications. On the other hand, increasing the throughput can also be carried out by increasing the symbol rate. Thus, the signal bandwidth may exceed the satellite multiplexing filters bandwidths leading to increased frequency selectivity in the satellite channel.

For both scenarios, an analysis of the nature and amount of interference is necessary in order to adopt adequate processing. Mitigation of the satellite channel impairments can be carried out either at the transmitter through pre-compensation and/or pre-distortion, or at the receiver by means of equalization. In this thesis, we are interested in receiver design for non linear satellite channels and the advanced waveforms allowing for a more efficient equalization at the receiver.

Structure of the manuscript

- **Chapter 1:** This chapter presents a description of the satellite systems under study. We are interested in broadband satellite services and more specifically in the Digital Video and Broadcasting standards. We present the DVB-S2 Amplitude and Phase Shift Keying schemes as well as related channel coding. We then present the satellite transponder constituting components, and show the impact of some system parameters such as the filters roll-offs, the signal bandwidth and the input back-off on the behaviour of the transponder. Moreover, we derive analytical symbol based description of the non linear interference by means of infinite Volterra series. For complexity considerations, this decomposition is truncated to reasonable third and five orders and the impact of this truncation on the model accuracy is analysed. Last but not least, we present the frequency domain equivalent Volterra series decomposition which is used later in the manuscript for frequency domain based processing.

- **Chapter 2:** This chapter deals with non iterative equalization for the non linear Volterra satellite channel. In the first part, we present a Markov chain description of the Volterra channel which then allows for the derivation of optimal symbol and sequence equalization. Due to the exponential complexity of the optimal equalizers, we investigate on sub-optimal linear and non linear equalization schemes in the time domain. More specifically, we derive expressions for the linear Minimum Mean Square Error estimator and two non linear Volterra decision feedback equalizers for the non linear channel. Then, similarly to the time domain, we present frequency domain linear and non linear equalization schemes. We specifically derive novel results on the hybrid time and frequency domain equalizer. Then, we compare these implementations in terms of bit error rates and complexity.

- **Chapter 3:** This chapter addresses iterative equalization and decoding for the non linear satellite channel. In the first part, we remind results on optimal iterative equalization for channels described by a trellis which we have shown to be the case of the Volterra non linear channel. Then, we derive novel results on time domain linear iterative equalizers based on the Volterra channel, and investigate on lower complexity approximations for the linear equalizer. We also analyse the frequency domain low complexity iterative equalizers. In a second part, we design and optimize the channel code so as to fit the equalizers output by the EXIT-chart curve fitting technique. To do so, we model the output of the equalizer as a mixture of Gaussians which we show is more accurate than the Gaussian approximation. Finally we illustrate the improvement in error rates for these approximations in comparison with non

optimized receivers.

- **Chapter 4:** In the chapter 4, we address the second throughput increasing technique relying on enlarging the signal bandwidth at the expense of increased frequency selectivity. Thus, to efficiently cope with the generated interference, we present a suitable single carrier transmission scheme which allows for simple frequency domain equalization at the receiver. We present both a frequency domain and a novel time domain model for this single carrier modulation which allows us to investigate on the spectrum characteristics and derive analytical expressions for its spectral density. Moreover, we investigate on the residual interference when linear equalizers are used and derive analytical expressions for the signal to interference and noise ratio, which allows for a good prediction of the system performance.

Main contributions

The main contributions of this thesis can be summarised as follows:

- Chapter 1: We study of the impact of the system parameters on the representation of the non linear satellite channel by Volterra series, and derive a test channel model given some system parameters which will be used later in simulations.
- Chapter 2: We derive a novel hybrid time and frequency domain equalizer for the Volterra description of the non linear interference and a detailed complexity analysis for different classes of equalizers.
- Chapter 3: We investigate on iterative linear time domain MMSE equalization [Benammar et al., 2013b] and frequency domain equalizers for the non linear satellite channel [Benammar et al., 2014a].
  We also model the output of the equalizer as a Gaussian Mixture instead. This approximation is used in the code design and optimization for a class of optimal and sub-optimal iterative receivers for the non linear channel [Benammar et al., 2014b].
- Chapter 4: We derive a time general representation of the Single Carrier -Orthogonal Frequency Division Multiplexing (SC-OFDM) modulation. We also derive analytical expressions for the spectral density [Benammar et al., 2013a] and signal to interference noise ratio for SC-OFDM.

Chapter 1

Digital communications over satellite channels

Contents

1.1 Introduction

New generation satellite broadcasting trends recommend using high order modulations to increase the spectral efficiency of the satellite link. Such high order modulations can be designed to allow a better resistance to noise (compared to amplitude shift keying), such as the new modulations suggested in the second generation broadcasting system. However, increasing the power efficiency does not come at no cost, since the resulting new waveforms have higher signal dynamics. This increased fluctuation has a direct impact on the operating region of non linear amplifiers on board satellites. Indeed, if the signal has large fluctuations, a non negligible back-off is required to the saturation power of the amplifier. The introduced back-offs decrease the energy efficiency of the power amplifier and thus impacts the overall link budget. If instead small back-offs are considered despite the large signal dynamics, the amplified signal is distorted and unless suitable mitigation techniques are used, the link budget is again impacted. It is thus important to understand the different technical issues involving the use of high order modulations and the corresponding RF design challenges. To do so, we start by introducing the context of satellite broadcasting systems. We then study the impact of different system configurations on the distortions induced by the non linear power amplifier. Then, we develop an analytical symbol based model for these distortions. Finally we investigate on equivalent representations of the non linear channel in the frequency domain, which will help us later develop frequency domain mitigation techniques.

1.2 Introduction (french)

Les nouvelles tendances concernant la diffusion par satellites, suggèrent l'utilisation de schémas de modulations d'ordre élevé afin d'améliorer l'efficacité spectrale des communications par satellites. Ces modulations d'ordre élevé peuvent être conçues afin de permettre une meilleure résistance au bruit (comparées aux modulations d'amplitude) à l'instar des modulations proposées dans la seconde génération des systèmes de diffusion. Cependant, l'amélioration de l'efficacité en puissance n'est pas gratuite, puisque les nouvelles formes d'ondes ainsi générées ont une plus forte dynamique du signal. Cette fluctuation additionnelle a un impact direct sur la zone de fonctionnement des amplificateurs non linéaires présents à bord des satellites. En effet, si le signal a une forte fluctuation, un recul non négligeable vis à vis de la puissance de saturation est nécessaire. Ceci représente un inconvénient majeur, puisque ces reculs diminuent l'efficacité énergétique des amplificateurs, et influent sur le bilan de liaison global. Si par contre, de faibles reculs par rapport à la puissance de saturation sont utilisés, le signal amplifié est distordu et à défaut de techniques adéquates d'élimination de ces distorsions, le bilan de liaison est impacté. Afin d'illustrer les enjeux liés à ces nouvelles modulations, nous commencerons par une

introduction des systèmes de diffusion par satellite. Nous étudierons ensuite l'effet de certains paramètres sur les distorsions générées par le canal nonlinéaire. Nous présenterons ensuite un modèle analytique au rythme symbole pour ces distorsions. Finalement, nous éudierons une représentation équivalente de ce modèle dans le domaine fréquentiel, ce qui nous permettra plus tard de développer des méthodes de traitement des distorsions dans le domaine fréquentiel.

1.3 Satellite communication system

A classical transparent satellite communication system consists of three distinct blocks:

- The ground station which is usually referred to as the hub.
  It consists for uplink communications of a transmitting dish or antenna fed by signals aggregated from different baseband signals. A power amplifier is used to cope with the sharp attenuation incurred by the transmitted signal when propagating through long distances to the satellite.

- The satellite or the space segment.
  It consists of three different components namely, the fuel component responsible for the propulsion, the Telemetric Tracking and Command (TT & C) system and the communication payload which usually contains several transponders. The TT & C system is used for all operations and commands concerning the deployment and the maintenance of the satellite in orbit. The transponder generally designated by the payload is responsible for all communications with the outside environment and thus for the Radio Frequency (RF) communications.
  Satellites can be classified into Fixed Satellite Services (FSS), Mobile Satellite Services (MSS) and Broadband Satellite Services (BSS). In this thesis, we focus on BSS systems with transparent satellites which unlike regenerative satellites do not demodulate the baseband signal but only repeat the incoming RF signal to the appropriate downlink channel with power amplification.

- The receiving station which can be a ground station, individual antennas or terminals directly located at the customer. For television applications, the satellite broadcasts signals over a wide area which can then be received by a large number of users with the use of small receiving antennas.

For satellite communications, the satellite transponder is generally the bottleneck of the system design, since it has limited resources and thus any required base-band processing should be located either at the transmitter station or at the receiving station.

Figure 1.1: DVB-S functional block diagram

1.4 Broadcasting Satellites standards

Broadcasting satellites are usually located in the geostationary orbit at about 37.000 km. The European Telecommunications Standards Institute (ETSI) committee has issued many standards regulating satellite broadcasting, depending on the type of the conveyed data.
Among the technologies of satellite broadcasting standards, we are interested in this thesis in Digital Video Broadcasting (DVB) standards and more specifically in DVB-S its 2nd generation evolution DVB-S2.

1.4.1 DVB-S standard

The standardised DVB-S [EN, 1997] is illustrated in Figure 1.1. It offers a $36MHz$ communication channel bandwidth and uses power efficient modulations namely the Binary Phase Shift Keying (BPSK) and Quadrature Phase Shift Keying (QPSK). Concatenated error correcting codes are used for channel coding. The inner code is based on a set of punctured Convolutional Codes (CC) constructed from a 1/2-rate convolutional code with constraint length equal to 7. The outer code is a shortened (N, K) Reed Solomon (RS) code $(N = 204, K = 188, T = 8)$ constructed on the Galois Field $GF(2^8)$ from a RS code $(N = 255, K = 239, T = 8)$ where is the length of the codewords, and K is the length of the information symbols and T is the correction capacity. It should be noted that the RS code shortening is realised by appending 51 null bytes to each block of 188 bytes and discarded at the end of the coding/decoding process. Since the RS code is systematic, the null bytes can be easily inserted and discarded at both ends of the coder and decoder. A convolutional interleaver is inserted between the two channel codes to offer a better correction capacity to the overall concatenated channel code.

1.4.2 DVB-S2 standard

The DVB-S2 standard depicted in Figure 1.2 has been proposed as a spectrally and power efficient transmission technology through using Amplitude and Phase Shift Keying (APSK) modulations and a class of capacity approaching block codes: Low Density Parity Check (LDPC) codes. The achieved system capacity gain over

Figure 1.2: DVB-S2 functional block diagram

the first generation DVB-S can reach 30%. Additionally, compared to the DVB-S standard, DVB-S2 offers the possibility of adapting the modulation and coding formats to the link quality with the so-called Adaptive Coding and Modulation (ACM) functionality.

DVB-S2 modulation schemes

The APSK modulation has been introduced in the DVB-S2 standard for its good trade-off between spectral and power efficiency. Indeed, for an equivalent spectral efficiency η, the APSK modulation has better robustness to Gaussian noise compared to PSK modulation. This power efficiency gain is achieved through dispatching the symbols over multiple rings allowing a better separation distance between symbols and yet carrying equivalent number of bits per modulated symbol. However, when compared to Quadrature an Amplitude modulations (QAM) constellations, APSK is less noise resistant but offers lower signal fluctuations which is a valuable feature especially for power amplifiers. Since APSK modulation symbols are distributed over multiple rings, it is convenient to define the ratio γ which characterises the relation between modulations radii. As such, for a 16APSK which consists of two concentric rings, the ratio γ writes as:

$$\gamma = \frac{R_2}{R_1} \tag{1.1}$$

where R_2 and R_1 are the outer and inner rings radii respectively. For a 32APSK, the DVB-S2 standard defines two ratios namely γ_1 and γ_2 describing the pairwise ratios and writing as follows:

$$\gamma_1 = \frac{R_2}{R_1} \text{ and } \gamma_2 = \frac{R_3}{R_2} \tag{1.2}$$

where R_3, R_2 and R_1 are the outer, intermediate and inner rings radii respectively. An illustration of the different proposed modulation schemes can be found in Figure 1.3. The modulation symbols s_i for these schemes can be written in a generic form as follows, :

$$s_i = R_n \exp(j2\pi\phi_k) \text{for} i = 1 : M \tag{1.3}$$

where R_n is one of the radii of the modulation scheme and ϕ_k is one of the allowed modulation phases for the ring radius R_n. Table 1.1 presents the different radii and phases for DVB-S2 mapping sets. The mapping used

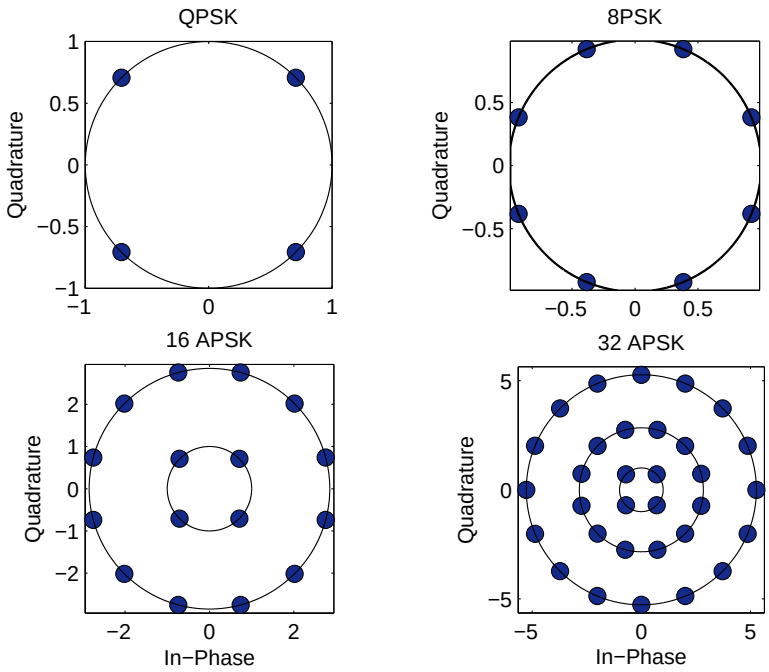

Figure 1.3: Scatter plot of the DVB-S2 modulation $\gamma = 2.85$ and $\gamma_1 = 2.84$ and $\gamma_2 = 5.27$

for PSK modulation is a Gray mapping whereas the mapping used for APSK modulations is a quasi-Gray mapping. It is important to notice that the performance of the APSK modulation, depends on the ratios γ_i, the number of constellation symbols on each ring, and the phase offsets between symbols. The minimum distance which measures the robustness to noise can be optimized to yield the targeted performance.

DVB-S2 coding schemes

The inner code of the DVB-S2 channel consists of a class of capacity approaching codes namely the LDPC codes. The proposed code is systematic with K_{LDPC} input bits and N_{LDPC} coded bits. The standard suggests two frame lengths consisting of short frames of length $N_{LDPC} = 16200$ and long frames of length $N_{LDPC} = 64800$.

The outer code is a Bose, Ray-Chaudhuri et Hocquenghem (BCH) block code with parameters (N_{BCH}, K_{BCH}, T) where T is the correction capacity of the code. A block interleaver is used between the two channel codes to cope with burst errors. This interleaver writes input stream in a matrix column-wise, and reads the elements line-wise. The dimensions of the interleaver matrix are given in [EN, 2009] for normal and short frames.

	Radii	Phases	Mapping in decimal
QPSK	$R = 1$	$k\frac{\pi}{2} + \frac{\pi}{4}$	$[0, 2, 3, 1]$
8PSK	$R = 1$	$k\frac{\pi}{4} + \frac{\pi}{4}$	$[0, 4, 6, 2, 3, 7, 5, 1]$
16APSK	$R_1 = 1$	$k\frac{\pi}{2} + \frac{\pi}{4}$	$[12, 14, 15, 13]$
	$R_2 = \gamma$	$k\frac{\pi}{6} + \frac{\pi}{12}$	$[4, 0, 8, 10, 2, 6, 7, 3, 11, 9, 1, 5]$
32APSK	$R_1 = 1$	$k\frac{\pi}{2} + \frac{\pi}{4}$	$[17, 21, 23, 19]$
	$R_2 = \gamma_1$	$k\frac{\pi}{6} + \frac{\pi}{12}$	$[16, 0, 1, 5, 4, 20, 22, 6, 7, 3, 2, 18]$
	$R_3 = \gamma_1\gamma_2$	$k\frac{\pi}{8}$	$[24, 8, 25, 9, 13, 29, 12, 28, 30, 14, 31, 15, 11, 27, 10, 26]$

Table 1.1: DVB-S2 modulation schemes parameters for QPSK, 8PSK, 16APSK and 32ASPK

Code rate	Modulation coding/spectral efficiency	γ
2/3	2,66	3,15
3/4	2,99	2,85
4/5	3,19	2,75
5/6	3,32	2,70
8/9	3,55	2,60
9/10	3,59	2,57

Table 1.2: Optimum constellation radius ratio for AWGN channel with 16APSK

In [De Gaudenzi et al., 2006], the overall DVB-S2 system has been optimized to yield the best system capacity. To do so, the radii of APSK modulations was jointly optimized with the coding rate to yield the best spectral efficiency. Table 1.2 and Table 1.3 summarize the designed optimal ratios γ and (γ_1, γ_2) for the couples (coding rate, spectral efficiency).

1.4.3 DVB-S2X

DVB-S2X [DVB-S2X, 2014] is an evolution of the standard DVB-S2 which relies on the same physical layer characteristics regarding the types of modulations and channel codes. However, there are some differences in the system parameters which can be summarised as follows:

- Small roll-offs (0.05 and 0.1) can be used leading to up to 15% gain in the system throughput.
- Finer modulations and coding rates
- The modulation ring ratios can be jointly chosen with coding rates for given amplifier back-offs.

Code rate	Modulation coding/spectral efficiency	γ_1	γ_2
3/4	3,74	2,84	5,27
4/5	3,99	2,72	4,87
5/6	4,15	2,64	4,64
8/9	4,43	2,54	4,33
9/10	4,49	2,53	4,30

Table 1.3: Optimum constellation radius ratio for AWGN channel with 32APSK

Using amplitude and phase shift keying modulations as originally proposed in the DVB-S2 standard has given rise to some challenges related to power amplifiers efficiency. Power amplifiers are located both at the transmitter (ground station) and on-board satellites. Yet, since there are less restrictions on the power supply of a hub or a gateway on a forward link, the limiting power amplifier is the one located in the satellite transponder. For a better understanding of the amplifiers effects, we present in the next section the satellite transponder constituent elements and how they impact the channel non linearity.

1.5 Transponder modelling

In this section we are interested in the elements constituting a transponder, and more specifically, the power amplifier and the input and output multiplexers. The considered amplifier is a memory-less device with a frequency independent amplification model. The input and output multiplexers placed before and after the power amplifier are meant to reject undesired spectral components. In the following, we give more insights on the classes of amplifiers and the multiplexing filter responses.

1.5.1 TWT and SSP Amplifiers

TWTA

Travelling Wave Tube Amplifier (TWTA) are wideband microwave amplifiers capable of amplifying a wide range of frequencies. Figure 1.4 depicts the structure of a TWT amplifier.
A cathode heated at thousands of degrees generates an electron beam which is accelerated by the anode using a high potential. These electrons propagate into a vacuum cavity containing a helix related to RF inputs and outputs. The interaction between the RF signal and the electron beam leads to a deceleration of the electrons, whose kinetic energy is transferred to the RF signal which is then amplified. At the end of their race, electrons

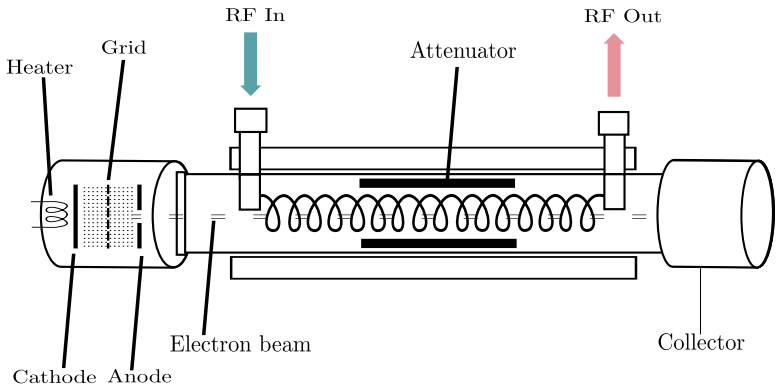

Figure 1.4: Structure of a Travelling Wave Tube Amplifier

are captured by the collector which receives the remaining electrons energy. TWTA have interesting high gain and low noise characteristics which makes them suitable for RF amplification [Gilmour, 2011].
The amplification process of a TWTA is usually described using two functions: Amplitude to Amplitude (AM-AM) and Amplitude to Phase (AM-PM). Theses functions relate the input amplitude to the output amplitude and phase rotation respectively. To describe a TWTA, Saleh in [Saleh, 1981] presented a frequency-independent model to characterise the AM-AM and AM-PM functions of a TWTA. The derived frequency-independent model of the amplifier only depends on the instantaneous input amplitude r. The AM-AM and AM-PM functions write as follows [Saleh, 1981]:

$$\begin{aligned} AM - AM(r) &= \frac{\alpha_a r}{1 + \beta_a r^2} \\ AM - PM(r) &= \frac{\alpha_\phi r.^2}{1 + \beta_\phi r^2} \end{aligned} \tag{1.4}$$

where r is the input signal amplitude and α_a, β_a, α_ϕ and β_ϕ are design parameters which characterise the AM-AM and AM-PM functions respectively. For instance, Figure 1.5 plots a TWTA amplifier functions using parameters $\alpha_a = 1.9638$, $\beta_a = 0.9945$, $\alpha_\phi = 2.5293$ and $\beta_\phi = 2.8168$. IBO and OBO stand for backoffs and are presented in the next section.

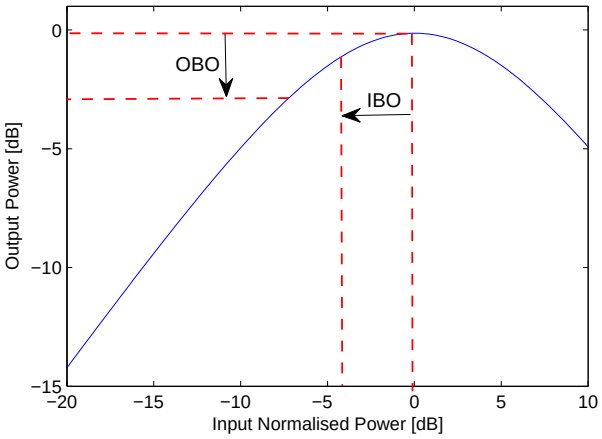

Figure 1.5: AM-AM characteristic using Saleh's model with parameters $\alpha_a = 1.9638$ and $\beta_a = 0.9945$

SSPA

A Solid State Power Amplifier (SSPA) is a device that uses Field Effect Transistors (FET) and thus relies on solid components unlike a TWTA which uses a vacuum tube. A SSPA is composed of serial/parallel combinations of FETs which used alone would have delivered limited gain. It usually consists of four stages using power combiners, dividers and medium power amplifiers. The power combiners are dissipative components which leads to a lower energy efficiency as their number increases.

In a similar fashion to TWTAs, SSPAs can be described by two functions namely AM-AM and AM-PM. Analytical models which can be used for representing these functions are different from Saleh's equations (1.4). In fact, two analytical models describing the SSPAs nonlinearity can be found in literature, the Rapp model [Rapp, 1991] [Costa and Pupolin, 2002] and the Ghorbani model [Ghorbani and Sheikhan, 1991] respectively. On the one hand, the Rapp's model defines AM-AM and AM-PM equation as follows:

$$\begin{aligned} AM-AM(r) &= v\frac{r}{\left(1+\left(\frac{vr}{A_0}\right)^{2p}\right)^{\frac{2}{2p}}} p>0, A_0 \geq 0, v \geq 0 \\ AM-PM(r) &= \alpha_\Phi \left(\frac{vr}{A_0}\right)^4 \end{aligned} \tag{1.5}$$

where r is the input signal amplitude, v is called the small-signal gain, A_0 is the saturation amplitude level and p is a factor that controls the smoothness of the curve before saturation. In the AM-PM conversion, α_Φ is generally set to zero since the phase rotation is considered negligible for a SSPA compared to TWTA. On the

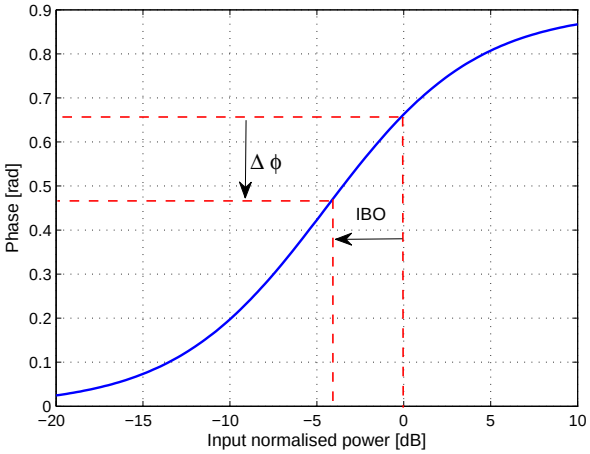

Figure 1.6: AM-PM characteristic using Saleh's model with parameters $\alpha_\phi = 2.5293$ and $\beta_\phi = 2.8168$

other hand, Ghorbani's model presents a different approximation of SSPA's AM-AM and AM-PM conversions. These conversions write as:

$$\begin{aligned} AM-AM(r) &= \frac{x_1 r^{x_2}}{1+x_3 r^{x_2}} + x_4 r \\ AM-PM(r) &= \frac{y_1 r^{y_2}}{1+y_3 r^{y_2}} + y_4 r \end{aligned} \tag{1.6}$$

where r is the input signal amplitude, x_1, x_2, x_3, x_4 and y_1, y_2, y_3, y_4 are adjusting coefficients. It can be seen, that the Ghorbani model can be written as a Saleh decomposition for special values of the adjusting parameters.

Comparison between TWTA and SSPA

For a comparison between the two classes of amplifiers to be carried out, one needs to determine what is the intended system use of these amplifiers. Indeed, each of the TWTAs and SSPAs have advantages and drawbacks, which implies they can only be assessed with regard to the application requirements. To do so, authors in [Maral and Bousquet, 2002] present a set of comparative characteristics between TWTAs and SSPAs which are presented in Table 1.4. On the one hand, SSPAs are lighter than TWTA but have less energy efficiency which makes them more suitable to small satellites in low orbits such as observation satellites. On the other hand, TWTAs have better efficiency and can operate over a wide range of frequencies which makes them suitable for telecommunication applications such as broadcasting satellites. In the remaining of this

Characteristic	**TWTA**	**SSPA**
Operating band (GHz)	C, Ku, Ka	L,C
Saturated power output (W)	$20-250$	$20-40$
Gain at saturation (dB)	~ 55	$70-90$
Intermodulation product relative level $(C/N)_{IM3}$ (dB)	$10-12$	$14-18$
AM/PM conversion coefficient $K_p(/dB)$	4.5	2
DC to RF efficiency	$50-65$	$30-45$
Mass including (kg)	$1.5-2.2$	$0.8-1.5$

Table 1.4: Comparative characteristics for TWTA and SSPA

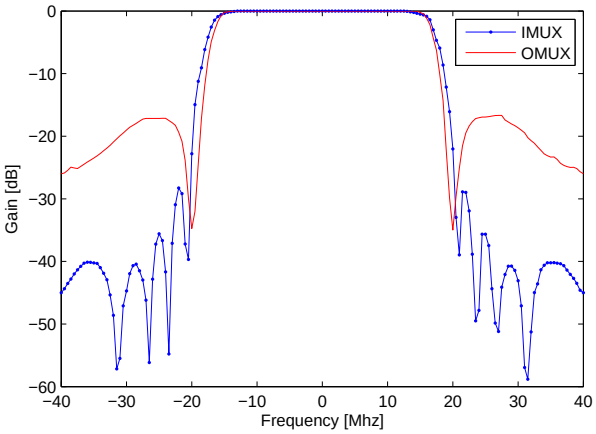

Figure 1.7: Gain for IMUX and OMUX

thesis, the considered amplifiers will be thus TWTAs, which will be modelled by Saleh's representation as in (1.4).

1.5.2 Input and output multiplexers

The Input MUltipleXer (IMUX) is a band-pass filter which aims at removing adjacent channels interference caused by other input channels. The Output MUltipleXer (OMUX) consists of a band-pass filter which rejects the out-of-band radiation due to the spectral growth induced by the non linear amplifier processing. The reader is referred to Section 1.6.1 for more details about the impact of the amplification on the power spectral density. Figure 1.7 and Figure 1.8 illustrate the gain and group delay of typical $36MHz$ IMUX and OMUX

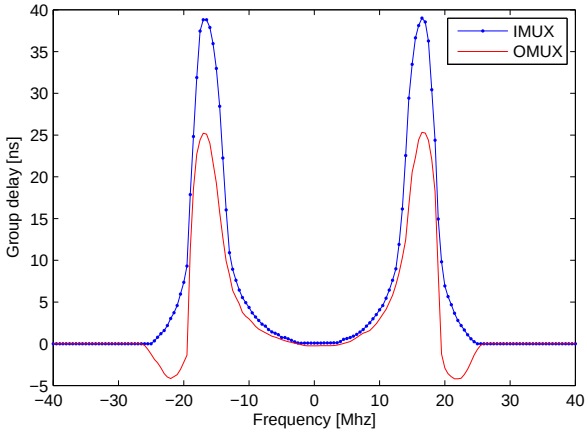

Figure 1.8: Group delay for IMUX and OMUX

filters. The phase response is applied by integrating the group delay (GD) following:

$$\phi(\omega) = \int GD(\omega) d\omega \tag{1.7}$$

where ω designates the frequency.

1.5.3 Saturation levels

In order to define the operating point of a power amplifier, it is useful to introduce two metrics which characterise the back-off towards the input saturation power and the output power respectively. We thus define the Input Back-Off (IBO) as the ratio between the input power P_{in} and the input saturation power $P_{in,sat}$ as follows:

$$IBO = -10 \log_{10} \frac{P_{in}}{P_{in,sat}} \tag{1.8}$$

Similarly we define the Output Back-Off (OBO) as the ratio between the output power P_{out} and the maximum output power delivered by the PA as follows:

$$OBO = -10 \log_{10} \frac{P_{out}}{P_{out,sat}} \tag{1.9}$$

Figure 1.5 and Figure 1.6 plot the TWTA transfer characteristics with its IBO and OBO operating points.

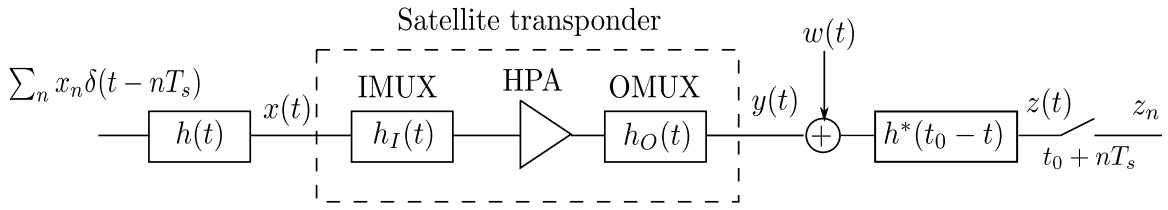

Figure 1.9: Satellite channel modelling

1.6 Impact of system parameters on the non linear channel

Let us consider the system depicted in Figure 1.9. A stream of symbols x_n with a symbol duration T_s is pulse shaped by a root raised cosine filter with roll-off α writing as:

$$h(t) = \frac{2\alpha}{\pi\sqrt{T_s}} \frac{\cos\left[(1+\alpha)\pi\frac{t}{T_s}\right] + \frac{sin\left[(1-\alpha)\pi\frac{t}{T_s}\right]}{4\alpha\frac{t}{T_s}}}{1-\left(4\alpha\frac{t}{T_s}\right)^2} \tag{1.10}$$

The resulting transmit signal is then sent to a satellite transponder where it is first filtered with the IMUX, amplified by the HPA and then filtered out by the OMUX. The output signal $y(t)$ is broadcast to the receiving station where an additive white Gaussian noise with variance σ_w^2. A matched receive filter is used before sampling at the corresponding Nyquist timing $t_0 + nT_s$. The resulting symbols z_n depend on the system parameters such as the root raised cosine roll-off, the signalling rate and on the HPA back-off, which hence has an impact on the resulting system performance. It is thus interesting to investigate on the impact of each of the aforementioned system parameters on the received symbols. To do so, we set the noise variance to zero to assess only the non linear interference.

1.6.1 Impact of IBO

The IBO as defined in Section 1.5.3 is a key factor in the amount of ISI generated by the non linear satellite channel. Figure 1.10 plots different scatter-plots for a 16APSK using a root raised cosine of roll-off $\alpha = 0.2$ and for $IBO = 0, 3, 6, 9dB$. The figure shows that the amount of ISI decreases with an increasing IBO which is due to the linear-like behaviour of the HPA for very high back-offs. It should be noted that the nonlinear ISI is not isotropic, since there seems to be a correlation between real and imaginary parts of the ISI owing to its elliptical shape. To illustrate this property, Figure 1.11 and Figure 1.12 plot the probability distribution function of the power of ISI around the average constellation point, which is often called a centroid. It can be seen that for low IBO values, the distribution of ISI of outer rings symbols is not a circular Gaussian

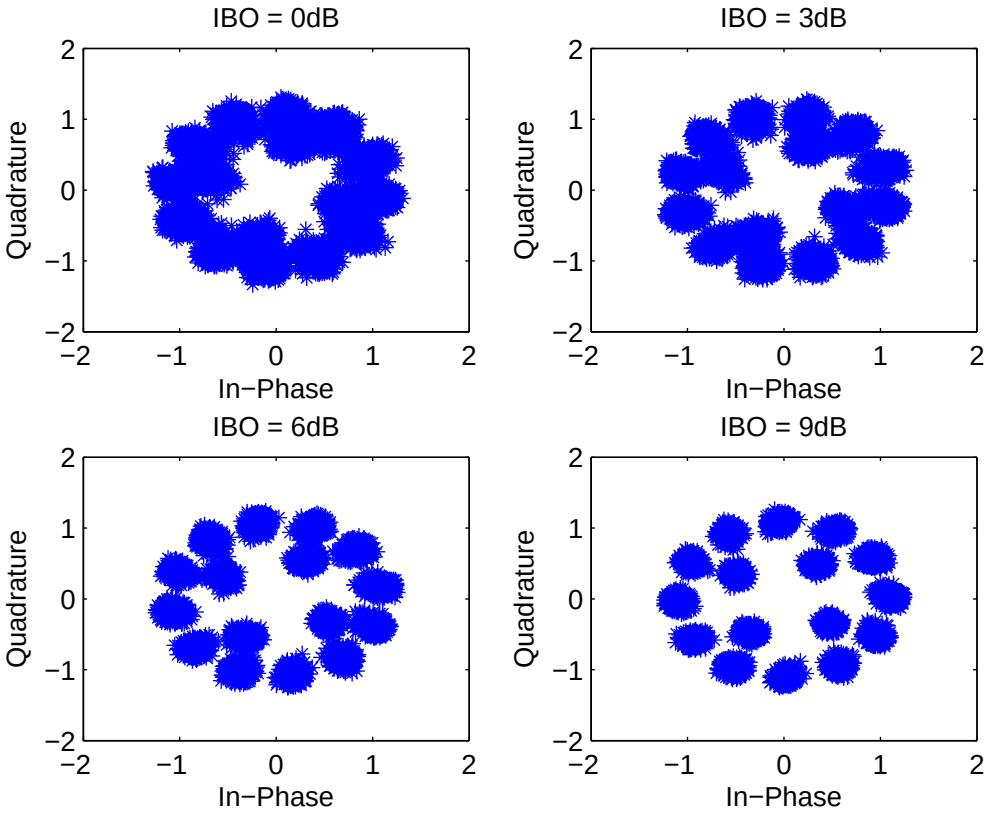

Figure 1.10: Constellation for 16APSK with roll-off $\alpha = 0.2$

distribution, since its imaginary and real part histograms are not similar. Yet, with increasing IBO values, the distribution of ISI becomes circular Gaussian which again is due to the linear operating region of the HPA for high IBOs.

When being amplified, the power spectral density of the signal is also modified by the non linear processing. The PSD is expanded leading to novel frequency components which is generally referred to as "spectral growth". The amount of spectral growth depends on the IBO values and is depicted in Figure 1.13. It is clear that the smaller the IBO, the larger the spectral growth, due to the increased nonlinearity of the power amplifier.

1.6.2 Impact of the root raised cosine roll-off

The root-raised cosine filter introduces a memory in the satellite system which combined with the memoryless non linear amplifier leads to the observed ISI in Figure 1.10. One can wonder what is the impact of the roll-off

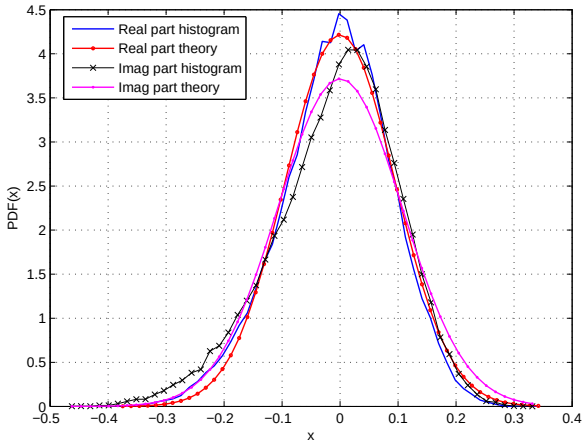

Figure 1.11: PDF of real and imaginary parts of one outer ring centroid at $IBO = 0dB$

Symbol rate \ IBO	0dB	-3dB	-6dB	-9dB
27.5 Mbauds	0.0561	0.0440	0.0373	0.0326
30 Mbauds	0.0863	0.0695	0.0585	0.0552
32.5 Mbauds	0.1505	0.1282	0.1186	0.1081

Table 1.5: ISI variance for different signal bandwidths

of the root raised cosine on the ISI power and shape. Figure 1.14 depicts the ISI variance for one of the outer ring constellation symbols using different IBOs and roll-offs. The higher the roll-offs, the lower the side lobes of the impulse response are, and thus the less the impact of the non linearity. It can be further noticed, that the dependence of the non linear interference power on the roll-off decreases for large IBO values. Ultimately, the roll-off influence vanishes for very high IBO values, since the amplifier consists then of a constant gain. Thus, this would yield to interference-free received symbols, since the root-raised cosine filters used in the chain are Nyquist shapes.

1.6.3 Impact of the signal bandwidth in the presence of IMUX and OMUX

The IMUX and OMUX filters present on both sides of the satellite non linear amplifiers control the input and output bandwidth of the satellite transponder signals. The multiplexing filters defined in Section 1.5.2 were designed for a $33MHz$ signal bandwidth, which for a certain roll-off α leads to a desired symbol rate $R_s = 33/(1+\alpha)Mbauds$. For example with a roll-off factor $\alpha = 0.2$, the desired symbol rate is $R_s = 27.5Mbauds$.

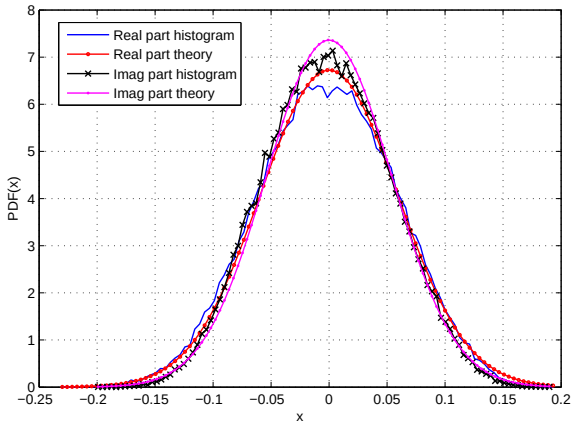

Figure 1.12: PDF of real and imaginary part of one outer ring centroid at $IBO = 9dB$

If the symbol rate is higher than $27.5Mbauds$, the filters will be more frequency selective and thus will lead to increased interference. In Table 1.5, the amount of ISI is expressed by means of the MSE between the received symbols and their centroids and different signal bandwidths are investigated. It can be seen that the larger the symbol rate in comparison with the reference $R_s = 27.5Mbauds$, the higher the MSE.

1.7 Non linear satellite channel models

The issue of modelling the satellite transponder effects on the received demodulated signals has been investigated in many previous studies. Indeed, modelling the satellite non linear channel is of primary importance in order to adopt the adequate processing techniques in order to cope with adverse effects occurring in the satellite link. Depending on the complexity of the channel model and the application type, mitigating the adverse effects of the satellite channel could be envisaged either at the transmitter through the so-called precoding/pre-compensation technique, or at the receiver using appropriate equalization schemes. When talking about the adverse effects of satellite power amplifiers it is usual to characterise the impact of the non linearities in terms of the intermodulation products. These intermodulation products are used to evaluate the amount of new generated frequencies due to spectral growth. In the following we present some of the models for the non linear channel:

- Authors in [J. C. Fuenzalida, 1973] presented a characterisation in the time domain of the intermodulation products by means of a Bessel series expansion. The resulting autocorrelation based time domain

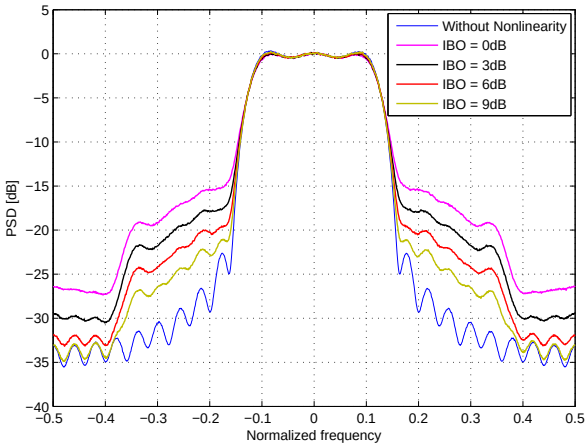

Figure 1.13: Power spectral density of the amplified signal for different IBO values

representation, was then used to compute the power spectral density of the intermodulation products.

- Blachman in [Blachman, 1968] derives a characterisation of the intermodulation products by using a Hermite polynomial decomposition, and shows that the output of a non linear process can be decomposed into the sum of uncorrelated elements.
- The author in [Burnet and Cowley, 2005], derived a linear experimental model based on the observation that the non linear channel can be decomposed into a combined triple effect as in [Uncini et al., 1999].
- Authors in [Benedetto and Biglieri, 1999] present a base-band non linear symbol based description of the non linear channel by means of a Volterra series decomposition presented in [Schetzen, 1980].

In this section, we are interested in the two last representations of the non linear channel namely the one derived by [Burnet and Cowley, 2005] which consists of a triple-effect linear model, and the representation of [Benedetto et al., 1979] which is a non linear symbol-based representation of the base-band satellite channel.

1.7.1 Linear model

In the linear model derived in [Uncini et al., 1999] and [Burnet and Cowley, 2005], the non linear channel is decomposed as a combination of three effects:

- Constellation warping: It occurs when the input signal to a non linear device has multiple amplitude values which thus are not similarly affected. Figure 1.15 illustrates how outer ring symbols of a 16APSK

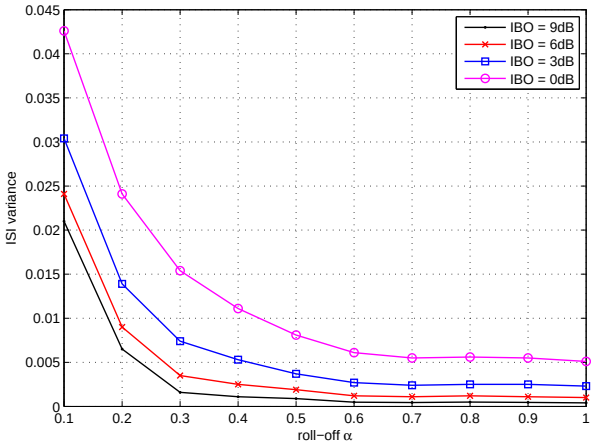

Figure 1.14: ISI variance function of the root raised cosine roll-off α

are differently amplified compared to inner ring symbols for $IBO = 0dB$ and $IBO = 3dB$. The reason is that outer rings symbols generally fall in the saturated operating region of the HPA and thus experience a clipping effect. The phase response AM-PM of the HPA also leads to a differential phase rotation of outer ring symbols compared to inner ring symbols. This selective phase and amplitude distortion leads to the so-called "constellation warping" [Burnet and Cowley, 2005].

- Non linear ISI: The non linear ISI arises from the combination of the effects of channel filter memories and the saturated HPA response, which leads to a general non linear ISI representation of the satellite channel. Figure 1.10 depicts the non linear ISI for different back-off values.

- Spectral spreading: Spectral spreading was discussed in Section 1.6.1. A spectral growth actually results in a signal attenuation as explained in [Burnet and Cowley, 2005].

This linear model is practical since it allows for the application of standard receiving techniques as those applied for a transmission over ISI channels with additive Gaussian noise. However, this model is too simplistic for multi-level modulations, since the impact of the non linear channel differs following the amplitude of symbols. In order to perfectly model the non linear channel, one needs to derive an analytical characterization of the non linear channel. This introduces the next subsection, where we study a modelling of the non linear channel by means of polynomial expansions, which leads to the so-called Volterra model.

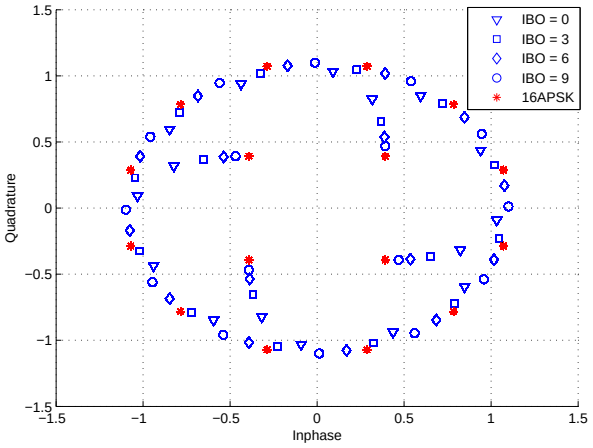

Figure 1.15: Constellation warping for 16APSK

1.7.2 Volterra model

Let us consider the system depicted in Figure 1.9. The baseband transmit signal $x(t)$ writes as follows:

$$x(t) = \sum_{n=\infty}^{\infty} x_n h(t - nT) \tag{1.11}$$

The signal is transposed into carrier frequency f_0 which is sent to a satellite transponder where $h_I(t)$ and $h_O(t)$ represent the time domain impulse responses of both the IMUX and OMUX filters, and $c(t)$ is the complex response of the power amplifier which writes as:

$$c(r) = A(r)\exp(j\Phi(r)) \tag{1.12}$$

where r is the input signal amplitude. As in [Benedetto and Biglieri, 1999] let us use the decomposition into polynomial series of the non linear Saleh's transfer function as follows:

$$c(r) = \sum_{i=0}^{\infty} \gamma_i r^i \tag{1.13}$$

where γ_i are complex coefficients representing the decomposition factors and taking into account both the AM-AM and AM-PM characteristics. It has been shown in [Benedetto and Biglieri, 1999] that due to the bandpass nature of the satellite transponder, only odd terms power coefficients are allowed for the series decomposition in (1.13). Even coefficients yield harmonics which are outside the transponder bandwidth and thus are not taken into account. Thus we define, $x_I(t)$ and $x_O(t)$ as the complex envelopes of the signals at the input

and output of the non linear amplifier characterised by $c(t)$. By writing the complex representation of the signal $x_I(t)$ as an amplitude $|x_I(t)|$ and a phase $\phi(t)$, the HPA's output signal $x_O(t)$ writes function of $x_I(t)$ as follows:

$$x_O(t) = \sum_{i=0}^{\infty} \frac{\binom{2i+1}{i}}{2^{2i+1}} \gamma_{2i+1} |x_I(t)|^{2i+1} \exp(j\phi(t)) \tag{1.14}$$

where the baseband signal $x_I(t)$ writes as follows:

$$\begin{aligned} x_I(t) &= x(t) * h_I(t) && (1.15)\\ &= \sum_{n=-\infty}^{\infty} x_n h(t-nT) * h_I(t) \\ &= \sum_{n=-\infty}^{\infty} x_n \tilde{h}_I(t-nT) \end{aligned}$$

$$(1.16)$$

and where we define the filter $\tilde{h}_I(t) = h(t) * h_I(t)$ as the overall input filter. The operation $a * b(t)$ stands for the convolution operator of signals $a(t)$ and $b(t)$ which writes as:

$$a * b(\tau) = \int_{\mathbb{R}} a(t) b(\tau - t) dt \tag{1.17}$$

Thus, the output base-band signal $x_O(t)$ can be written in a expanded form as follows:

$$\begin{aligned} x_O(t) &= \sum_{i=0}^{\infty} \frac{\binom{2i+1}{i}}{2^{2i+1}} \gamma_{2i+1} |x_I(t)|^{2i+1} \exp(j\phi(t)) \\ &= \sum_{i=0}^{\infty} \frac{\binom{2i+1}{i}}{2^{2i+1}} \gamma_{2i+1} x_I(t)^i x_I^{*i}(t) |x_I(t)| \exp(j\phi(t)) \\ &= \sum_{i=0}^{\infty} \frac{\binom{2i+1}{i}}{2^{2i+1}} \gamma_{2i+1} x_I(t)^{i+1} x_I^{*i}(t) \\ &= \sum_{i=0}^{\infty} \frac{\binom{2i+1}{i}}{2^{2i+1}} \gamma_{2i+1} \sum_{n_1} \cdots \sum_{n_{i+1}} \sum_{n_{i+2}} \cdots \sum_{n_{2i+1}} x_{n_1} \ldots x_{n_{i+1}} \ldots x^*_{n_{i+2}} x^*_{n_{2i+1}} \\ &\quad \tilde{h}_I(t-n_1T) \ldots \tilde{h}_I(t-n_{i+1}T) \tilde{h}^*_I(t-n_{i+2}T) \ldots \tilde{h}^*_I(t-n_{2i+1}T) \end{aligned} \tag{1.18}$$

The transponder base-band output signal $y(t)$ writes thus as:

$$y(t) = x_O(t) * h_O(t) \tag{1.19}$$

The satellite transmitted signal is broadcast to the receiving station where an additive noise at the receiver is added. The sampled signal at time $t_0 + nT_s$ writes then as follows:

$$z_n \triangleq z(t_0 + nT)$$

$$
\begin{aligned}
&= y(t) * h(t)|_{t_0+nT} + w(t) * h(t)|_{t_0+nT} \\
&= x_O(t) * \tilde{h}_O(t)|_{t_0+nT} + w_n \\
&= \sum_{i=0}^{\infty} \sum_{n_1} \cdots \sum_{n_{i+1}} \sum_{n_{i+2}} \cdots \sum_{n_{2i+1}} x_{n-n_1} \ldots x_{n-n_{i+1}} x^*_{n-n_{i+2}} \ldots x^*_{n-n_{2i+1}} k^{(i)}(n_1, \ldots n_{2i+1}) + w_n
\end{aligned}
$$

where we define the OMUX-receive filter $\tilde{h}_O(t)$ as:

$$\tilde{h}_O(t) = h(t) * h_O(t) \tag{1.20}$$

and where the non linear interference kernels $k^{(i)}(n_1, \ldots n_{2i+1})$ write as:

$$k^{(i)}(n_1, \ldots n_{2i+1}) = \frac{\binom{2i+1}{i}}{2^{2i+1}} \gamma_{2i+1} \int \tilde{h}_I(u-n_1T) \ldots \tilde{h}_I(u-n_{i+1}T) \tilde{h}^*_I(u-n_{i+2}T) \ldots \tilde{h}^*_I(u-n_{2i+1}T) \tilde{h}_O(t_0+nT-u) du \tag{1.21}$$

It should be noted, that when the chain filters are memoryless e.g. rectangular shaped with length equal to the symbol period, Volterra kernels $k^{(i)}(n_1, \ldots n_{2i+1})$ are zero for all $i \in \mathbf{N}$ and for all $k^{(0)}(n)$ with $n > 0$, which yields to a memoryless linear channel.

1.7.3 Volterra coefficients design

Symmetries exploitation

The infinite series decomposition of Volterra kernels induces unfortunately a large and unpractical complexity in the time domain expression (1.20). Since working with infinite series decomposition is not possible in real scenarios, some channel reduction is needed. A first step in reducing the number of coefficients is to look at the different symmetries in the Volterra kernels. Indeed, the decomposition in (1.20), involves products of symbols $x_{n-n_1} \ldots x_{n-n_{i+1}} x^*_{n-n_{i+2}} x^*_{n-n_{2i+1}}$ which may lead to the same symbols for specific values of the set $n_{p_{p\in 0,\ldots 2i+1}}$. As a result, the number of Volterra kernels can be reduced when exploiting the symmetries in the non linear interfering symbols. To illustrate this reduction, let us consider the 3^{rd} and 5^{th} order terms of a Volterra decomposition. It is clear that the triplets of indexes (n_1, n_2, n_3) lead to the same value of symbols products $x_{n-n_1} x_{n-n_2} x^*_{n-n_3}$ for any permutation of symbols (n_1, n_2), which are in the number of 2 for any couple of indexes (n_1, n_2). For 5^{th} order decomposition and with quintuplets $(n_1, n_2, n_3, n_4, n_5)$, any permutation of the symbol indexes (n_1, n_2, n_3) and any permutation of the symbols conjugates indexes (n_4, n_5) lead to the same expression of the products of symbols. By exploiting these symmetries, major reduction in the number of indexes quintuplets $(n_1, n_2, n_3, n_4, n_5)$ can be achieved providing a reduced yet equivalent description of the non linear Volterra decomposition. We select thus one representing kernel for all

symmetric kernels $h^{(i)}(n_1, \dots n_{2i+1})$ which we denote as:

$$h^{(i)}(n_1, \dots n_{2i+1}) = \sum k^{(i)} \left(\Pi(n_1, \dots n_{i+1}), \Pi(n_{i+2}, \dots, n_{2i+1})\right) \tag{1.22}$$

where $\Pi(n_1, \dots n_{i+1})$ denotes all the permutations of the i-tuples $(n_1, \dots n_{i+1})$ which are in the number of $(i+1)!$.

Constant amplitude modulations

The number of Volterra kernels can also be decreased using special characteristics of the symbols x_n, and more specifically when they are drawn from constant amplitude modulations such as PSK. Indeed, due to the presence of symbols conjugates, products of $x_n x_n^* = |x_n|^2$ can be exploited when the symbols satisfy $|x_{n_i}|^2 = C$. To illustrate this reduction, let us consider the 3^{rd} order Volterra decomposition indexes (n_1, n_2, n_3) related to the product $x_{n_1} x_{n_2} x_{n_3}^*$. For all triplets writing as (n_1, n_2, n_1), the product $x_{n_1} x_{n_2} x_{n_3}^* = |x_{n_1}|^2 x_{n_2} = C x_{n_2}$. This product will thus only contribute to first order inter symbol interference. This reduction is also valid for (n_1, n_2, n_2) triplets since n_1 and n_2 are symmetrical. For 5^{th} order interference, the same reduction can be carried out leading to simplified third order terms whenever the product $\delta(n_1, n_4)\delta(n_1, n_5)\delta(n_2, n_4)\delta(n_2, n_5)\delta(n_3, n_4)\delta(n_3, n_5) = 0$, and $\delta(i, j)$ is the kronecker function. It can be noted that for 16APSK, an approximation consisting of assimilating $|x_n|^2$ to its mean value which is $E[|x_n|^2] = R_1^2/4 + R_2^2/12$, can allow us using the same reduction as for PSK modulations.

Truncation

A third step in reducing the number of Volterra coefficients, which this time induces some degradation in the system model consists of truncating the Volterra series expansion. This truncation is applied to the degree of the Volterra decomposition, and to the allowed memory in all these approximations. As such, the Volterra decomposition writes as:

$$\begin{aligned} z_n \quad = \quad & \sum_{i=0}^{v} \gamma_{2i+1} \sum_{n_1=-(M-1)}^{M-1} \cdots \sum_{n_{i+1}=-(M-1)}^{M-1} \sum_{n_{i+2}=-(M-1)}^{M-1} \cdots \sum_{n_{2i+1}=-(M-1)}^{M-1} \\ & x_{n-n_1} \dots x_{n-n_{i+1}} x_{n-n_{i+2}}^* \dots x_{n-n_{2i+1}}^* h^{(i)}(n_1, \dots n_{2i+1}) \end{aligned} \tag{1.23}$$

where the parameter v is the decomposition order of the Saleh's polynomial expansion, and where M controls the channel memory size. The higher the order v, the more accurate the approximation gets, but

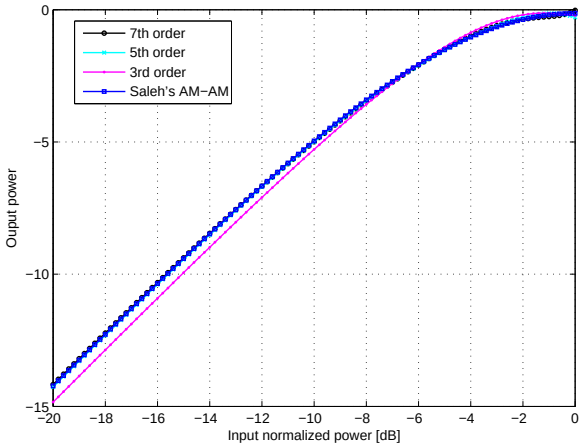

Figure 1.16: Polynomial decomposition for AM-AM Saleh's function

Polynomial order	MSE
7th order	$2.1005e-5$
5th order	$4.4702e-4$
3rd order	0.0040
1st order	0.0106

Table 1.6: Table of MSE for different polynomial order decompositions

the more coefficient have to be dealt with. Figure 1.16 and Figure 1.17 illustrate the decomposition of the Saleh transfer function for different orders v using the parameters in Figures 1.5 and 1.6. Table 1.6 presents the MSE between the real channel output, and the channel output when Saleh's HPA model is replaced by a polynomial expansion of orders 3, 5 and 7 for $IBO = 6dB$. It can be seen that the polynomial expansions yield better approximations with higher orders.

As far as the decomposition memory is concerned, a long channel memory allows a better channel approximation. Figure 1.18 depicts the scatterplots obtained for values of the channel memory from 2 to 4 for $IBO = 3dB$ using a Volterra decomposition order equal to 5. Higher memory values lead to a large computational complexity due to the resulting high cardinality of channel coefficients. Indeed, for a memory M of the channel which is equivalent to $2M-1$ coefficients, the number of Volterra kernels for a degree i decomposition is $(2M-1)^i$. Thus, it is valuable to find a trade-off between the channel memory and the approximation accuracy. It can be noticed that in comparison with the true received symbols, a channel memory of 4 leads

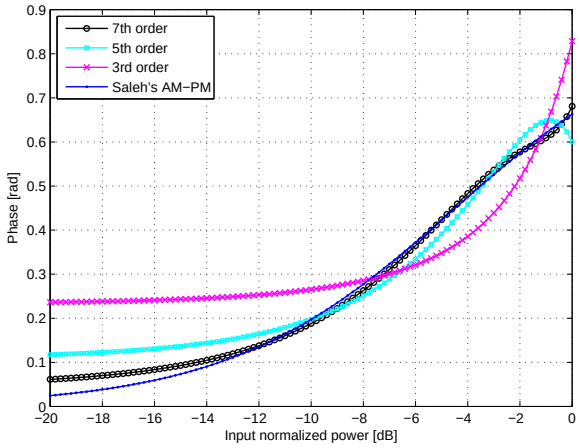

Figure 1.17: Polynomial decomposition for AM-PM Saleh's function

to a fair approximation of the channel output. It should be noted that in practice we only consider a causal representation of the Volterra series which introduces some degradation and only retain coefficients having a value not less than a threshold. Since this truncation introduces a bias in the Volterra decomposition, we could resort to a further Least Mean Square identification to improve the identification of Volterra kernels based on the truncated model. The final decomposition thus writes as:

$$z_n = \sum_{i=0}^{v} \gamma_{2i+1} \sum_{n_1=0}^{M-1} \cdots \sum_{n_{i+1}=0}^{M-1} \sum_{n_{i+2}=0}^{M-1} \cdots \sum_{n_{2i+1}=0}^{M-1} x_{n-n_1} \ldots x_{n-n_{i+1}} x^*_{n-n_{i+2}} \ldots x^*_{n-n_{2i+1}} h^{(i)}(n_1, \ldots n_{2i+1}) \quad (1.24)$$

1.7.4 Volterra decomposition for test channels

Characteristics	Test channel 2
Modulation	16APSK
Roll-off	0.2
Symbol rate	$30Mbauds$
IBO	$1.2dB$
Volterra order	3
Channel memory	3

Table 1.7: Test channels characteristics

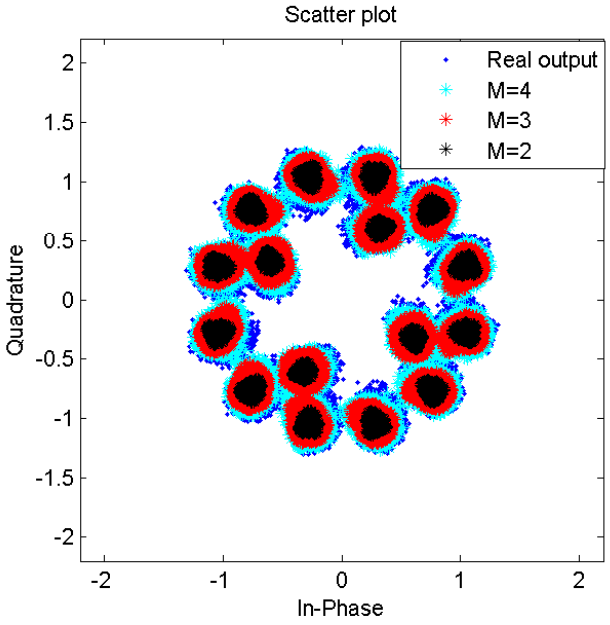

Figure 1.18: Scatterplots of 16APSK with roll-off $\alpha = 0.2$ at $IBO = 3dB$

In this section, we present Volterra decomposition kernels for two test scenarios which will be our benchmark for the remaining of this thesis. The test channel 1 coefficients are excerpted from [Ampeliotis et al., 2008] and consist of a 8PSK modulation with butterworth filters as explained in [Benedetto and Biglieri, 1999]. The test channel 2 is computed using the Volterra decomposition for a 16PASK modulationusing the system configuration in Table 1.7. The obtained Volterra decomposition kernels were fed to a LMS system identifier to reduce the resulting estimation error. Table 1.8 summarizes the obtained kernels. It can be noticed that only $1st$ order and $3rd$ order decomposition kernels are retained. Moreover, for all simulations, we assume perfect receiver synchronisation.

Similarly to the linear channel, we would like to investigate on an equivalent representation in the frequency domain of the non linear Volterra channel. Actually, we can show that such a modelling exists using only mono-dimensional Fourier analysis and this will be discussed in the following section.

Kernels Channel	Test channel 1	Test channel 2
$1st$ order kernels	$h_0 = 0.8529 + 0.4502i$	$h_0 = -0.0802 + 0.9387i$
	$h_1 = 0.0881 - 0.0014i$	$h_1 = -0.0108 + 0.1652i$
	$h_2 = -0.0336 - 0.0196i$	$h_2 = 0.0165 - 0.1500i$
	$h_3 = 0.0503 + 0.0433i$	$h_3 = -0.0126 + 0.1398i$
$3rd$ order kernels	$h^{(3)}_{002} = 0.1091 - 0.0615i$	$h^{(3)}_{001} = -0.0091 - 0.0232i$
	$h^{(3)}_{330} = 3300.0503 - 0.0503i$	$h^{(3)}_{003} = -0.0030 - 0.0108i$
	$h^{(3)}_{001} = 0.0979 - 0.0979i$	$h^{(3)}_{110} = -0.0168 - 0.0453i$
	$h^{(3)}_{003} = -0.1119 - 0.0252i$	$h^{(3)}_{112} = 0.0077 + 0.0271i$
	$h^{(3)}_{110} = -0.0280 - 0.0475i$	$h^{(3)}_{220} = -0.0031 - 0.0088i$
		$h^{(3)}_{221} = 0.0045 + 0.0087i$
		$h^{(3)}_{223} = -0.0016 - 0.0124i$

Table 1.8: Volterra kernels for test channels

1.8 Frequency domain Volterra model

Since the time domain Volterra model consists of linear and non linear combinations of symbols, it is not straightforward to analytically express the Volterra channel in the frequency domain. To do so, we will introduce a set of tools relying on multi-dimensional Fourier analysis, that allow us to represent the non linear channel in the frequency domain.

1.8.1 Multi-dimensional Fourier Transforms

Let $\mathbf{F}$ be the 1-Dimensional Discrete Fourier Transform (1D-DFT) matrix of size N. The matrix element $F_{i,j}$ is:

$$\mathbf{F}_{i,j} = W_N^{-ij} \tag{1.25}$$

where $W_N^k = e^{\frac{\sqrt{-1}2\pi k}{N}}$. We then have $F^H = NF^{-1}$. Let $\mathbf{H}$ a circulant matrix of size $(N \times N)$. It can be diagonalised using the DFT matrix $\mathbf{F}$ and more precisely:

$$\mathbf{H} = \mathbf{F}^{-1}\mathbf{H}\mathbf{F} \tag{1.26}$$

where the notation $\mathbf{H}_d$ stands for the diagonal matrix containing the eigenvalues of $\mathbf{H}$ respectively. We also derive some useful properties which are then going to be used further in this manuscript. Let H and G be two circulant matrices of size $(N \times N)$. A circulant matrix can be diagonalised using the DFT matrix $\mathbf{F}$. More

precisely:

$$H = \mathbf{F}^{-1} H_d \mathbf{F} \qquad (1.27)$$
$$G = \mathbf{F}^{-1} G_d \mathbf{F}$$

where the notation $\mathbf{H}_d$ and $\mathbf{G}_d$ stands for the diagonal matrix containing the eigenvalues of $\mathbf{H}$ and $\mathbf{G}$ respectively. $\mathbf{H}$ and $\mathbf{G}$ satisfy the following properties:

1. $\mathbf{HG}$ is a circulant matrix and $HG = \mathbf{F}^{-1}\mathbf{H}_d\mathbf{G}_d\mathbf{F}$.

2. $\mathbf{H}^H$ is a circulant matrix $H^H = \mathbf{F}^{-1}\mathbf{H}_d^H\mathbf{F}$.

3. $\mathbf{H}^{-1}$ is a circulant matrix and $H^{-1} = \mathbf{F}^{-1}\mathbf{H}_d^{-1}\mathbf{F}$.

4. $\forall (n,m) \in \{0,\dots,N-1\}^2, \quad \mathbf{u}_m^T \mathbf{H} \mathbf{u}_m = \mathbf{u}_n^T \mathbf{H} \mathbf{u}_n \quad$ where $\mathbf{u}_m = [\mathbf{0}_m \; 1 \; \mathbf{0}_{N-m-1}]^T$

In order to understand the behaviour of a non linear channel in the frequency domain, we shall present a glimpse on mono and multi-dimensional circular convolution. By definition, the N-3D normalised DFT of 3D symbols $y^{(3)}_{m,n,l}$ for $m,n,l \in \{0,\dots,N-1\}$ is:

$$Y^{(3)}_{p,q,r} \triangleq \sum_{m=0}^{N-1}\sum_{n=0}^{N-1}\sum_{l=0}^{N-1} y^{(3)}_{m,n,l} W_N^{-mp} W_N^{-nq} W_N^{-lr} \qquad (1.28)$$

Similarly, the N-3D normalised IDFT of 3D frequency symbols $Y^{(3)}_{p,q,r}$ writes as follows:

$$y^{(3)}_{m,n,l} \triangleq \frac{1}{N^3} \sum_{p=0}^{N-1}\sum_{q=0}^{N-1}\sum_{r=0}^{N-1} Y^{(3)}_{p,q,r} W_N^{mp} W_N^{nq} W_N^{lr} \qquad (1.29)$$

1.8.2 Frequency domain Volterra model

Let us consider the scheme depicted in Figure 1.19. In order to be able to characterise the non linear channel in the frequency domain, the proposed system uses a cyclic prefix. For a linear channel, using a cyclic prefix which length is chosen greater or equal to the channel memory, circularises the channel matrix, and the resulting system can be efficiently described in the frequency domain as a scalar multiplication instead of the linear convolution in the time domain. For non linear channels, using a cyclic prefix leads to the so-called multi-dimensional circular convolution. To illustrate the non linear channel behaviour with CP, let us consider

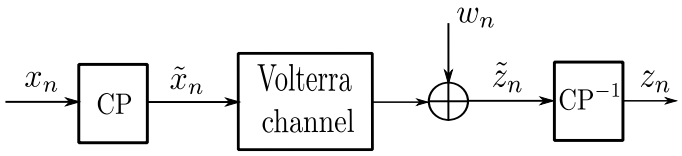

Figure 1.19: System model description in the frequency domain

blocks of N transmitted symbols which are cyclically shifted by the insertion of a cyclic prefix of length equal to the channel memory M and sent through the Volterra channel in (1.24). The received symbols thus write for:

$$\tilde{z}_n = \sum_{i=0}^{M-1} h_i \tilde{x}_{n-i} + \sum_{i=0}^{M-1}\sum_{j=0}^{M-1}\sum_{k=0}^{M-1} h_{ijk}\tilde{x}_{n-i}\tilde{x}_{n-j}\tilde{x}^*_{n-k} + w_n \tag{1.30}$$

After removing the cyclic prefix, the received samples in (1.30) can be expressed for $n \in [0, \ldots, N-1]$ as follows:

$$\begin{aligned} z_n &= \sum_{i=0}^{M-1} h_i x_{<n-i>_N} + \sum_{i=0}^{M-1}\sum_{j=0}^{M-1}\sum_{k=0}^{M-1} h_{ijk} x_{<n-i>_N} x_{<n-j>_N} x^*_{<n-k>_N} + w_n \\ &\triangleq z^{(1)}_n + z^{(3)}_{n,n,n} + w_n \end{aligned} \tag{1.31}$$

The RHS of (1.31) consists of a sum of both a circular convolution $z^{(1)}_n$ and a third order circular convolution $z^{(3)}_{n,n,n}$ expressed as follows:

$$\begin{aligned} z^{(1)}_n &= \sum_{i=0}^{M-1} h_i x_{(n-i)_N} \\ z^{(3)}_{m,n,l} &= \sum_{i=0}^{M-1}\sum_{j=0}^{M-1}\sum_{k=0}^{M-1} h_{ijk} x_{<m-i>_N} x_{<n-j>_N} x^*_{<l-k>_N} \end{aligned} \tag{1.32}$$

In the frequency domain, the 1D-DFT of the circular convolution in (1.32) translates into an element-wise multiplication of the 1D-DFT linear filter coefficients and the 1D-DFT of symbols x_n as follows:

$$Z^{(1)}_m = \mathbf{H}_d(m) X_m \tag{1.33}$$

where $0 \leq m \leq N-1$. For general values of (m, n, r), it can be shown that the 3D-DFT of $z_{m,n,l}$ is [Im and Powers, 1996]:

$$\begin{aligned} Z^{(3)}_{p,q,r} &\triangleq \sum_{m=0}^{N-1}\sum_{n=0}^{N-1}\sum_{l=0}^{N-1} z^{(3)}_{m,n,l} W_N^{-mp} W_N^{-nq} W_N^{-lr} \\ &= \sum_{m=0}^{N-1}\sum_{n=0}^{N-1}\sum_{l=0}^{N-1}\sum_{i=0}^{M-1}\sum_{j=0}^{M-1}\sum_{k=0}^{M-1} h^{(3)}_{i,j,k} x_{<m-i>_M} x_{<n-j>_M} x^*_{<l-k>_M} W_N^{-mp} W_N^{-nq} W_N^{-lr} \end{aligned}$$

$$= \mathbf{H}^{(3)}_{p,q,r} X_p X_q \overline{X}_r \tag{1.34}$$

where $\overline{X}$ is the N 1D-DFT of conjugate symbols x^*_n and $\mathbf{H}^{(3)}_{p,q,r}$ are the N-3D-DFT of 3^{rd} order Volterra kernels $h_{i,j,k}$. Equivalently for $m = n = l$, the time domain symbols $z^{(3)}_{n,n,n}$ can be expressed as:

$$\begin{aligned} z^{(3)}_{n,n,n} &= \frac{1}{N^3} \sum_{p=0}^{N-1} \sum_{q=0}^{N-1} \sum_{r=0}^{N-1} Z^{(3)}_{p,q,r} W_N^{n(p+q+r)} \qquad (1.35) \\ &= \frac{1}{N^3} \sum_{\alpha=0}^{3(N-1)} \sum_{p+q+r=\alpha} \mathbf{H}^{(3)}_{p,q,r} X_p X_q \overline{X}_r W_N^{n\alpha} \\ &= \frac{1}{N^3} \sum_{\alpha=0}^{N-1} W_N^{n\alpha} \Big[\sum_{p+q+r=\alpha} \mathbf{H}^{(3)}_{p,q,r} X_p X_q \overline{X}_r + \sum_{p+q+r=\alpha+N} \mathbf{H}^{(3)}_{p,q,r} X_p X_q \overline{X}_r + \sum_{p+q+r=\alpha+2N} \mathbf{H}^{(3)}_{p,q,r} X_p X_q \overline{X}_r \Big] \\ &= \frac{1}{N^3} \sum_{\alpha=0}^{N-1} W_N^{n\alpha} \sum_{p=0}^{N-1} \sum_{q=0}^{N-1} \sum_{r=0}^{N-1} \mathbf{H}^{(3)}_{p,q,r} X_p X_q \overline{X}_r \delta_N(p+q+r-\alpha) \end{aligned}$$

where the delta-function modulo N is defined as follows:

$$\delta_N(m) = 1 \; if \; < m >_N = 0 \tag{1.36}$$

Equation (1.36) shows that $z^{(3)}_{n,n,n}$ is the mono-dimensional N-1D-IDFT of a combination of N-3D-DFT Volterra kernels. The non linear interference can thus be projected on a 1D-DFT instead of a 3D-DFT. The m^{th} N-1D-DFT output of the received symbols can thus be written as follows:

$$Z_m = \mathbf{H}_d(m) X_m + \frac{1}{N^2} \sum_{p=0}^{N-1} \sum_{q=0}^{N-1} \sum_{r=0}^{N-1} \mathbf{H}^{(3)}_{p,q,r} X_p X_q \overline{X}_r \delta_N(p+q+r-m) + W_m \tag{1.37}$$

It should be noted, that triplets (p, q, r) satisfying $\delta_N(p+q+r-m) = 1$ are disjoint for different frequency indexes m. Thus we are able to characterise the non linear Volterra channel in the frequency domain using only 1D Fourier analysis. However, the frequency domain model requires computations of triple sums over N elements which will constitute a dramatic complexity increase. We will show later in this manuscript how to overcome this limitation.

1.9 Conclusion

In this chapter, we presented a satellite system description which consists the core of our study. A special focus was given to the satellite transponder which contains the satellite amplifier. We showed that for the considered DVB-S and DVB-S2 technologies we are considering, the presence of this power amplifier yields to major

limitations. Indeed, increasing the spectral efficiency using the modulations proposed in the DVB-S2 standard is limited due to the non linear effects of the HPA. We studied the impact of different system parameters on the amount of distortions generated by this power amplifier. In the sake of representing these distortions, we presented a symbol-based formalism for non linear channels based on Volterra decomposition. Moreover, we discussed the design of the Volterra decomposition kernels and evaluated the impact of some parameters on the accuracy and the complexity of this decomposition. Besides, for study purposes, we derived the Volterra decomposition of two test channels which will constitute reference scenarios later in this manuscript. Furthermore, we investigated the expression of the Volterra series decomposition in the frequency domain which will allow us to derive frequency-based compensation methods for the non linear channel distortions.

1.10 Conclusion (french)

Dans ce chapitre, nous avons décrit le système satellite qui fera l'objet de notre étude. Nous avons porté notre attention sur le transpondeur du satellite qui contient l'amplificateur de puissance. Nous avons montré que pour les technologies que nous considérons, DVB-S et DVB-S2, la présence de l'amplificateur de puissance entrainait certaines limitations. En effet, l'augmentation de l'efficacité spectrale en utilisant des modulations telles que celles proposées dans le standard DVB-S2, entrainent des effets nonlinéaires dus aux amplificateurs. Nous avons étudié l'impact de différents paramètres du système sur l'intensité des distorsions générées par ces amplificateurs. De plus, nous avons présenté quelques éléments sur le calcul des coefficients de Volterra, et étudié les paramètres qui influent sur la précision et la complexité de cette décomposition. Par ailleurs, et à des fins d'évaluation, nous avons dérivé la décomposition de Volterra pour deux canaux de test qui feront office de scénarios de référence lors des tests effectués plus tard dans le manuscrit. Finalement, nous avons étudié l'expression de la décomposition de Volterra dans le domaine fréquentiel, ce qui va nous permettre de dériver plus tard des méthodes fréquentielles de compensation des nonlinéarités du canal satellite.

Chapter 2

Mitigation of non linear satellite channels interference

Contents

2.1 Introduction

In the previous chapter, we studied the impact of non linear amplifiers on the received symbols and presented the Volterra symbol-based decomposition of the underlying channel. In order to mitigate the linear and non linear interference caused by the satellite non linear amplifiers, several techniques can be considered. As the choice of equalizers is usually driven by the trade-off between complexity and performance, we investigate on different implementations of the satellite channel mitigation techniques. Similarly to linear channels, non linear channel equalization can be classified into linear and non linear processing. If linear equalizers usually involve less computational complexity, they are generally less efficient when compared to non linear equalizers. A reduction in the complexity can be further achieved for linear equalizers by using the frequency domain model of the non linear channel. In this chapter, non iterative linear and non linear equalizers for the non linear channel are investigated and novel results are presented. The computational complexity and error performance of all versions of the non linear satellite channel equalizers are then compared in terms of the achievable complexity/performance trade-off.

2.2 Introduction (French)

Dans le chapitre précédent, nous avons étudié l'impact des amplificateurs nonlinéaires sur les symboles reçus, et présenté un formalisme symbole basé sur la décomposition de Volterra du canal sous-jacent. Afin de compenser les non linéaires causées par l'amplificateur, plusieurs méthodes peuvent être envisagées. Outre les méthodes dites de pré-compensation localisées au sein de l'émetteur, nous nous intéresserons plus particulièrement aux techniques en réception. Comme le choix de l'égaliseur est souvent régi par le compromis complexité-performance, nous étudierons différentes implémentations d'égaliseurs du canal non linéaire satellite. A l'instar des canaux linéaires, les techniques d'égalisation pour les canaux non linéaires sont classées en méthodes linéaires et non linéaires. Si les égaliseurs linéaires ont généralement une faible complexité calculatoire, ils sont souvent moins performants comparés aux égaliseurs non linéaires parmi lesquels nous pouvons citer les égaliseurs optimaux. Si de plus, nous utilisons des égaliseurs fréquentiels, la complexité peut être d'avantage réduite. Dans ce chapitre, nous étudions des égaliseurs non itératifs linéaires et non linéaires pour le canal satellite. La complexité calculatoire des différentes implémentations des égaliseurs du canal satellite est présentée afin de permettre une comparaison équitable.

2.3 Optimal time domain equalization

In this section, we are interested in optimal time domain detection. As for the linear ISI channel, the non linear ISI channel can be represented by a Markov chain, which allows for the derivation of optimal detection. It is thus interesting to investigate on processing techniques that exploit the known structure of the non linear interference, and this will be presented in the following section.

2.3.1 Trellis based structure of the non linear channel

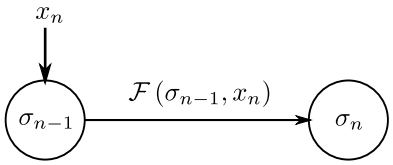

Figure 2.1: Trellis representation of the non linear channel

Let z_n be the received symbol at time n. For practical considerations, we will derive analytical expression of equalizers based on a third order truncation of the satellite channel which yields the received symbols of (1.30):

$$z_n = \sum_{i=0}^{M-1} h_i x_{n-i} + \sum_{i=0}^{M-1}\sum_{j=0}^{M-1}\sum_{k=0}^{M-1} h_{ijk} x_{n-i} x_{n-j} x_{n-k}^* + w_n \tag{2.1}$$

Although the channel output is a non linear combination of time domain symbols x_n, the channel model still can be considered as a finite state machine, relating a set of past symbols x_{n-i} where $i \in \mathcal{I} = \{1, \ldots, M-1\}$ in association with a current symbol x_n to an observed output value y_n writing as:

$$\begin{aligned} y_n &= \sum_{i=0}^{M-1} h_i x_{n-i} + \sum_{i=0}^{M-1}\sum_{j=0}^{M-1}\sum_{k=0}^{M-1} h_{ijk} x_{n-i} x_{n-j} x_{n-k}^* \\ &= \mathcal{F}\left((x_{n-i})_{i\in\mathcal{I}}, x_n\right) \end{aligned} \tag{2.2}$$

where $\mathcal{F}$ is the observation output for each transition in the state machine. By defining the memory state at time n as $\sigma_{n-1} = \{(x_{n-i})_{i\in\{1,\ldots,M-1\}}\}$, then the new memory state σ_n is fully defined given the couple (σ_{n-1}, x_n) and the corresponding channel observation is $\mathcal{F}(\sigma_{n-1}, x_n)$, or equivalently $\mathcal{F}(\sigma_{n-1}, \sigma_n)$. Figure 2.1 depicts the structure of the non linear channel trellis. Based on this structure we will derive the corresponding optimal symbol and sequence based equalizers in the following subsections.

2.3.2 Symbol based detection: MAP

Let us first start with the optimal symbol-based detection known as the Maximum A Posteriori (MAP) equalizer. The MAP criterion consists of maximising the probability for a symbol x_n to be transmitted, given a length N observed sequence $\mathbf{z} = [z_0, \ldots, z_{N-1}]$. We remind that given the notations in (2.2), a received symbol z_n writes as $z_n = y_n + w_n$, where w_n is the noise sample. The MAP solution writes as:

$$\begin{aligned} \hat{x}_n &= \arg\max_{\tilde{x}} P\left(x_n = \tilde{x}|\mathbf{z}\right) \\ &\propto \arg\max_{\tilde{x}} P\left(x_n = \tilde{x}; \mathbf{z}\right) \\ &\propto \arg\max_{s,s' \in \mathcal{S}_{\tilde{x}}} \sum_{s,s' \in \mathcal{S}_{\tilde{x}}} P\left(\sigma_{n-1} = s, \sigma_n = s', \mathbf{z}\right) \end{aligned} \tag{2.3}$$

where $\mathcal{S}_{\tilde{x}}$ designates the set of states (σ_{n-1}, σ_n) where the input was the symbol $\tilde{x}$. An efficient implementation of the MAP equalizer can be realized by the Bahl, Cocke, Jelinek and Raviv (BCJR) algorithm [Bahl et al., 1974]. It relies on the Markov chain structure of the general ISI channel and can be decomposed into three metrics as shown in the following:

$$\begin{aligned} \hat{x}_n &= \arg\max_{s,s' \in \mathcal{S}_{\tilde{x}}} \sum_{s,s' \in \mathcal{S}_{\tilde{x}}} P\left(\sigma_{n-1} = s, \sigma_n = s', \mathbf{z}\right) \\ &= \arg\max_{s,s' \in \mathcal{S}_{\tilde{x}}} \sum_{s,s' \in \mathcal{S}_{\tilde{x}}} P\left(\sigma_{n-1} = s, \sigma_n = s', (z_0, \ldots, z_{n-1}), z_n, (z_{n+1}, \ldots, z_{N-1})\right) \\ &= \arg\max_{s,s' \in \mathcal{S}_{\tilde{x}}} \sum_{s,s' \in \mathcal{S}_{\tilde{x}}} \underbrace{P\left(\sigma_{n-1} = s, z_0, \ldots, z_{n-1}\right)}_{\alpha_n(s)} \underbrace{P\left(z_n, \sigma_n = s' | \sigma_{n-1} = s\right)}_{\gamma_n(s,s')} \underbrace{P\left(z_{n+1}, \ldots, z_{N-1} | \sigma_n = s'\right)}_{\beta_n(s')} \\ &= \arg\max_{s,s' \in \mathcal{S}_{\tilde{x}}} \sum_{s,s' \in \mathcal{S}_{\tilde{x}}} \alpha_n(s)\gamma_n(s,s')\beta_n(s') \end{aligned} \tag{2.4}$$

The forward metric $\alpha_n(s)$, the backward metric $\beta_n(s')$ and the branch transition metric $\gamma_n(s,s')$ can be computed in a recursive form as follows: $\forall (s,s') \in \mathcal{S}_{\tilde{x}}^2$

$$\begin{aligned} \alpha_n(s) &= \sum_{s' \in \mathcal{S}_{\tilde{x}}} \alpha_{n-1}(s')\gamma_{n-1}(s,s') \\ \beta_n(s) &= \sum_{s' \in \mathcal{S}_{\tilde{x}}} \beta_{n+1}(s')\gamma_n(s',s) \\ \gamma_n(s,s') &\propto \exp\left(\frac{-|z_n - \mathcal{F}(s,s')|^2}{\sigma_w^2}\right) P(x_n = \tilde{x}) \end{aligned} \tag{2.5}$$

$\mathcal{F}(s,s')$ is the output of the non linear Volterra channel for an initial state s with input symbol $\tilde{x}$ and $P(x_n = \tilde{x}) = \frac{1}{\mathcal{M}}$ which is a consequence of the independence and equal distribution of the transmitted symbols x_n.

2.3.3 Sequence based detection: MLSE

In this section we investigate on another optimal detection technique over ISI channels, which is sequence-optimal and is based on the Maximum Likelihood Sequence Equalization (MLSE). For a length N observed sequence $\mathbf{z} = [z_0 \dots z_{N-1}]$, the MLSE sequence $\hat{\mathbf{x}} = [\hat{x}_0, \dots \hat{x}_{N-1}]$ maximises the likelihood between the transmitted sequence and the noisy observed sequence. The MLSE thus writes as:

$$\begin{aligned}
\hat{\mathbf{x}} &= \arg\max_{\tilde{\mathbf{x}}} P(\mathbf{z}|\tilde{\mathbf{x}}) \\
&= \arg\max_{\tilde{\mathbf{x}}} \prod_{n=0}^{N-1} P(z_n|\tilde{\mathbf{x}}) \\
&= \arg\max_{\tilde{\mathbf{x}}} \prod_{n=0}^{N-1} \exp\left(-\frac{|z_n - \mathcal{F}((\tilde{x}_{n-i})_{i\in\mathcal{I}}, \tilde{x}_n)|^2}{\sigma_w^2}\right) \\
&= \arg\min_{\tilde{\mathbf{x}}} \sum_{n=0}^{N-1} |z_n - \mathcal{F}((\tilde{x}_{n-i})_{i\in\mathcal{I}}, \tilde{x}_n)|^2
\end{aligned} \tag{2.6}$$

The optimization over transmitted symbols $\tilde{x}_n$, can be equivalently carried out on the set of states σ_n since there is a total correspondence between the set of transmitted symbols and the set of channel states. As such, we can write the MLSE solution as:

$$\hat{\mathbf{x}} = \arg\min_{\sigma_0,\dots\sigma_{N-1}} \sum_{n=0}^{N-1} |z_n - \mathcal{F}(\sigma_{n-1}, \sigma_n)|^2 \tag{2.7}$$

The Viterbi algorithm [Viterbi, 1967] is one of the efficient implementations of the MLSE in the sense, that it uses the structure of the trellis to cumulate the sum of Euclidean distances over the trellis branches, and thus selects the branch having the smallest distance for the following branch metrics computation. In other words, let us define the two following quantities for a branch at time n with a state σ_n:

$$\begin{aligned}
\Lambda_n(\sigma_n) &= \arg\min_{\sigma_0,\dots\sigma_n} \sum_{k=0}^{n} |z_k - \mathcal{F}(\sigma_{k-1}, \sigma_k)|^2 \\
\lambda_n(\sigma_{n-1}, \sigma_n) &= |z_n - \mathcal{F}(\sigma_{n-1}, \sigma_n)|^2
\end{aligned} \tag{2.8}$$

Then it can be shown that the cumulated Viterbi metric at time n of state σ_n, $\Lambda_n(\sigma_n)$, writes as a function of the past cumulated metrics as follows:

$$\Lambda_n(\sigma_n) = \arg\min_{\sigma_{n-1}\to\sigma_n} \Lambda_{n-1}(\sigma_{n-1}) + \lambda_n(\sigma_{n-1}, \sigma_n) \tag{2.9}$$

where $\sigma_{n-1} \to \sigma_n$ stands for the possible transitions from σ_{n-1} to σ_n. It can be noted that by means of Bayes rule, the MLSE is strictly equivalent to the MAP criterion when the input symbols are independent and equally

likely. Non linear optimal equalization techniques achieve the best processing performance but unfortunately suffer from a large computational complexity, since the number of states in a trellis grows exponentially in the channel memory. Indeed, for each section of the trellis, there are $M^{\mathcal{M}}$ states involved in the branch metrics, where M is the channel memory and $\mathcal{M}$ is the constellation size. This urges to investigate on alternative sub-optimal equalization schemes which are discussed in the following sections.

2.4 Linear time domain equalization

In this section, we are interested in time domain linear Finite Impulse Response (FIR) equalizers. The motivation behind using linear equalizers for a non linear channel stems from their low computational complexity yet with sub-optimal performance. Let us consider the Volterra channel defined in (1.30).

As far as Zero Forcing equalization is concerned, Schetzen in [Schetzen, 1976] has derived the p-th inverse Volterra series. Under constraints on the minimal phase of the linear part of the Volterra channel, the p^{th} order inverse forces to zero all Volterra terms not larger than p. The impact on the terms of order higher than p depends on the characteristics of the Volterra decomposition.

In our study, we are interested in the linear equalizer based on Minimum Mean Square Error (MMSE) equalization. Authors in [Krall et al., 2008] have presented a framework for linear MMSE equalization over nonlinear second order Volterra models. The performance of the designed equalizers was then compared to Least Mean Square adaptive equalization. In this section, we will derive general MMSE solutions for the Volterra channel model with no special restrictions on the decomposition order. The linear MMSE estimated symbols [Poor, 1994] are affine transformations of the received symbols. Let us consider the MMSE solution $\mathbf{a}$ consisting of $N = N_1 + N_2 + 1$ elements where N_1 is the symbols post-cursor length and N_2 is the symbols precursor. The estimated symbols write then as follows:

$$\hat{x}_n = \sum_{i=-N_2}^{N_1} a_i z_{n-i} + b \tag{2.10}$$

For ease of notation, let us consider the vectorial representation of the non linear channel in (1.20). To do so, we define the following vectors:

$$\begin{aligned} \mathbf{z}_n &\triangleq [z_{n-N_1}, \ldots, z_{n+N_2}]^T \\ \mathbf{x}_n &\triangleq [x_{n-N_1-M+1}, \ldots, x_{n+N_2}]^T \\ \mathbf{w}_n &\triangleq [w_{n-N_1}, \ldots, w_{n+N_2}]^T \end{aligned}$$

where $\mathbf{z}_n$, $\mathbf{x}_n$ and $\mathbf{w}_n$ are the vectorial representation of the received symbols, the transmitted symbols and noise respectively. Let us also define the channel matrices, $\mathbf{H}$ representing the linear interference and $\mathbf{H}_{ijk}$ representing the non linear interference as:

$$\mathbf{H} \triangleq \begin{pmatrix} h_{M-1} & \dots & h_0 & 0 & \dots & 0 \\ 0 & h_{M-1} & \dots & h_0 & 0 & 0 \\ \vdots & \ddots & & & \dots & \vdots \\ 0 & \dots & 0 & h_{M-1} & \dots & h_0 \end{pmatrix} \tag{2.11}$$

and

$$\mathbf{H}_{ijk} \triangleq \begin{pmatrix} h_{i,j,k} & 0 & \dots & 0 \\ 0 & h_{i,j,k} & 0 & 0 \\ 0 & 0 & \ddots & 0 \\ 0 & \dots & 0 & h_{i,j,k} \end{pmatrix}$$

where $\mathbf{H}$ is a linear convolution Toeplitz matrix, and $\mathbf{H}_{ijk}$ are diagonal matrices containing on their diagonal the same value h_{ijk}. Let us also define the corresponding non linear interfering symbols $\mathbf{x}_n^{ijk}$ which write as:

$$\mathbf{x}_n^{ijk} \triangleq \begin{bmatrix} x_{n-N_1-i}x_{n-N_1-j}x^*_{n-N_1-k} \\ \vdots \\ x_{n+N_2-i}x_{n+N_2-j}x^*_{n+N_2-k} \end{bmatrix}$$

It follows that the received symbol vector of size N writes as follows:

$$\mathbf{z}_n = \mathbf{H}\mathbf{x}_n + \sum_{i=0}^{M-1}\sum_{j=0}^{M-1}\sum_{k=0}^{M-1} \mathbf{H}_{ijk}\mathbf{x}_n^{ijk} + \mathbf{w}_n$$

The linear estimated MMSE symbols $\hat{x}_n$ write for a linear MMSE equalizer as:

$$\hat{x}_n = \mathbf{a}\mathbf{z}_n + b \tag{2.12}$$

where $\mathbf{a} = [a_{N_1}, \dots, a_{N_2}]$ is the MMSE solution filter which along with the constant b need to minimize the mean square of the estimation error as follows:

$$(\mathbf{a}, b) = \arg\min_{\mathbf{a},b} E[|\hat{x}_n - x_n|^2] \tag{2.13}$$

By deriving the Jacobian $J(\mathbf{a}, b)$ of the MMSE of the estimated symbols, we can write:

$$J(\mathbf{a}, b) = E[|\hat{x}_n - x_n|^2] \quad = \quad E[(\hat{x}_n - x_n)(\hat{x}_n - x_n)^*]$$

$$\begin{aligned} &= \mathbf{a}E[\mathbf{z_n}\mathbf{z_n}^H]\mathbf{a}^H + \mathbf{a}b^*E[\mathbf{z}_n] + bE[\mathbf{z}_n^H]\mathbf{a}^H + bb^* - \mathbf{a}E[\mathbf{z}_n x_n^*] + bE[x_n^*] \\ &\quad -E[x_n\mathbf{z}_n^H]\mathbf{a}^H - b^*E[x_n] + E[x_n x_n^*] \end{aligned} \tag{2.14}$$

To find the optimal MMSE solution $(\mathbf{a}, b)$, the derivatives of the MMSE with respect to $\mathbf{a}$ and b need to be computed which can be done using the complex derivation properties in [Haykin, 2008]. The derivatives of the MMSE write then as follows:

$$\begin{aligned} \frac{\partial J(\mathbf{a},b)}{\partial \mathbf{a}} &= \mathbf{a}E[\mathbf{z}_n\mathbf{z}_n] + bE[\mathbf{z}_n^H] - E[x_n\mathbf{z}_n^H] \\ \frac{\partial J(\mathbf{a},b)}{b} &= \mathbf{a}E[\mathbf{z}_n] + b + E[x_n] \end{aligned} \tag{2.15}$$

Setting these derivatives to zero, yields to the well-known MMSE solution:

$$\begin{aligned} \mathbf{a} &= Cov(x_n, \mathbf{z}_n)Cov(\mathbf{z}_n, \mathbf{z}_n)^{-1} \\ b &= -aE[\mathbf{z}_n] - E[x_n] \end{aligned} \tag{2.16}$$

where we used the covariance operator defined as $Cov(X,Y) \triangleq E[XY^H] - E[X]E[Y^H]$ and $(.)^H$ being the Hermitian operator. In order to compute the MMSE solution, we need to investigate on the high order moments of non linear interference symbols. Indeed, as far as first order terms are concerned, the expectation of symbols vector $E[\mathbf{z}_n]$ writes as the sum of the linear and non linear interference terms expectations:

$$E[\mathbf{z}_n] = \mathbf{H}E[\mathbf{x}_n] + \sum_{i=0}^{M-1}\sum_{j=0}^{M-1}\sum_{k=0}^{M-1}\mathbf{H}_{ijk}E[\mathbf{x}_n^{ijk}] \tag{2.17}$$

Equation (2.17) involves the linear symbols expectations which for zero-mean symbols is equal to 0, and non linear symbols expectations. Since non linear symbols expectations include product of symbols which might have the same indexes, it is not straightforward how their expectations write. It should be noted that two simplifications are needed to efficiently compute these expectations and they are:

- Assumption 1: The symbols have constant or quasi-constant modulus (PSK and APSK modulation) and are independent.
- Assumption 2: The Volterra system is in its reduced form where symmetries discussed in Section 1.7.4 have already been used to eliminate triplets (i,j,k) in the form $i = k$ or $j = k$.

Under these conditions, it has been shown in [Ampeliotis et al., 2008] that the expectation of first order symbols writes as:

$$E[\mathbf{x}_{i,j,k}] = \mathbf{0}_{N\times 1} \tag{2.18}$$

Thus $E[z_n] = 0$ and consequently $b = 0$.

As far as the MMSE filter solution $\mathbf{a}$ is concerned, computing the covariances of linear and non linear symbols requires evaluating moments of x_n up to the power 6 containing a mixture of symbols and symbols conjugates. Authors in [Benedetto et al., 1979], presented a useful formalism that consists of enumerating the number of occurrences of each of the symbols indexes and then, using the independence of symbols, are transforming the moment to products of smaller moments. In other words, the expectation of a product of p symbols and $q-p$ symbol conjugates writes as follows:

$$\begin{aligned} E\left[x_{n-i_1}x_{n-i_2}\dots x_{n-i_p}x^*_{n-i_{p+1}}\dots x^*_{n-i_q}\right] &= \prod_j E\left[x^{v_j}_{n-i_j}\left(x^{*v^*_j}_{n-i_j}\right)\right] \\ &= \prod_j \frac{1}{\mathcal{M}}\sum_{m=1}^{\mathcal{M}} s_m^{v_j}\left(s_m^{*v^*_j}\right) \end{aligned} \tag{2.19}$$

where v_j and v_j^* represent the number of occurrences of symbol x_{n-i_j} and $x^*_{n-i_j}$ in the product average respectively, and $s_m \quad m \in [1\dots\mathcal{M}]$ is the m^{th} constellation symbol. More specifically, applying (2.19), the covariance $Cov(x_{n-i_1}, x_{n-i_2}x_{n-i_3}x^*_{n-i_4})$ writes as:

$$E\left[x_{n-i_1}x^*_{n-i_2}x^*_{n-i_3}x_{n-i_4}\right] = E[|x_n|^2]^2\left(\delta(i_1,i_2)\delta(i_3,i_4) + \delta(i_1,i_3)\delta(i_2,i_4)\right) = 0 \tag{2.20}$$

where the Volterra kernel reduced model in "Assumption 2" yields $\delta(i_3,i_4) = \delta(i_2,i_4) = 0$. Similarly, for the covariances of third order non linear terms writing as $Cov(x_{n-i_1}x_{n-i_2}x^*_{n-i_3}, x_{n-i_4}x_{n-i_5}x^*_{n-i_6})$ is equal to:

$$E\left[x_{n-i_1}x_{n-i_2}x^*_{n-i_3}x^*_{n-i_4}x^*_{n-i_5}x_{n-i_6}\right] = E[|x_n|^2]^3\delta(i_1,i_4)\delta(i_2,i_5)\delta(i_3,i_6) \tag{2.21}$$

The properties in (2.20) and (2.21) allow us thus to write the following covariances:

$$\begin{aligned} &\forall n \quad \forall(i,j,k) \quad E\left[\mathbf{x}_n^{ijk}\right] = \mathbf{0}_{N\times 1} \\ &\forall n \quad \forall(i,j,k) \quad Cov\left(\mathbf{x}_n, \mathbf{x}_n^{ijk}\right) = \mathbb{O}_{N+M\times N} \\ &\forall n \quad \forall(i,j,k) \quad Cov\left(\mathbf{x}_n^{ijk}, \mathbf{x}_n\right) = \mathbb{O}_{N\times N+M} \\ &\forall n \quad \forall(i,j,k) \neq (i',j',k') \quad Cov\left(\mathbf{x}_n^{ijk}, \mathbf{x}_n^{i'j'k'}\right) = \mathbb{O}_{N\times N} \\ &\forall n \quad \forall(i,j,k) \quad Cov\left(\mathbf{x}_n^{ijk}, \mathbf{x}_n^{ijk}\right) = E[|x_n|^2]^3\mathbb{I}_N \end{aligned} \tag{2.22}$$

where $\mathbf{0}_{N\times 1}$ is the size $(N\times 1)$ all-zero vector, and $\mathbb{O}_{N+M\times N}$ is the size $(N+M\times N)$ all zero matrix and $\mathbb{I}_N$ is te identity matrix of size N.

Thus it can be concluded that using the assumptions 1 and 2, the non linear interference is uncorrelated from the linear interference, and each pair of non linear terms are uncorrelated. It should be noted, that these

terms are uncorrelated but not independent since unless they are drawn form a Gaussian distribution the independence is not guaranteed. Based on the properties in (2.22), and assuming $E[|x_n|^2] = 1$ (or ≈ 1 for APSK) the covariance of the received symbols write as:

$$\begin{aligned}
Cov\left(\mathbf{z}_n, x_n\right) &= \mathbf{H}Cov\left(\mathbf{x}_n, x_n\right) + \sum_{i=0}^{M-1}\sum_{j=0}^{M-1}\sum_{k=0}^{M-1}\mathbf{H}_{ijk}Cov\left(\mathbf{x}_n^{ijk}, x_n\right) \\
&= \mathbf{H}\mathbf{u}_n \\
Cov\left(\mathbf{z}_n, \mathbf{z}_n\right) &= \sigma_w^2\mathbb{I}_N + \mathbf{H}Cov\left(\mathbf{x}_n, \mathbf{x}_n\right)\mathbf{H}^H \\
&+ \sum_{i=0}^{M-1}\sum_{j=0}^{M-1}\sum_{k=0}^{M-1}\mathbf{H}_{ijk}Cov\left(\mathbf{x}_n^{ijk}, \mathbf{x}_n\right)\mathbf{H}^H + \sum_{i=0}^{M-1}\sum_{j=0}^{M-1}\sum_{k=0}^{M-1}\mathbf{H}Cov\left(\mathbf{x}_n, \mathbf{x}_n^{ijk}\right)\mathbf{H}_{ijk}^H \\
&+ \sum_{i=0}^{M-1}\sum_{j=0}^{M-1}\sum_{k=0}^{M-1}\sum_{i'=0}^{M-1}\sum_{j'=0}^{M-1}\sum_{k'=0}^{M-1}\mathbf{H}_{ijk}Cov\left(\mathbf{x}_n^{ijk}, \mathbf{x}_n^{i'j'k'}\right)\mathbf{H}_{i'j'k'}^H \\
&= \sigma_w^2\mathbb{I}_N + \sum_{i=0}^{M-1}\sum_{j=0}^{M-1}\sum_{k=0}^{M-1}|h_{i,j,k}|^2\mathbb{I}_N
\end{aligned} \tag{2.23}$$

where $\mathbf{u}_n = [\mathbf{0}_{1\times N_1+M}, 1, \mathbf{0}_{1\times N_2}]^T$. From (2.23), it appears that the non linear interfering terms are equivalent to a Gaussian noise with variance $\sigma_{\tilde{w}}^2 = \sum_{i=0}^{M-1}\sum_{j=0}^{M-1}\sum_{k=0}^{M-1}|h_{i,j,k}|^2$. Thus the MMSE solution of the non linear channel is similar to that of a linear channel with an additive Gaussian noise with complex variance $\sigma_w^2 + \sigma_{\tilde{w}}^2$. The MMSE solution thus writes as:

$$\mathbf{a} = \mathbf{u}_n^T H^H\left(\mathbf{H}\mathbf{H}^H + \left(\sigma_w^2 + \sigma_{\tilde{w}}^2\right)\mathbb{I}_N\right)^{-1} \tag{2.24}$$

Complexity analysis

The computational complexity for a block of L estimated symbols can be decomposed into two parts. On the one hand, the computation of the MMSE solution $\mathbf{a}$, requires the inversion of a $(N \times N)$ Toeplitz matrix which we assume is done with complexity $3N^2$ [Lusicus et al., 1984]. The computation of the MMSE matrix $\left(\mathbf{H}\mathbf{H}^H + \left(\sigma_w^2 + \sigma_{\tilde{w}}^2\right)\mathbb{I}_N\right)$ is done with complexity (MN^2) Complex Multiplies (CM) and $(M-1)N^2 + N$ Complex Adds (CA) given the fact that $\mathbf{H}$ has at most M non zero elements per line/column. On the other hand, the computation of one symbol estimate which is equivalent to linear filtering requires (N) CM and $(N-1)$ CA. Finally, using the fact that 1 complex multiply requires 4 real multiplies and 2 real adds, the total number of operations per block of L symbols is equal to:

$$\begin{aligned}
\text{Real multiplications} &= 4(M+3)N^2 + 4(M+L)N \\
\text{Real adds} &= 2(M+5)N^2 + 4(M+L)N - 2L
\end{aligned} \tag{2.25}$$

The afore-studied linear equalizer, is only able of detecting the interference symbols as noise, and thus yields a coarse processing of the non linear interference. Thus, we are interested in non linear equalization techniques which are classified into adaptive and decision driven techniques.

2.5 Non linear sub-optimal equalization

2.5.1 Non linear adaptive Volterra equalization

In [Benedetto and Biglieri, 1983], a non linear Volterra based equalizer is used to cope with the non linear interference. To do so, a non linear combiner is used to produce non linear functions of the observed symbols. These combinations are linearly filtered to produce estimated symbols which write as follows:

$$\hat{x}_n = \sum_{i=0}^{M-1} c_i z_{n-i} + \sum_i \sum_j \sum_k c_{i,j,k} z_{n-i} z_{n-j} z^*_{n-k} \tag{2.26}$$

As such, writing the equalizer output in a vectorial form yields the following estimated symbols vector:

$$\hat{x}_n = \mathbf{C}\mathbf{z}_n \tag{2.27}$$

where $\mathbf{C} = [c_0, \ldots, c_{N-1}, c_{0,0,0}, \ldots c_{M-1,M-1,M-1}]^T$ is the global processing filter and the combined symbols write as $\mathbf{z}_n = [z_n, \ldots, z_{n-M-1}, z_n z_n z^*_n, \ldots z_{n-M+1} z_{n-M+1} z^*_{n-M+1}]^T$. It can be noticed that the proposed Volterra equalizer in [Benedetto and Biglieri, 1983] processes up to the fifth order received symbols, but we truncated it to a third order equalizer since we are dealing with up to the third order Volterra channel. It is argued in [Benedetto and Biglieri, 1983], that a judicious choice of the equalizer indexes (i, j, k) is to use the same non zero Volterra kernels indexes (i, j, k) in the channel model. The solution $\mathbf{C}$ that minimizes the mean square error of the estimated symbols with the transmitted symbol delayed by a decision time D, $e_n = \hat{x}_n - x_{n-D}$ writes as:

$$\mathbf{C} = Cov(x_{n-D}, \mathbf{z}_n) Cov(\mathbf{z}_n, \mathbf{z}_n)^{-1} \tag{2.28}$$

To simplify the computation of the covariances in (2.28), [Gutierrez and Ryan, 2000] proposed an adaptive implementation of the aforementioned Volterra equalizer where the Volterra coefficients $\mathbf{C}$ are updated following the adaptation:

$$\mathbf{C}(n+1) = \mathbf{C}(n) + \mu e_n \mathbf{z}^*_n \tag{2.29}$$

where μ is the step size, which by experience was chosen equal to a linear equalizer step, i.e. when $\mathbf{C}$ only consists of linear taps. The step size should thus satisfy $0 < \mu < 2/(N\lambda_{max})$ where λ_{max} is the maximum eigenvalue of the tap input linear MMSE equalizer. It should be noted that the proposed adaptive equalizer

relies on the approximation that the non linear combiner outputs are independent, which is actually not accurate but yields acceptable results.

Complexity analysis

Let us compute the complexity of the adaptive implementation of the Volterra equalizer. As in the linear MMSE scenario, we compute the complexity per block of L estimated symbols. Let us consider there are $(\mathcal{I})$ non zero non linear terms. For each estimated symbol, to construct the vector of observations $\mathbf{z}_n$, each non linear Volterra term requires 2 complex multiplies which yields $(2\mathcal{I})$ complex multiplies. The term $\mu e_n \mathbf{z}_n^*$ requires 1 real multiply and 2 complex multiplies per symbol and there are $\mathcal{I}+N$ symbols, which yields $2(\mathcal{I}+N)$ complex multiplies and $(\mathcal{I}+N)$ real multiplies. Then for the update of the equalizer coefficients, $(N+\mathcal{I})$ complex adds are required. Finally the computation of the estimated symbols in (2.27) requires $(\mathcal{I}+N)$ complex multiplies and $(\mathcal{I}+N-1)$ complex adds. The required complexity for the Volterra equalizer writes thus as:

$$\begin{aligned} \text{Real Multiplies} &= 21L\mathcal{I} + 13NL \\ \text{Real Adds} &= 14L\mathcal{I} + 10NL - 2 \end{aligned} \tag{2.30}$$

The computational complexity of the Volterra equalizer scales in $O(LN) + O(\mathcal{I}L)$. It can be noticed that the number of the Volterra coefficients $0 < \mathcal{I} < (M-1)^3$, so the actual complexity can reach $O(LM^3)$.

2.5.2 Decision Feedback Equalization: DFE

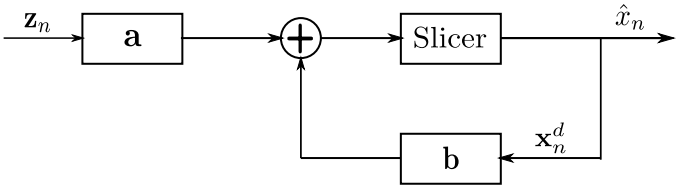

Figure 2.2: DFE with linear feedback

Decision Feedback (DFE) with linear feedback

In this section we are interested in decision directed non linear equalization and more specifically, on Decision Feedback Equalization (DFE). Two implementations are going to be presented, one that consists of a linear

feedback of the estimated symbols and will be denominated as a short DFE, and one that consists of linear and non linear feedback and will be designated by long DFE. Let us start with the first implementation depicted in Figure 2.2 which only uses the feedback of linear past decided symbols [Fisher et al., 1991]. The estimated symbols thus write as:

$$\hat{x}_n = \mathbf{a}\mathbf{z_n} + \mathbf{b}\mathbf{x_n^d} + c \tag{2.31}$$

where $x_n^d = [\hat{x}_{n-N_b}, \ldots, \hat{x}_{n-1}]^T$ stands for the past hard-decided symbols through a symbol slicer. The length of the post-cursor past decided symbols is chosen so as to cope with the channel memory by letting $N_b = M-1$. As for the length of the precursor filter it is meant to process non-causal received symbols $z_n, \ldots, z_{n+N_2}$, which leads to $N_1 = 0$ and $N_2 = N-M-1$ where N is set invariant among different implementations of the non linear equalizers as explained in [Tuchler, 2000]. In a similar fashion to [Tuchler, 2000], by defining the extended vector $[\mathbf{z}_n x_n^d]$, the MMSE solution should satisfy:

$$[\mathbf{a}, \ \mathbf{b}] = \left[Cov(x_n, \mathbf{z_n}), \ Cov(x_n, \mathbf{x_n^d})\right] \begin{pmatrix} Cov(\mathbf{z_n}, \mathbf{z_n}) & Cov(\mathbf{z_n}, \mathbf{x_n^d}) \\ Cov(\mathbf{z_n}, \mathbf{x_n^d})^H & Cov(\mathbf{x_n^d}, \mathbf{x_n^d}) \end{pmatrix}^{-1} \tag{2.32}$$

$$c = -\mathbf{a}E[\mathbf{z}] - \mathbf{b}E[\mathbf{x_n^d}] + E[x_n] \tag{2.33}$$

In order to compute the MMSE-DFE solution, an approximation needs to be made. Indeed, we will assume that the past symbols have been correctly decided i.e. x_n^d are the transmitted symbols. It results that $Cov(x_n, \mathbf{x_n^d}) = \mathbf{0}_{1\times N_b}$. Using the block matrices inversion lemma [1]. The resulting MMSE-DFE solution writes as follows:

$$\begin{aligned} \mathbf{a} &= Cov(x_n, \mathbf{z}_n)\mathbf{R}_n^{-1} \\ \mathbf{b} &= -\mathbf{a}Cov(\mathbf{z_n}, \mathbf{x_n^d})Cov(\mathbf{x_n^d}, \mathbf{x_n^d})^{-1} \\ \mathbf{R}_n &= Cov(\mathbf{z_n}, \mathbf{z_n}) - Cov(\mathbf{z_n}, \mathbf{x_n^d})Cov(\mathbf{x_n^d}, \mathbf{x_n^d})^{-1}Cov(\mathbf{z_n}, \mathbf{x_n^d})^H \end{aligned} \tag{2.35}$$

Taking into account the properties in (2.22), we can compute the MMSE-DFE solution for PSK and APSK modulations. The covariance between the received symbols and the past decided symbols using the assumption that they have been correctly estimated writes as follows:

$$Cov\left(\mathbf{z_n}, \mathbf{x_n^d}\right) = \mathbf{H}\mathbb{I}_{fb}^T \tag{2.36}$$

[1] The block matrix inversion lemma

$$\begin{pmatrix} A & B \\ C & D \end{pmatrix}^{-1} = \begin{pmatrix} (A-BD^{-1}C)^{-1} & -(A-BD^{-1}C)^{-1}BD^{-1} \\ (D-CA^{-1}B)^{-1}CA^{-1} & (D-CA^{-1}B)^{-1} \end{pmatrix} \tag{2.34}$$

where $\mathbb{I}_{fb} = [\mathbb{I}_{N_b \times N_b} \mathbb{O}_{N_b \times N-1}]$ accounts for the fact that the decided symbols only take values in the past indexes $[n - N_b, \ldots, n-1]$. The matrix $\mathbf{R}_n$ can also be simplified using properties in (2.22) as follows:

$$\mathbf{R}_n = \left((\sigma_w^2 + \sum_{i,j,k} |h_{ijk}|^2) \mathbb{I}_N + \mathbf{H} \left(\mathbb{I}_N - \mathbb{I}_{fb}^T \mathbb{I}_{fb} \right) \mathbf{H}^H \right) \tag{2.37}$$

where it can be noted that the resulting matrix:

$$\mathbb{I}_N - \mathbb{I}_{fb}^T \mathbb{I}_{fb} = \begin{pmatrix} \mathbb{O}_{N_b \times N_b} & \mathbb{O}_{N_b \times N-1} \\ \mathbb{O}_{N-1 \times N_b} & \mathbb{I}_{N-1 \times N-1} \end{pmatrix} \tag{2.38}$$

shows the impact of decision feedback which consists of removing the power of the past decided symbols in the computation of the MMSE-DFE solution which thus writes as:

$$\begin{aligned} \mathbf{a} &= \mathbf{u}_n^T \mathbf{H}^H \left((\sigma_w^2 + \sum_{i,j,k} |h_{ijk}|^2) \mathbb{I}_N + \mathbf{H} \left(\mathbb{I}_N - \mathbb{I}_{fb}^T \mathbb{I}_{fb} \right) \mathbf{H}^H \right)^{-1} \\ \mathbf{b} &= -\mathbf{a} \mathbf{H} I_{fb}^T \end{aligned} \tag{2.39}$$

Complexity analysis

The computational complexity of the equalizer coefficients $\mathbf{a}$ is unchanged compared to the linear MMSE complexity. However, the computation of the feedback filter $\mathbf{b}$ adds a complexity of $(N_b M)$ CM and $N_b(M-1)$ CA. An additional complexity equal to (N_b) CM and $(N_b - 1)$ CA which corresponds to the feedback filtering. Thus the overall complexity is:

$$\begin{aligned} \text{Real Multiplies} &= 4(M+3)N^2 + 4(M+L)N + 4(N_b + L)M \\ \text{Real Adds} &= 2(M+5)N^2 + 4(M+L)N - 4L + 2N_b(L + M - 1) \end{aligned} \tag{2.40}$$

The presented short DFE improves the system performance since it relies on cancelling some of the decided symbols, which clearly can enhance the system performance in the high SNR regime. This enhancement can be further increased when designing a decision feedback equalizer which uses also combinations of past decided non linear symbols, which is investigated in the following subsection.

Decision Feedback Equalizer with Non Linear feedback (DFE-NL)

To exploit the non linear structure of the interference, we introduce in addition to the feed-forward and feedback filters $\mathbf{a}$ and $\mathbf{b}$ previously defined in (2.31), non linear channel feedback scalars $c_{i,j,k}$. Each of these scalars

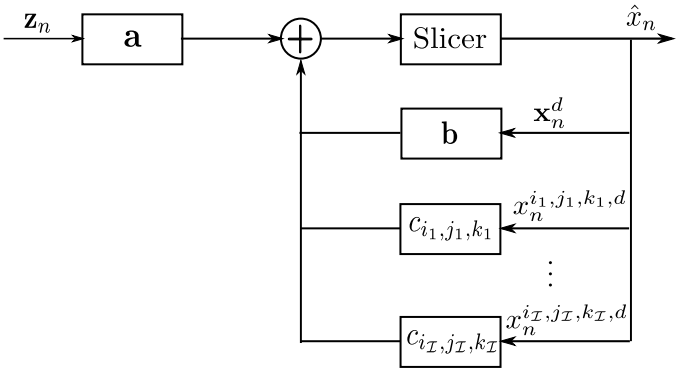

Figure 2.3: DFE with non linear feedback

is associated to a non linear decided interference term $\mathbf{x}_{ijk,d}$. As depicted in Figure 2.3, the MMSE-DFE-NL solution writes as follows:

$$\hat{x}_n = \mathbf{a}\mathbf{z_n} + \mathbf{b}\mathbf{x_n^d} + \sum_{i=1}^{M-1}\sum_{j=1}^{M-1}\sum_{k=1}^{M-1} c_{ijk}x_n^{ijk,d} \tag{2.41}$$

where the non linear decided symbols write as $x_n^{ijk,d} = [\hat{x}_{n-i}\hat{x}_{n-j}\hat{x}^*_{n-k}]$. The summation of third order indexes (i,j,k) starts at 1 since 0 indexes require not decided yet symbols $\hat{x}_n$. For ease of notations, let us consider there are $\mathcal{I}_3$ non zero non linear kernels, $0 \leq \mathcal{I}_3 \leq (M-1)^3$. Let us define the vector of decided non linear symbols $\mathbf{x}_n^{3,d} = [x_n^{i_1,j_1,k_1,d}, \ldots, x_n^{i_{\mathcal{I}_3},j_{\mathcal{I}_3},k_{\mathcal{I}_3},d}]$, the long MMSE-DFE solution writes as follows:

$$\begin{aligned}[\mathbf{a}\ \mathbf{b}\ c_{i_1,j_1,k_1},\ \ldots c_{i_{\mathcal{I}_3},j_{\mathcal{I}_3},k_{\mathcal{I}_3}}] \quad &= \quad \left[Cov(x_n,\mathbf{z_n}),\ \ Cov(x_n,\mathbf{x_n^d}),\ \ Cov(x_n,\mathbf{x}_n^{3,d})\right] \\ &\left(\begin{array}{ccc} Cov(\mathbf{z_n},\mathbf{z_n}) & Cov(\mathbf{z_n},\mathbf{x_n^d}) & Cov(\mathbf{z_n},\mathbf{x}_n^{3,d}) \\ Cov(\mathbf{z_n},\mathbf{x_n^d})^H & Cov(\mathbf{x_n^d},\mathbf{x_n^d}) & Cov(\mathbf{x}_n^d,\mathbf{x}_n^{3,d}) \\ Cov(\mathbf{z_n},\mathbf{x}_n^{3,d})^H & Cov(\mathbf{x_n^d},\mathbf{x}_n^{3,d})^H & Cov(\mathbf{x}_n^{3,d},\mathbf{x}_n^{3,d}) \end{array}\right)^{-1}\end{aligned} \tag{2.42}$$

After tedious calculations, we can show that the long MMSE-DFE solution writes as:

$$\begin{aligned} \mathbf{a} \quad &= \quad \mathbf{u}_n^T\mathbf{H}^H\left(\sigma_w^2\mathbb{I}_N + \sum_{i,j,k}|h_{ijk}|^2(\mathbb{I}_N - \mathbb{I}^{(0)}_{N\times N}) + \mathbf{H}\left(\mathbb{I}_N - \mathbb{I}^T_{fb}\right)\mathbf{H}^H\right)^{-1} \\ \mathbf{b} \quad &= \quad -\mathbf{a}\mathbf{H}\mathbb{I}^T_{fb} \\ \forall(i,j,k)\ c_{i,j,k} \quad &= \quad -\mathbf{a}\mathbf{H}_{i,j,k}\mathbf{u}_0 \end{aligned} \tag{2.43}$$

where $\mathbf{u}_0 = [1,\ \mathbf{0}_{1\times N-1}]^T$ and $\mathbb{I}^{(0)}_{N\times N} = \mathbf{u}_0\mathbf{u}_0^T$. It can be noticed, that the MMSE solutions $c_{i,j,k}$ are equivalent to filtering by $\mathbf{a}$ a reconstructed hard interference $h_{i,j,k}x_n^{i,j,k}$, where in the computation of $\mathbf{a}$, the contribution of this term is cancelled through the matrix $\mathbb{I}_N - \mathbb{I}^{(0)}_{N\times N}$.

Complexity analysis

In addition to the linear feedback DFE complexity, the DFE with non linear feedback has additional complexity due to the cancellation of non linear interference as well. The resulting complexity is increased first by the computation of the solutions $c_{i,j,k}$ which require $(\mathcal{I}_3)$ CM and $(\mathcal{I}_3)$ CA. The subtraction of the estimated non linear interference adds $(3\mathcal{I}_3)$ CM and $(\mathcal{I}_3)$ CA for each estimated symbol. The total number of operations for a block of L estimated symbols writes thus as:

$$\begin{aligned} \text{Real Multiplies} &= 4(M+3)N^2 + 4(M+L)N + 4(N_b+L)M + 16L\mathcal{I}_3 \\ \text{Real Adds} &= 2(M+5)N^2 + 4(M+L)N - 4L + 2N_b(L+M-1) + 18L\mathcal{I}_3 \end{aligned} \tag{2.44}$$

In the MMSE-DFE-NL solution (2.41), we were only able of cancelling the contribution of the post-cursor interference. Indeed, based on past decided symbols we are only able of reconstructing the Volterra interference not containing the current symbol which corresponds to indexes different from 0 for a Volterra kernel $h_{i,j,k}$. For example, among the 7 kernels of the test channel 2 in Table 1.7, only 3 kernels can be used for past decided symbols $h_{1,1,2}$, $h_{2,2,1}$ and $h_{2,2,3}$. Based on this limitation, authors in [Biglieri et al., 1984] proposed an interference canceller using a delay line to compute tentative decisions, which can supply to the need of undecided yet symbols. Tentative decisions are then used as well as decided symbols to construct the post and pre-cursor interference. Authors in [Sands and Cioffi, 1994] have also identified this issue and proposed an alternative to the computation of the feedback which is called multiplying DFE. The considered implementation of the DFE relies on the look-up table or RAM-DFE with a multiplicative processing of the past and received symbols. The principle relies on expressing the transmitted symbols x_n as a linear transformation of the received symbols z_n and past symbols using some approximations on the power of Volterra kernels. The resulting expression is then used to compute an adequate unbiased estimator.

The performance of the different implementations of the DFE equalizer compared to non-decision directed methods are enhanced due to the exploitation of past decided symbols either through linear or non linear processing. However, it is this same advantage which can at low SNR worsen the performance of DFE equalization schemes due to the so-called error propagation. Indeed, under strong noise, the past decisions are more likely to be unreliable, and using a decision directed equalizer will lead to the propagation of estimation errors along the estimation process. A possible alternative to the DFE error propagation is the DFE with noise prediction [Belfiore and Park, 1979] which is equivalent to the standard DFE when the length of the feed-forward filter is infinite. Yet for a finite implementation, it performs worse than the DFE but has the

advantage of yielding lower errors at small SNRs. The principle of the noise predictor equalizer is that the feed-forward and feed-back filters can be optimized separately, which allows them to have independent behaviour and thus limits the error propagation phenomenon.

2.6 Frequency domain equalization

2.6.1 Linear MMSE -FD equalization

In order to decrease the complexity of the linear and non linear equalizer in the time domain, we are interested in this section in the frequency domain implementations of the previously studied linear equalizers. The complexity of a frequency domain equalizer can be reduced thanks to the use of the equivalence between circular convolution in the time domain and DFT multiplication in the frequency domain. The circular (or cyclic) convolution can be realised inserting a cyclic prefix before the Volterra channel and removing it at the entry of the receiver as shown in Figure 1.19. The length of this cyclic prefix needs to account for the whole channel memory, which in our system is assumed to be equal to M. We have shown earlier in (1.37) that the time and resulting frequency domain Volterra channel symbols write as:

$$\begin{aligned} z_n &= \sum_{i=0}^{M-1} h_i x_{<n-i>_N} + \sum_{i=0}^{M-1}\sum_{j=0}^{M-1}\sum_{k=0}^{M-1} h_{ijk} x_{<n-i>_N} x_{<n-j>_N} x^*_{<n-k>_N} + w_n \\ Z_m &= \mathbf{H_d}(m) X_m + \frac{1}{N^2}\sum_{p=0}^{N-1}\sum_{q=0}^{N-1}\sum_{r=0}^{N-1} \mathbf{H}^{(3)}_{p,q,r} X_p X_q \overline{X}_r \delta_N(p+q+r-m) + W_m \end{aligned} \tag{2.45}$$

The frequency domain non linear Volterra channel does not reduce to a scalar multiplication in the frequency domain, since the channel output not only depends on the transmitted frequency X_m but also on a set of past and future symbols X_p, X_q and $\overline{X}_r$. Since the received time domain symbols are obtained by cyclic convolutions of the transmitted symbols with the channel kernels, it seems natural to process these symbols by means of cyclic equalization as well. Hence, the frequency domain detector will consist of scalar symbol by symbol based equalization.

In the time domain there are two ways of designing the equalizer. A circular convolution of the equalizer $\mathbf{a}$ with the received symbols can be envisaged as one of the two following conventions:

- **Convention 1**: A time varying solution $\mathbf{a}_n$ to process a fixed symbol vector $\mathbf{z}_0 \triangleq [z_0, \ldots, z_{N-1}]^T$. In this case, the estimated symbols write as:

$$\hat{x}_n = \sum_{m=0}^{N-1} z_m a_{<n-m>_N} + b = \mathbf{a'}_n \mathbf{z}_0 + b \tag{2.46}$$

The time varying solutions $\mathbf{a'}_n$ are cyclic shifts of the first solution $\mathbf{a'}_0$. The impulse response of the equalizer writes then as $\mathbf{a} = [\mathbf{a'}_0(0)\mathbf{a'}_0(N-1), \ldots, \mathbf{a'}_0(1)]$.

- **Convention 2**: A fixed time solution $\mathbf{a}$ and time varying symbol vectors $\mathbf{z}_n$ which are **cyclic** shifts of the vector $\mathbf{z}_0$. The estimated symbols thus write as:

$$\hat{x}_n = \sum_{m=0}^{N-1} a_m z_{<n-m>_N} + b = \mathbf{a'}\mathbf{z}_n + b \tag{2.47}$$

where the time domain filter is then gain $\mathbf{a} = [a'_0, a'_{N-1}, \ldots, a'_1]$.

To illustrate the derivation of the MMSE-FD solutions, let us introduce the following length N vectors and Fourier transforms:

$$\begin{aligned}
\mathbf{z_0} &= [z_0, \ldots, z_{N-1}]^T \\
\mathbf{x_0} &= [x_0, \ldots, x_{N-1}]^T \\
\mathbf{w_0} &= [w_0, \ldots, w_{N-1}]^T \\
\mathbf{x}_0^{ijk} &\triangleq \begin{bmatrix} x_{<0-i>_N} x_{<0-j>_N} x^*_{<0-k>_N} \\ \vdots \\ x_{<N-1-i>_N} x_{<N-1-j>_N} x^*_{<N-1-k>_N} \end{bmatrix} \\
\mathbf{Z} &= \mathbf{F}\mathbf{z_0} \triangleq [Z_0, \ldots, Z_{N-1}]^T \\
\mathbf{X} &= \mathbf{F}\mathbf{x_0} \triangleq [X_0, \ldots, X_{N-1}]^T \\
\mathbf{W} &= \mathbf{F}\mathbf{w_0} \triangleq [W_0, \ldots, W_{N-1}]^T
\end{aligned} \tag{2.48}$$

For the derivation of the linear MMSE-FD solution, we will use the **convention 1**. Using the afore-defined quantities we can write a compact block representation of the N-output Voterra channel as:

$$\mathbf{z}_0 = \mathbf{H}\mathbf{x}_0 + \sum_{i=0}^{M-1}\sum_{j=0}^{M-1}\sum_{k=0}^{M-1} \mathbf{H}_{ijk}\mathbf{x}_0^{ijk} + \mathbf{w}_0 \tag{2.49}$$

Let us also define the frequency domain MMSE estimates X_m as:

$$\hat{X}_m = A_m Z_m + B_m \tag{2.50}$$

where A_m and B_m are the MMSE coefficients to be optimized such that they minimise the frequency domain estimation error as follows:

$$(A_m, B_m) = \min_{A,B} E[\left|\hat{X}_m - X_m\right|^2] \tag{2.51}$$

The MMSE criterion solution yields the following expression for A_m and B_m:

$$\begin{aligned} A_m &= \frac{Cov(X_m, Z_m)}{Cov(Z_m, Z_m)} \\ B_m &= -A_m E[Z_m] - E[X_m] \end{aligned} \tag{2.52}$$

To compute the MMSE solutions, we need to investigate on the properties of frequency domain transmitted and received symbols. There are actually two different ways of computing moments of the frequency domain symbols. The first one consists of using the Fourier transform definition to compute expectations of products of symbols. The second approach, which we will be presenting in the following consists of using the vectorial time domain properties in (2.22), in order to compute the equivalent frequency domain properties. Using the properties in (2.22), we can first compute the expectation of transmitted and received frequency domain symbols as:

$$\begin{aligned} E[\mathbf{X}] &= FE[\mathbf{x}_0] = \mathbf{0}_{N\times 1} \\ E[\mathbf{Z}] &= FE[\mathbf{z}_0] = \mathbf{0}_{N\times 1} \end{aligned} \tag{2.53}$$

To compute the covariance between transmitted and received symbols we can notice that $Cov(X_m, Z_m)$ can be written as a function of the time domain covariances as follows:

$$\begin{aligned} Cov(X_m, Z_m) &= \mathbf{u}_m^T Cov(\mathbf{X}, \mathbf{Z})\mathbf{u}_m = \mathbf{u}_m^T \mathbf{F} Cov(\mathbf{x}_0, \mathbf{z}_0)\mathbf{F}^H \mathbf{u}_m \\ &= \mathbf{u}_m^T \mathbf{F}\mathbf{H}^H \mathbf{F}^H \mathbf{u}_m = N\mathbf{u}_m^T \mathbf{H}_d^H \mathbf{u}_m \\ &= NH_m^* \end{aligned} \tag{2.54}$$

where we used the m-index vector $\mathbf{u}_m = [\mathbf{0}_{m-1\times 1} 1 \mathbf{0}_{N-m}]^T$. It can be noticed that similarly to the time domain properties, a frequency domain symbol X_m is uncorrelated from the non linear interference appearing in Z_m, i.e. products of X_p, X_q and $\overline{X}_r$ such that $\delta_N(p+q+r-m) = 1$. To compute the covariance of symbols Z_m a similar derivation can be used which yields the following:

$$\begin{aligned} Cov(Z_m, Z_m) &= \mathbf{u}_m^T Cov(\mathbf{Z}, \mathbf{Z})\mathbf{u}_m \\ &= \mathbf{u}_m^T \mathbf{F} Cov(\mathbf{z}_0, \mathbf{z}_0)\mathbf{F}^H \mathbf{u}_m \\ &= \mathbf{u}_m^T \mathbf{F} \left(\mathbf{H}\mathbf{H}^H + \sigma_w^2 \mathbb{I}_N + \sum_{i=0}^{M-1}\sum_{j=0}^{M-1}\sum_{k=0}^{M-1} |h_{i,j,k}|^2 \mathbb{I}_N \right) \mathbf{F}^H \mathbf{u}_m \\ &= \mathbf{u}_m^T \left(\mathbf{H}_d \mathbf{H}_d^H + \sigma_w^2 \mathbb{I}_N + \sum_{i=0}^{M-1}\sum_{j=0}^{M-1}\sum_{k=0}^{M-1} |h_{i,j,k}|^2 \mathbb{I}_N \right) \mathbf{u}_m \end{aligned}$$

$$= N(|H_m|^2 + \sigma_w^2 + \sum_{i=0}^{M-1}\sum_{j=0}^{M-1}\sum_{k=0}^{M-1}|h_{i,j,k}|^2) \quad (2.55)$$

Again it can be noticed that the time domain properties are conserved when going to the frequency domain, and more specifically, the non linear interference is detected as additive white noise with variance $\sigma_{\tilde{w}}^2 = \sum_{i=0}^{M-1}\sum_{j=0}^{M-1}\sum_{k=0}^{M-1}|h_{i,j,k}|^2$. The frequency domain estimated symbols write consequently as:

$$\hat{X}_m = \frac{H_m^*}{|H_m|^2 + \sigma_w^2 + \sigma_{\tilde{w}}^2} Z_m \quad (2.56)$$

Complexity analysis

To provide a fair comparison with the time domain equalizers, we will compute the complexity for a block of L estimated symbols. We assume that a DFT of size L takes $2L\log_2(L)$ real multiplications and $3L\log_2(L)$ real additions. In the MMSE-FD equalization, three (3) Fourier transforms are needed to compute the DFT of symbols $\mathbf{z}_0$, the linear filter coefficients A_m and the IDFT of estimated symbols $\hat{x}$. Each scalar factor A_m requires 4 real adds, and two (2) real multiplies and one reciprocal operation which is neglected. Thus the overall complexity for a block of L estimated symbols is:

$$\begin{aligned} \text{Real Multiplies} &= 6L\log_2(L) + 2L \\ \text{Real Adds} &= 9L\log_2(L) + 4L \end{aligned} \quad (2.57)$$

Since the proposed linear MMSE solution treats the non linear interference as additive noise, the performance of the equalizer will be limited in a similar way to the time domain linear MMSE equalizer. In order to better mitigate the frequency domain non linear interference, we would like to investigate on non linear equalizers and more specifically the Frequency domain implementation of the decision feedback equalizer. Some causality issues arise when using the frequency domain DFE, and this yields us to the following section which investigates on an alternative hybrid frequency-time domain DFE.

2.6.2 Hybrid time and frequency domain DFE

On the causality of the Block DFE

A frequency domain DFE is a special case of block DFE using circular feed-forward filters. More generally, discarding the circular convolution, a block DFE requires processing a length N received symbols vector $\mathbf{z}_0$ as well as block of decided symbols $\hat{\mathbf{x}}$. In other words, the block DFE MMSE solution would write as:

$$\hat{\mathbf{x}} = \mathbf{A}\mathbf{z}_0 + \mathbf{B}\hat{\mathbf{x}} \quad (2.58)$$

It is thus clear that to compute estimated symbols, the block MMSE DFE requires future decisions on these symbols which is unrealisable because of the non causality of the above relationship. Consequently, frequency domain DFE is unrealisable in its original form, i.e. when the feedback decided symbols are treated block-wise.

On the causality of the non linear frequency domain feedback

An additional issue arising when designing frequency domain DFE which this time is inherent to the Volterra model is explained in the following. The expression of the frequency domain channel model in (1.37) suggests that a non linear feedback in the frequency domain DFE would write as an interference canceller i.e.:

$$\hat{X}_m = A_m Z_m + B_m \hat{X}_m + \sum_{p=0}^{N-1}\sum_{q=0}^{N-1}\sum_{r=0}^{N-1} C^{(3)}_{p,q,r}\hat{X}_p\hat{X}_q\overline{\hat{X}}_r\delta_N(p+q+r-m) \tag{2.59}$$

Unfortunately for each $m \in \{0,\ldots,N-1\}$, $\hat{X}_m$ would involve $\hat{X}_n$ where $n > m$. To illustrate this causality issue, let us consider $m = 0$, then among the triples (p,q,r) satisfying $\delta_N(p+q+r) = 1$ the triplet $(N-1,1,0)$ which involves non causal estimated symbols $\hat{X}_1$ and $\hat{X}_{N-1}$. To solve the two aforementioned causality issues, we will use a hybrid time-frequency domain decision feedback equalizer which consists of processing the past decisions on a per symbol basis allowing for the resolution of the causality issue. Detailed analysis is given in the following subsection.

Hybrid time and frequency domain DFE

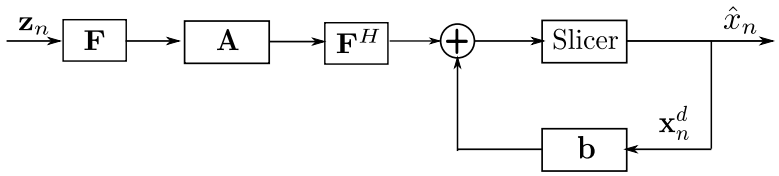

Figure 2.4: Hybrid Time and frequency time domain equalizer

The idea behind the hybrid time and frequency domain DFE is to exploit the block processing in the frequency domain for the feed-forward filter, and to process the feedback filter in the time domain. As such the issue of the causality of the past decided symbols is alleviated. Figure 2.4 depicts the principle of the proposed hybrid decision feedback equalizer. The estimated symbols at time n write using the **Convention 2** as:

$$\hat{x}_n = \sum_{m=0}^{N-1} a_m z_{<n-m>_N} + \sum_{m=1}^{N_b} b_m \hat{x}_{n-m} + c$$

$$= \mathbf{a}'\mathbf{z}_n + \mathbf{b}\mathbf{x}_n^d + c \tag{2.60}$$

where we use the following definitions:

$$\begin{aligned}
\mathbf{z}_n &\triangleq [z_n, z_{n+1}, \ldots, z_{N-1}, z_0, \ldots, z_{n-1}]^T \\
\mathbf{x}_n &\triangleq [x_n, x_{n+1}, \ldots, x_{N-1}, x_0, \ldots, x_{n-1}]^T \\
\mathbf{w}_n &\triangleq [w_n, w_{n+1}, \ldots, w_{N-1}, w_0, \ldots, w_{n-1}]^T \\
\mathbf{x}_n^{ijk} &\triangleq \begin{bmatrix} x_{n-i}x_{n-j}x_{n-k}^* \\ \vdots \\ x_{n-1-i}x_{n-1-j}x_{n-1-k}^* \end{bmatrix}
\end{aligned} \tag{2.61}$$

Since the feed-forward filtered symbols are the result of a circular convolution in the time domain, the estimated symbol thus writes as:

$$\hat{x}_n = u_n^T \mathbf{F^{-1}} \mathbf{A}\mathbf{Z} + \mathbf{b}\mathbf{x}_n^d + c \tag{2.62}$$

where $\mathbf{A}$ is the frequency domain feed-forward coefficients, and $\mathbf{Z}$ is the Fourier transform of the received symbols $\mathbf{z}_0$.

The block received symbols are written in terms of transmitted symbols as follows:

$$\mathbf{z}_n = \mathbf{H}\mathbf{x}_n + \sum_{i=0}^{M-1}\sum_{j=0}^{M-1}\sum_{k=0}^{M-1} \mathbf{H}_{ijk}\mathbf{x}_n^{ijk} + \mathbf{w}_n \tag{2.63}$$

The covariance of the received symbols remains unchanged, however some cross-correlation terms between transmitted, decided and received symbols are slightly modified. Indeed, we can write:

$$\begin{aligned}
Cov(\mathbf{x}_n^d, \mathbf{z}_n) &= \mathbb{I}'_{f_b}\mathbf{H}^H \\
\mathbb{I}'_{f_b} &= [\mathbb{O}_{N_b \times N - N_b}\mathbb{I}_{N_b \times N_b}] \\
Cov(x_n, \mathbf{z}_n) &= \mathbf{u}_0^T\mathbf{H}^H
\end{aligned} \tag{2.64}$$

It results from these modifications, that the hybrid MMSE FD-DFE solutions write as:

$$\begin{aligned}
\mathbf{a}' &= \mathbf{u}_0^T\mathbf{H}^H\left((\sigma_w^2 + \sum_{i,j,k}|h_{ijk}|^2)\mathbb{I}_N + \mathbf{H}\left(\mathbb{I}_N - \mathbb{I}'^T_{fb}\mathbb{I}'_{fb}\right)\mathbf{H}^H\right)^{-1} \\
\mathbf{b} &= -\mathbf{a}'\mathbf{H}\mathbb{I}'^T_{f_b}
\end{aligned} \tag{2.65}$$

The frequency domain coefficients are then computed by $\mathbf{A} = \mathbf{F}[a'_0, a'_{N-1}, \ldots, a'_1]^T$. It can be noticed, that due to the presence of the term $\mathbb{I}_N - \mathbb{I}'^T_{fb}\mathbb{I}'_{fb}$ in (2.65), the matrix in the MMSE solution $\mathbf{a}'$ is no longer circulant,

and thus is not simply inverted in the frequency domain which does not improve the computational complexity as much as in the linear frequency domain equalizer. There is yet still a gain in performing the feed-forward filtering in the frequency domain. This limitation can also be inferred from an alternative derivation of the MMSE FD-DFE solutions in [Falconer and Ariyavisitakul, 2002] and [Benvenuto and Tomasin, 2002]. Indeed, the feed-forward and feedback filters computed in [Falconer and Ariyavisitakul, 2002] are as follows:

$$\begin{aligned} A_k &= \frac{H_k^*(1-\sum_{i=1}^{N_b} b_{N_b-i}\Omega_N^{-ki})}{|H_k|^2+\sigma_w^2+\sum_{i,j,k}|h_{i,j,k}|^2} \\ V\tilde{\mathbf{b}} &= -v \end{aligned} \tag{2.66}$$

where we define $\tilde{\mathbf{b}} = -[b_{N_b}^*, \ldots, b_1^*]$ and the following quantities:

$$\begin{aligned} v &= [v_0, \ldots, v_{Nb}] \\ V &= \begin{pmatrix} v_0 & v_{k1-k2} & \cdots & v_{k_1-k_{N_b}} \\ v_{k2-k1} & v_0 & \cdots & v_{k_3-k_{N_b}} \\ \cdots & \vdots & \ddots & \vdots \\ v_{k_1-k_{N_b}} & \cdots & \cdots & v_0 \end{pmatrix} \\ v_i &= \frac{\sigma_w^2+\sum_{i,j,k}|h_{i,j,k}|^2}{N}\sum_{l=0}^{N-1}\frac{\Omega_N^{li}}{|H_l|^2+\sigma_w^2+\sum_{i,j,k}|h_{i,j,k}|^2} \end{aligned} \tag{2.67}$$

The approach adopted in these two references somehow joins that of [Al-Dhahir and Cioffi, 1995] in the sense that the feed-forward filter $\mathbf{a}$ is first written function of the feed-back $\mathbf{b}$ filter. The feed-back filter is then solved in [Falconer and Ariyavisitakul, 2002] and [Benvenuto and Tomasin, 2002] by means of a linear system resolution whereas, in [Al-Dhahir and Cioffi, 1995] the feed-back filter is computed using the Cholesky factorisation. This linear problem yields to a Toeplitz matrix inversion which proves to be less complex than the matrix inversion in (2.65).

Complexity analysis

The complexity of the Hybrid time and frequency domain equalizer, consists of the complexity of the linear FD-MMSE and additional complexity related to solving the linear system in (2.67). The linear system resolution can be solved using reduced Levinson-Durbin algorithm [Benvenuto et al., 2010] which exploits the Toeplitz structure of the matrix, and thus yields $3N_b^2$ complexity. This results in an overall computational complexity equal to:

$$\text{Real Multiplies} = 7N_b^2 + 6L\log_2(L) + 4LN_b + 4N_b + 6L$$

Equalizer	Solution	Complexity
Linear Time MMSE	$\hat{x}_n = \mathbf{a}\mathbf{z}_n$ $\mathbf{a} = \mathbf{u}_n^T H^H \left(\mathbf{H}\mathbf{H}^H + \left(\sigma_w^2 + \sum_{i,j,k} \lvert h_{ijk}\rvert^2\right)\mathbb{I}_N\right)^{-1}$	$O(N^2)$
Linear Freq MMSE	$\hat{X}_m = \frac{H_m^*}{\lvert H_m\rvert^2+\sigma_w^2+\sigma_{\tilde{w}}^2} Z_m$	$O(L\log_2(L) + L)$
Linear feedback Time DFE-MMSE	$\hat{x}_n = \mathbf{a}\mathbf{z_n} + \mathbf{b}\mathbf{x_n^d}$ $\mathbf{a} = \mathbf{u}_n^T\mathbf{H}^H \left((\sigma_w^2 + \sum_{i,j,k} \lvert h_{ijk}\rvert^2)\mathbb{I}_N + \mathbf{H}\left(\mathbb{I}_N - \mathbb{I}_{fb}^T\mathbb{I}_{fb}\right)\mathbf{H}^H\right)^{-1}$ $\mathbf{b} = -\mathbf{a}\mathbf{H}I_{fb}^T$	$O(N^2)$
Non linear feedback Time DFE-MMSE-NL	$\hat{x}_n = \mathbf{a}\mathbf{z_n} + \mathbf{b}\mathbf{x_n^d} + \sum_{i=1}^{M-1}\sum_{j=1}^{M-1}\sum_{k=1}^{M-1} c_{ijk}x_n^{ijk,d}$ $\mathbf{a} = \mathbf{u}_n^T\mathbf{H}^H \left(\sigma_w^2\mathbb{I}_N + \sum_{i,j,k} \lvert h_{ijk}\rvert^2(\mathbb{I}_N - \mathbb{I}_{N\times N}^{(0)}) + \mathbf{H}\left(\mathbb{I}_N - \mathbb{I}_{fb}^T\right)\mathbf{H}^H\right)^{-1}$ $\mathbf{b} = -\mathbf{a}\mathbf{H}\mathbb{I}_{fb}^T$ $\forall(i,j,k)\ \ c_{i,j,k} = -\mathbf{a}\mathbf{H}_{i,j,k}\mathbf{u}_0$	$O(N^2)$
Hybrid Freq-Time DFE-MMSE-Hybrid	$\hat{x}_n = u_n^T\mathbf{F^{-1}}\mathbf{A}\mathbf{Z} + \mathbf{b}\mathbf{x}_n^d$ $\mathbf{a} = \mathbf{u}_0^T\mathbf{H}^H \left((\sigma_w^2 + \sum_{i,j,k} \lvert h_{ijk}\rvert^2)\mathbb{I}_N + \mathbf{H}\left(\mathbb{I}_N - \mathbb{I'}_{fb}^T\mathbb{I'}_{fb}\right)\mathbf{H}^H\right)^{-1}$ $\mathbf{b} = -\mathbf{a}\mathbf{H}\mathbb{I'}_{f_b}^T$	$O(N_b^2)$ $O(L\log_2(L)$ $+L)$

Table 2.1: Comparison of linear and non linear Volterra channel equalizers

$$\text{Real Adds} \quad = \quad 8N_b^2 + 9L\log_2(L) + 4LN_b + 5L + 4N_b - 2 \tag{2.68}$$

2.7 Equalization schemes comparison

2.7.1 Complexity comparison

In this section, we present a summary of previous linear and non linear time and frequency domain equalization schemes. For a fixed channel length $M = N_b$ and a fixed number of feedback Volterra coefficients $\mathcal{I}_3$ the algorithms complexities are reported in terms of the length of the feed-forward N and number of estimated symbols L. A summary of the MMSE derived solutions can be found in Table 2.7.1. In Figure 2.6, we depict the computational complexity of the different MMSE implementations, taking the channel test 2 parameters namely $N_b = M - 1 = 3$ and $\mathcal{I}_3 = 3$. The complexity of the linear Time domain and Decision Feedback with its two implementations (linear and non linear decision cancelling), have similar complexity yet with small differences owing to the additional processing required between the linear and non linear MMSE. As far as the

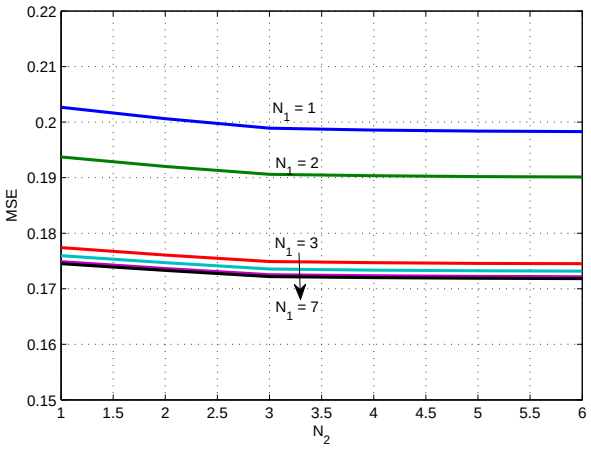

Figure 2.5: Mean Square Error for the MMSE time domain equalizer function of the feed-forward filter lengths N_1 and N_2

frequency domain equalizer, its complexity only depends on the length of the estimated symbols. The hybrid time and frequency domain equalizer has additional complexity inherent to the linear system solving and the feedback filtering.

2.7.2 Performance comparison

The design of an equalizer is an important step in finding the suitable filter length for the affordable trade-off performance-complexity. As a reference, we find the suitable operating filter lengths for the MMSE linear time domain equalizer which will then be length for a comparison of the overall performance of the equalizers. This section presents some results on the application of linear and non linear equalizers for the test channels in Table 1.7. Figure 2.5 depicts the evolution of the mean squared error of the output of the MMSE time domain equalizer for the test channel 2. It can be seen that the MSE decays for large global length $N = N_1 + N_2$. However, starting from a length $N_1 = 3$ and $N_2 = 3$, the evolution of the MSE is slower. We thus take these numerical values as reference for the remaining of the simulation results. The simulated system is based on the parameters of channel test 2. Figure 2.7 plots the obtained results for the time and frequency domain implementations of the different equalizers. As expected, the time domain linear equalizer is sub-optimal compared to DFE time domain implementations. Additionally, the enhancement between the short and long time domain DFE is slight since, not all the non linear Volterra kernels would be dealt with. However, when using the tentative decisions previously presented in [Biglieri et al., 1984], the performance can be enhanced.

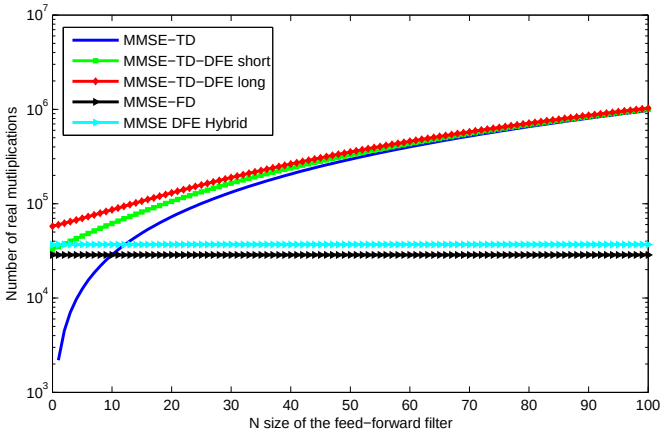

Figure 2.6: Number of complex MMSE operations for a block of estimated symbols $L = 512$

Moreover, the short frequency domain hybrid DFE joins the Time domain DFE short equalizer.

2.8 Conclusion

In this chapter, we have investigated on different implementations of the linear and non linear time and frequency domain equalizers for the non linear Volterra channel. It has been shown, that linear time and frequency domain equalizer only regarded the non linear interference as additive noise, which does not allow for a fine mitigation of the non linear interference. We also investigated on some optimal and sub-optimal non linear equalization techniques, which we showed improved the system performance at the cost of increased complexity. To cope with this increased complexity, we investigated on the hybrid time and frequency domain implementation of the non linear decision feedback equalizer and showed it did only slightly degrade the computational complexity. Thus, the question arising is whether we can envisage new advanced processing techniques such as iterative equalization to further enhance the performance of the equalizers and what is the impact of these equalization techniques on the system computational complexity.

2.9 Conclusion (french)

Dans ce chapitre, nous avons abordé différentes implantations des égaliseurs linéaires et non linéaires dans les domaines fréquentiel et temporel. Nous avons montré que les égaliseurs linéaires temporels et fréquentiels considéraient l'interférence non linéaire comme étant du bruit additif ce qui ne permet hélas pas de traiter

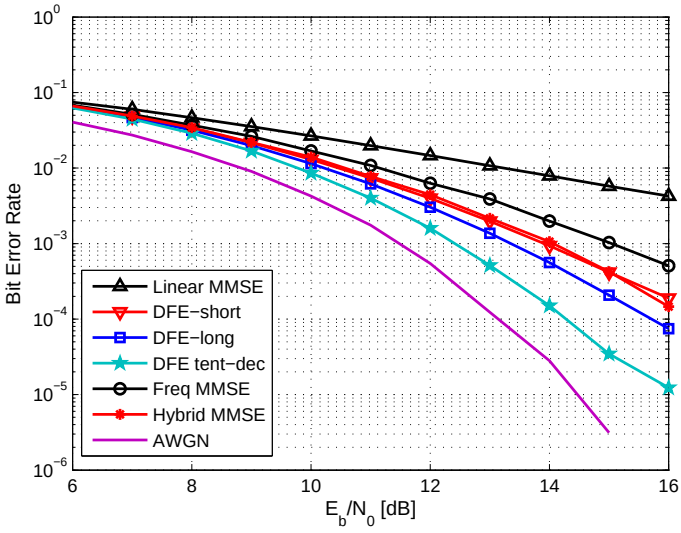

Figure 2.7: Bit Error Rate performance of the equalizers over the channel test 2

d'une manière efficace ces non linéarités. Nous avons aussi étudié des égaliseurs non linéaires optimaux et sous optimaux et avons montré que les performances du système étaient certes améliorées mais non sans impact sur la complexité qui est en conséquent augmentée. Afin de pallier cette hausse de complexité, nous avons étudié la version hybride temporelle et fréquentielle de l'égaliseur non linéaire à retour de décisions, et avons montré que cela dégradait faiblement la complexité calculatoire du système. Ainsi, la question qui se pose est si nous pouvons envisager des techniques de traitements avancées à l'instar des méthodes itératives afin d'améliorer les performances du système et quel impact cela pourrait avoir sur la complexité calculatoire.

Chapter 3

Iterative equalization and decoding

Contents

3.1 Introduction

In the previous chapter, we presented a state of the art of linear and non linear non iterative time domain equalizers as well as some contributions on the frequency domain hybrid decision feedback equalizer for the non linear satellite channel. In this chapter, we are interested in iterative equalizers for the non linear satellite channel. The motivation behind using iterative equalization techniques lies in their excellent ISI mitigating performance for ISI channels as presented in the pioneering work of [Douillard et al., 1995] [Roumy, 2000] [Laot et al., 2001]. As such, we investigate on optimal and sub-optimal iterative time domain detection. We will show how the derived linear equalizer encompass some of the state of the art equalizers. Furthermore, using the frequency domain model of the non linear satellite channel, we will present new results on linear frequency domain iterative equalizers. The complexity of all equalizers is then being compared and their performance presented in comparison with existing non linear satellite channel turbo-equalizers. In a second part of this chapter, we will design optimized channel codes to further improve the performance over a non linear ISI channel. In our optimization, we will show that using a Gaussian mixture approximation allows for a better design of the channel codes and we will compare the obtained codes with ISI-free optimized channel codes.

3.2 Introduction (French)

Dans le chapitre précédent, nous avons présenté un état de l'art des égaliseurs linéaires et non linéaires non itératifs pour les canaux non linéaires, ainsi que certaines contributions concernant l'égaliseur hybride à retour de décisions dans le domaine fréquentiel. Dans ce chapitre, nous nous intéressons aux égaliseurs itératifs pour les canaux non linéaires. L'intérêt porté aux égaliseurs itératifs provient de leur excellente capacité à réduire l'interférence entre symboles pour des canaux à mémoire comme présenté dans les travaux majeurs de [Douillard et al., 1995] [Roumy, 2000] [Laot et al., 2001]. Ainsi, nous étudierons les égaliseurs itératifs optimaux et sous optimaux dans le domaine temporel. Nous démontrerons comment certaines structures proposées par l'état de l'art peuvent être vues comme des cas particuliers des égaliseurs proposés. Par ailleurs, nous utiliserons l'expression du canal non linéaire dans le domaine fréquentiel afin de dériver un égaliseur fréquentiel itératif. La complexité de tous ces égaliseurs sera étudiée et et leurs performances comparées à certains égaliseurs proposés dans la littérature. Dans une seconde partie de ce chapitre, nous optimiserons le codage canal afin qu'il soit le mieux adapté aux égaliseurs itératifs utilisés. Une telle optimisation a déjà été proposée pour des canaux linéaires et se base sur une approximation Gaussienne de la sortie de l'égaliseur. Nous allons

montrer qu'en utilisant une approximation en mélange de Gaussiennes, nous pouvons construire des codes ayant de meilleures performances qu'en utilisant l'approximation Gaussienne, et nous comparerons les codes obtenus à des codes optimisés pour un canal sans mémoire.

3.3 Turbo equalization principle

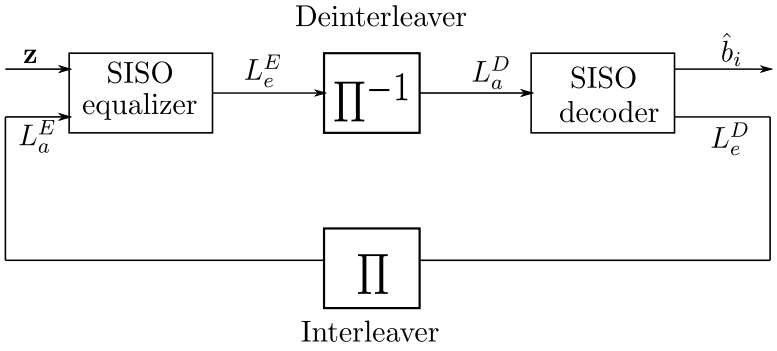

Figure 3.1: Structure of a turbo equalizer

The concatenation of the channel code with an ISI channel can be regarded as serially concatenated codes, with an inner channel code, and a rate 1 outer code represented by the ISI channel. Optimal global detection and decoding over such a scheme requires constructing a global trellis for the concatenation of both the channel code and the ISI channel which then would allow the derivation of symbol and sequence optimal decoding. However, the number of states of the resulting trellis grows exponentially in the product of the channel memory and the encoder number of states. A practical way to counteract this complexity, is using separate optimal equalization and decoding, within an iterative process. Hence, building upon the principle of turbo-decoding [Berrou et al., 1993] for concatenated codes, [Douillard et al., 1995] [Laot et al., 2001] suggested using iterative equalization and decoding for the detection of coded modulations in ISI channels. In a similar way to the turbo-decoder, the turbo equalizer depicted in Figure 3.1 consists of Soft Input Soft Output (SISO) modules which exchange *extrinsic soft information* used in different stages of the iterative receiver. This soft information can be assimilated to the reliability upon the detection of each symbol/bit at the receiver. By iterating the exchange of soft information between the SISO equalizer and SISO decoder, the reliability on the information bits is increased until reaching a point of convergence beyond which no further improvement is observed. In order to grant bit/symbol independence, bit interleaving is used between the SISO equalizer and the SISO decoder. When involved in a detection process, the information on the coded bits can be represented by hard

or soft estimations. In the case of hard information, the bit is either decided '0' or '1' for binary codes. The soft information is instead richer than the hard information in the sense that it allows for both hard and soft information processing. In [Hagenauer and Hoeher, 1989] for example, the soft information on the bits is presented in the form of a ratio of the logarithm of probabilities for the bits to be either 0 or 1. The log likelihood ratios (LLR) write for a coded bit c_i as:

$$L(c_i) = \log \frac{P(c_i = 0)}{P(c_i = 1)} \tag{3.1}$$

The coded bits probabilities can thus be written from the LLRs as follows:

$$P(c_i = b) = \frac{\exp(-bL(c_i))}{1 + \exp(-L(c_i))} \tag{3.2}$$

where b takes the value in $(0, 1)$ for binary valued codes c_i. Let us consider that $\log_2(\mathcal{M})$ coded bits $c_{n,i}$ are mapped into a symbol x_n. The SISO equalizer consists of a two-stage processing, namely soft symbol estimation and soft demapping. The soft symbol estimation process is used to provide probabilities of symbols x_n using the observed noisy channel outputs and the input a priori LLR $L_a^E(c_{n,i})$. From the resulting symbol probabilities, the soft demapper computes bit log likelihood ratios. The probability for a bit $c_{n,i}$ at position i in the symbol x_n to be equal to b is the marginalisation over all probabilities of symbols whose i^{th} bit is equal to b, and more precisely:

$$P(c_{n,i} = b) = \sum_{\tilde{x} \in \mathcal{X}_b^i} P(x_n = \tilde{x}) \tag{3.3}$$

where $\mathcal{X}_b^i$ denotes the set of symbols where the i^{th} bit is equal to b for $b \in \{0, 1\}$. The soft information exchanged then with the decoder is made extrinsic so that only the innovation of the a posteriori LLRs is transmitted to the next processing stage. As such, the extrinsic LLRs are computed from the a posteriori LLRs L_{ap}^E and the received symbols $\mathbf{z}$ as follows:

$$L_e^E(c_{n,i}) = L_{ap}^E(c_{n,i}|\mathbf{z}, L_a^E) - L_a^E(c_{n,i}) \tag{3.4}$$

In a similar way, it is possible to compute the symbol a priori probability based on the a priori bits log likelihood ratios $L_a c_{n,i}$, using the independence assumption granted by the use of interleavers between the equalizer and decoder. Th symbol probability writes then as

$$P(x_n = \tilde{x}|L_a^E) = \prod_{i=0}^{\log_2(\mathcal{M})-1} P(c_{n,i} = \tilde{x}_i|L_a^E) = \prod_{i=0}^{\mathcal{M}-1} \frac{\exp(-\tilde{x}_i L_a^E(c_{n,i}))}{1 + \exp(-L_a^E(c_{n,i}))} \tag{3.5}$$

where $\tilde{x}_i$ is the i^{th} bit in the symbol $\tilde{x}$. The decoder receives a soft LLR $L_a^E(c_{n,i})$ and computes two corresponding LLRs, the aposteriori information bits LLRs $L_{ap}^D(b_i)$ and the extrinsic coded bits LLRs $L_e^D(c'_{n,i})$ which after deinterleaving will constitute the apriori LLRs for the equalizer $L_a^E(c_{n,i})$.

3.4 Optimal SISO MAP equalization

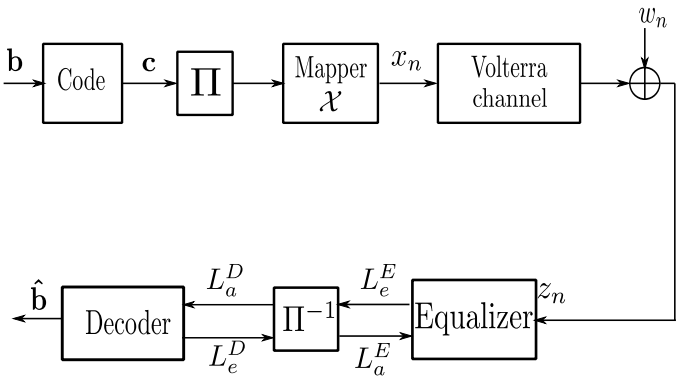

Figure 3.2: Iterative Volterra receiver for the non linear channel

Let us consider the general transmission scheme depicted in Figure 3.2 modelling the iterative receiver for a non linear Volterra channel. Similarly to the non iterative equalization schemes, SISO equalizers can be separated into optimal and sub-optimal symbol and sequence detectors. In this section we are interested in optimal symbol iterative detection. As far as linear ISI channels are concerned, numerous references have dealt with turbo optimal detection e.g. [Douillard et al., 1995], [TuĹchler and Singer, 2011]. As far as non linear channels are concerned authors in [Su et al., 2002] [Gutierrez and Ryan, 2000] have used the structure of the non linear channel trellis to derive MAP SISO equalizers which we are presenting in this section.
Let us consider a block of noisy channel observations $[z_0, \ldots, z_{N-1}]$ generated by a trellis structure as in Figure 2.1. The SISO map equalizer computes the probability for symbol x_n to take on a value $\tilde{x}$ using both the channel observations and the input a priori LLRs L_a^E as follows:

$$P(x_n = \tilde{x}|\mathbf{z}, L_a^E) \quad \propto \quad \sum_{s,s' \in \mathcal{S}_{\tilde{x}}} P\left(\sigma_{n-1} = s, \sigma_n = s', \mathbf{z}, L_a^E\right) \tag{3.6}$$

The a priori information is involved in the computation of symbol a priori probabilities following (3.5). Using the BCJR efficient implementation of the MAP criterion, this information can be exploited in the computation of $\gamma_n(s, s')$ for $(s, s') \in \mathcal{S}_{\tilde{x}}$ as follows:

$$\begin{aligned}
\gamma_n(s, s') &= P\left(z_n, \sigma_n = s'|\sigma_{n-1} = s, L_a^E\right) \\
&= P\left(z_n|\sigma_n = s', \sigma_{n-1} = s\right) P(\sigma_n = s'|\sigma_{n-1} = s, L_a^E) \\
&= P\left(z_n|\sigma_n = s', \sigma_{n-1} = s\right) P(x_n = \tilde{x}[L_a^E)
\end{aligned}$$

$$= P\left(z_n|\sigma_n = s', \sigma_{n-1} = s\right) \prod_{i=0}^{\log_2(\mathcal{M})-1} P(c_{n,i} = \tilde{x}_i|L_a^E)$$
$$= \exp\left(\frac{-|z_n - \tilde{x}|^2}{\sigma_w^2}\right) \prod_{i=0}^{\log_2(\mathcal{M})-1} P(c_{n,i} = \tilde{x}_i|L_a^E) \quad (3.7)$$

As such, the aposteriori coded bit LLRs output by the soft demapper write as follows:

$$L_{app}^E(c_{n,i}) = \log\left(\frac{\sum_{\tilde{x}\in\mathcal{X}_0^i} P(x_n = \tilde{x}[\mathbf{z}, L_a^E)}{\sum_{\tilde{x}\in\mathcal{X}_1^i} P(x_n = \tilde{x}|\mathbf{z}, L_a^E)}\right) \quad (3.8)$$

where

$$P(x_n = \tilde{x}[\mathbf{z}, L_a^E) \propto \sum_{s,s'\in\mathcal{S}_{\tilde{x}}} \alpha_n(s)\gamma_n(s,s')\beta_n(s') \quad (3.9)$$

and the extrinsic LLRs write as:

$$L_e^E(c_{n,i}) = L_{app}^E(c_{n,i}) - L_a(c_{n,i}) \quad (3.10)$$

Similarly to the non iterative case, the MAP optimal SISO equalizer suffers from exponential complexity in the order $O(\mathcal{M}^M)$ which thus motivates the need for low complexity implementations of the SISO equalization module.

Different candidate receivers have been investigated in the case of linear ISI channels such as: reduced states BCJR [Colavolpe et al., 2001], factor graph equalizers [Kschischang et al., 2001], neural network equalizers [Yee et al., 2003] and linear equalizers [Glavieux et al., 1997] and [Tuchler et al., 2002]. In the next section, we derive a linear MMSE turbo equalizer for the non linear channel and show how it is actually able of efficiently mitigating non linear interference in contrast with the linear non iterative MMSE equalizer presented in Section 2.4.

3.5 Linear MMSE turbo-equalization

Linear MMSE turbo equalization has been proposed as two different implementations of a reduced complexity linear iterative processing for coded modulations in ISI channels namely in [Glavieux et al., 1997], [Laot et al., 2005] and in an alternative way by [Tuchler et al., 2002]. Authors in [Glavieux et al., 1997] have derived a linear soft interference canceller where the feed-forward processes received symbols and the feedback filter processes the reconstructed soft interference. In [Tuchler et al., 2002], the proposed MMSE consists of a linear feed-forward processing of the received symbols, which yields after derivations to the same MMSE soft interference canceller structure as in [Glavieux et al., 1997].

As far as non linear channels are concerned, authors in [Liu and Fitz, 2012] and [Ampeliotis et al., 2008] have

proposed MMSE "non linear" equalizers for the non linear channel. The *non linear* derived solutions do not mean actually non linear processing of the received symbols, but rather a *non linear* soft interference canceller. In fact, authors have imposed a structure on the MMSE solution as a *linear* filtering of the input symbols in conjunction with a *non linear* interference canceller. In this section, we show that using only *linear* symbol processing, we can derive a soft interference canceller which we will show encompasses the two implementations of the afore-mentioned non linear iterative equalizers.

3.5.1 Linear MMSE time varying solution

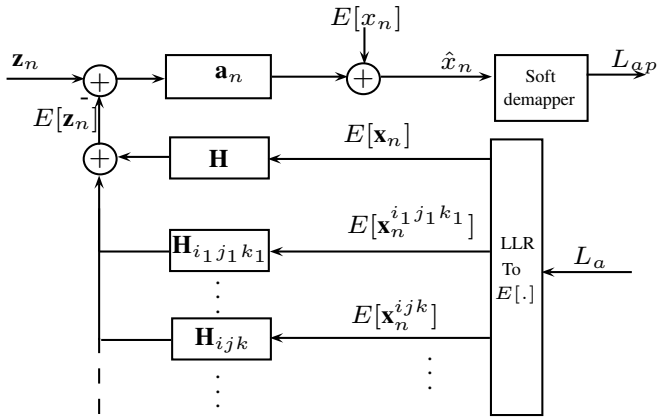

Figure 3.3: Linear MMSE time domain solution

Exact MMSE solution

The MMSE estimate of the transmitted symbols writes similarly to the non iterative equalizer as follows:

$$\hat{x}_n = \mathbf{a}_n \mathbf{z}_n + b_n \tag{3.11}$$

where the subscript under in $\mathbf{a}_n$ indicates that the MMSE iterative solution is a time varying solution for each symbol estimate x_n. The solution $(\mathbf{a}_n, b_n)$ minimizes the mean square error between estimated and transmitted symbols $E\left[|\hat{x}_n - x_n|^2\right]$ and are given as in (2.16):

$$\begin{cases} \mathbf{a}_n = Cov\left(x_n, \mathbf{z}_n\right) Cov\left(\mathbf{z}_n, \mathbf{z}_n\right)^{-1} \\ b_n = E\left[x_n\right] - \mathbf{a}_n E\left[\mathbf{z}_n\right] \end{cases} \tag{3.12}$$

leading to estimated symbols writing as:

$$\hat{x}_n = \mathbf{a}_n \left(\mathbf{z}_n - E\left[\mathbf{z}_n\right] \right) + E\left[x_n\right] \tag{3.13}$$

where

$$E\left[\mathbf{z}_n\right] = \mathbf{H} E\left[\mathbf{x}_n\right] + \sum_i \sum_j \sum_k \mathbf{H}_{ijk} E\left[\mathbf{x}_n^{ijk}\right] \tag{3.14}$$

We recognise in (3.13) and Figure 3.3 the structure of a soft interference canceller where linear and non linear ISI terms appearing in $E\left[\mathbf{z}_n\right]$ are cancelled. Note that in order not to cancel the current symbol to be estimated, the a priori LLR (L_a) for the n^{th} symbol should not be taken into account in the linear ISI terms by considering $E[x_n] = 0$ and $var(x_n) \triangleq v_n = 1$. Since the non linear ISI also contains the current symbol, it is preferable not to cancel the contribution of the current symbol in this nonlinear ISI since it needs to be integrally removed. Authors in [Liu and Fitz, 2012] removed the contribution of the current symbol in the non linear interference as well, and this resulted in poor performance of their proposed equalizer compared to a linear channel equalizer. Equations (3.12) of the MMSE equalizer can then be detailed as follows:

$$\begin{aligned}
Cov\left(\mathbf{z}_n, \mathbf{z}_n\right) &= \sigma_w^2 \mathbb{I}_N + \mathbf{H} Cov\left(\mathbf{x}_n, \mathbf{x}_n\right) \mathbf{H}^H + (1 - v_n) \mathbf{h}_n \mathbf{h}_n^H \\
&+ \sum_{i,j,k} \mathbf{H}_{ijk} Cov\left(\mathbf{x}_n^{ijk}, \mathbf{x}_n\right) \mathbf{H}^H + \sum_{i,j,k} \mathbf{H} Cov\left(\mathbf{x}_n, \mathbf{x}_n^{ijk}\right) \mathbf{H}_{ijk}^H \\
&+ \sum_{i,j,k} \sum_{i',j',k'} \mathbf{H}_{ijk} Cov\left(\mathbf{x}_n^{ijk}, \mathbf{x}_n^{i'j'k'}\right) \mathbf{H}_{i'j'k'}^H \\
Cov\left(\mathbf{z}_n, x_n\right) &= \mathbf{H} Cov\left(\mathbf{x}_n, x_n\right) + (1 - v_n) \mathbf{h}_n + \sum_{i,j,k} \mathbf{H}_{ijk} Cov\left(\mathbf{x}_n^{ijk}, x_n\right) \\
E\left[\mathbf{z}_n\right] &= \mathbf{H} E\left[\mathbf{x}_n\right] - \mathbf{h}_n E\left[x_n\right] + \sum_{i,j,k} \mathbf{H}_{ijk} E\left[\mathbf{x}_n^{ijk}\right]
\end{aligned} \tag{3.15}$$

where $\mathbf{h}_n = \mathbf{H} \times [\mathbf{0}_{1\times N_1+M-1}, 1, \mathbf{0}_{1\times N_2}]^T$.

To obtain the exact MMSE coefficients one needs to compute expectations of products of 3,4 and 6 symbols and symbols conjugates at different time instants as mentioned in (2.19) from the input bit a priori LLRs. Due to the presence of the interleaver between the decoder and the equalizer, symbols can be considered to be mutually independent. Thus, we can write the average of a product of p symbols and $q-p$ symbol conjugates as follows:

$$\begin{aligned}
E\left[x_{n-i_1} x_{n-i_2} \ldots x_{n-i_p} x_{n-i_{p+1}}^* \ldots x_{n-i_q}^*\right] &= \prod_j E\left[x_{n-i_j}^{v_j} x_{n-i_j}^{*v_j^*}\right] \\
&= \prod_j \sum_{m=0}^{\mathcal{M}} \tilde{x}_m^{v_j} \tilde{s}_m^{*v_j^*} P(x_{n-i_j} = \tilde{x}_m)
\end{aligned} \tag{3.16}$$

where $P(x_{n-i_j} = \tilde{x}_m)$ is computed using the input a priori LLR L_a following (3.5).

Soft demapper

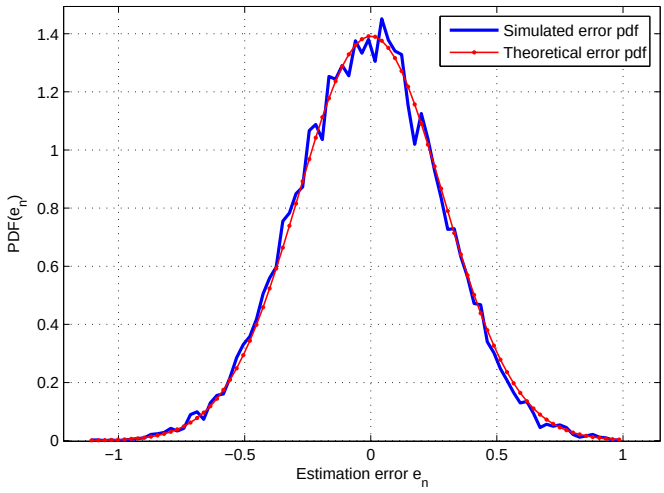

Figure 3.4: Estimation error PDF

In order to map the output of the equalizer into code LLRs, we define the residual equalizer output error $e_n = \hat{x}_n - \kappa_n x_n$. For practical considerations, this error is assumed to be Gaussian. The bias κ_n can be computed using the correlation between estimated and transmitted symbols as follows:

$$\kappa_n = Cov(\hat{x}_n, x_n) \tag{3.17}$$

The characteristics of the estimation error thus write as:

$$\begin{aligned} E[e_n] &= 0 \\ var(e_n) &= Cov(\hat{x}_n, \hat{x}_n) - |\kappa_n|^2 \\ &= \mathbf{a}_n Cov(\mathbf{z}_n, \mathbf{z}_n)\mathbf{a}_n^H - |\kappa_n|^2 \\ &= \kappa_n^* - |\kappa_n|^2 \end{aligned} \tag{3.18}$$

The Gaussian approximation of the estimation error is a plausible assumption as depicted in Figure 3.4 which plots the probability distribution function of the estimation error compared to the afore-presented Gaussian assumption. The equalizer output $\hat{x}_n \sim \mathcal{N}(\kappa_n x_n, var(e_n))$ and the output *a posteriori* LLR L_{ap} can finally be

written as:

$$
\begin{aligned}
L_{ap}(c_{n,i}|\hat{x}_n) &\triangleq \log \frac{P\left(c_{n,i}=0|\hat{x}_n\right)}{P\left(c_{n,i}=1|\hat{x}_n\right)} \\
&= \log \frac{\sum_{\tilde{x}_j \in \mathcal{X}_0^i} exp\left(\frac{-|\hat{x}_n-\kappa_n\tilde{x}_j|^2}{var(e_n)}\right) \prod_k P(c_{n,k}=\tilde{x}_{j,k})}{\sum_{\tilde{x}_j \in \mathcal{X}_1^i} exp\left(\frac{-|\hat{x}_n-\kappa_n\tilde{x}_j|^2}{var(e_n)}\right) \prod_k P(c_{n,k}=\tilde{x}_{j,k})}
\end{aligned}
\tag{3.19}
$$

The a posteriori LLRs are made extrinsic (L_e) by subtracting the a priori probability fed by the decoder:$L_e(c_{n,i}) = L_{ap}(c_{n,i}|\hat{x}_n) - L_a(c_{n,i})$.

Complexity analysis

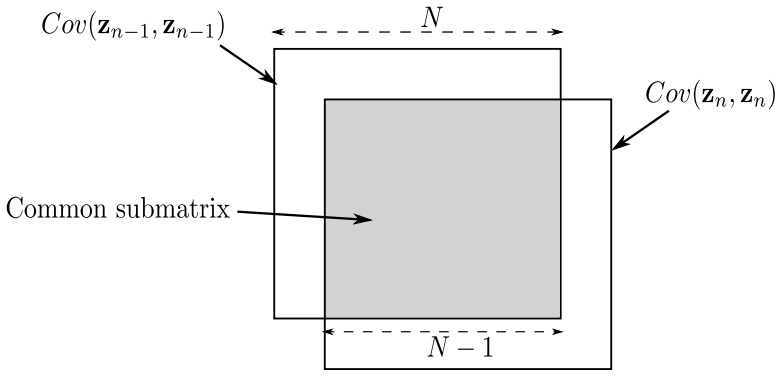

Figure 3.5: Common sub-matrix in the MMSE solution

In terms of computational complexity, there are two bottleneck steps which render the exact MMSE solution rather complex. For a linear ISI channel, the major complexity stems form the computation of the inverse matrix in (3.12). In the case of a Volterra non linear channel, the computational complexity is also impacted by the number of Volterra kernels. Indeed, there are two major computational issues:

- On the one hand, the computation of the inverse of the received symbols covariance matrix yields a non negligible complexity per estimated symbol. However, inspired by adaptive filtering fast recursion solutions, as for example in [Haykin, 2008], authors in [Tuchler et al., 2002] have exploited the presence of common sub-matrices in the covariance matrix for successive time domain received symbols $\mathbf{z}_{n-1}$, $\mathbf{z}_n$, $\mathbf{z}_{n+1}$ to derive a fast covariance matrix computation. These common sub-matrices are depicted in Figure 3.5 and one can notice that only $2N-1$ terms need to be updated from $Cov(\mathbf{z}_{n-1}, \mathbf{z}_{n-1})$ to construct the covariance matrix $Cov(\mathbf{z}_n, \mathbf{z}_n)$, whereas a full complexity construction would have required computing

N^2 covariance elements. This recursive structure of the covariance of received symbols, has then been exploited to reduce the matrix inversion from $O(LN^3)$ to $O(LN^2)$ for a block of L estimated symbols.

- A further complexity issue arises from the computation of non linear soft symbols covariances in the covariance of received symbols. Unlike the linear channel, computing the covariance of received symbols in (3.15) can yield large complexity depending on the number of non linear Volterra kernels. To illustrate this limitation, let us consider, there are only two non linear Volterrra kernels with indexes (i_0, j_0, k_0) and (i_1, j_1, k_1). In this case, five covariance matrices need to be computed: the covariances between linear and non linear symbols $Cov(\mathbf{x}_n, \mathbf{x}_n^{i_0,j_0,k_0})$, $Cov(\mathbf{x}_n, \mathbf{x}_n^{i_1,j_1,k_1})$, and covariances of non linear symbols: $Cov(\mathbf{x}_n^{i_0,j_0,k_0}, \mathbf{x}_n^{i_0,j_0,k_0})$, $Cov(\mathbf{x}_n^{i_0,j_0,k_0}, \mathbf{x}_n^{i_1,j_1,k_1})$ and $Cov(\mathbf{x}_n^{i_1,j_1,k_1}, \mathbf{x}_n^{i_1,j_1,k_1})$. The first two covariances require computation of the expectation of four symbol products which is done with a maximum complexity $(4\mathcal{M}+3)$ [1]CM and $(4\mathcal{M})$ [2]CA. Since these covariances are of size $(N+M-1 \times N)$, then the complexity for computing these matrices elements is equal to $N(N+M-1)(4\mathcal{M}+3)$ CM and $(4N\mathcal{M}(N+M-1))$ CA. Fortunately, this complexity can be reduced using the common sub-matrices simplification. Thus only the last column and line of these sub-matrices need to be computed which yields a complexity of the order $(2N+M-2)(4\mathcal{M}+3)$ CM and $(4\mathcal{M}(2N+M-2))$ CA.
  As far as the covariances of non linear terms $Cov(\mathbf{x}_n^{i_1,j_1,k_1}, \mathbf{x}_n^{i_0,j_0,k_0})$ are concerned, each matrix component can be computed with a maximum complexity $(6\mathcal{M}+5)$ CM and $6\mathcal{M}$ CA where the exponent 6 owes to the computation of expectations of products of six symbols and symbol conjugates. Since these matrices are of size $N \times N$ and using the common sub-matrices simplification, this complexity is reduced to $((6\mathcal{M}+5)(2N-1))$ CM and $(6\mathcal{M}(2N-1))$ CA.

If we consider now the general case, assuming there are $\mathcal{I}$ non zero Volterra kernels, the computation of a block of L MMSE estimates requires:

- Computing L linear covariances $\mathbf{H}Cov(\mathbf{x}_n, \mathbf{x}_n)\mathbf{H}^H$ which requires $3L(M^2)$ CM and $2LM(M-1)$ CA using sub-matrices recursive computation.
- Computing $L\mathcal{I}$ non linear covariances $\mathbf{H}Cov(\mathbf{x}_n, \mathbf{x}_n^{i,j,k})\mathbf{H}_{i,j,k}^H$ which requires $L\mathcal{I}(N(2M+1)+N(N+M-1)(4\mathcal{M}+3))$ CM and $4L\mathcal{I}(2(M-1)N+\mathcal{M}N(N+M-1))$ CA taking into account the sub-matrices simplification.
- Computing $L\frac{\mathcal{I}(\mathcal{I}-1)}{2}$ non linear covariances $\mathbf{H}_{i,j,k}Cov(\mathbf{x}_n^{i,j,k}, \mathbf{x}_n^{i',j',k'})\mathbf{H}_{i',j',k'}^H$ which requires $L\frac{\mathcal{I}(\mathcal{I}-1)}{2}(2N+(2N-1)(6\mathcal{M}+5))$ CM and $3L\mathcal{I}(\mathcal{I}-1)\mathcal{M}$ CA per block of L estimated symbols.

[1]Complex Multiplication
[2]Complex Add

- Computing L inverses of the MMSE solution which we consider can be done with $O(LN^3)$ complexity.
- Computing the soft linear and non linear ISI which can be simplified using the existence of sub-matrices. For one estimated symbol, computing the linear soft ISI can be done with complexity (M) CM and $(M-1)$ CA, the $(\mathcal{I})$ non linear ISI with $(\mathcal{I})$ CM and $(\mathcal{I}-1)$ CA which yields for a block of L estimated symbols to $L(M+\mathcal{I})$ CM and $L(M+\mathcal{I}-2)$ CA.
- Linearly filtering the received symbols with a complexity (LN) CM and $L(N-1)$ CA.
- Computing the error variance which is done by a complexity of (M) CM and $(M-1)$ CA.

Finally the overall number of real multiplications is:

$$\begin{aligned} \text{Real Multiplies} \quad &\approx \quad LN^3 + N^2(L\mathcal{I}(4\mathcal{M}+3)) + NL(\mathcal{I}(2M+1+(M-1)(4\mathcal{M}+3)) \\ &+ \quad \mathcal{I}(\mathcal{I}-1)(1+6\mathcal{M}+5)+1) + (L+M)\mathcal{I} + L\mathcal{I}\frac{\mathcal{I}-1}{2}(-6\mathcal{M}-5) + M \end{aligned} \tag{3.20}$$

The computational complexity of the mean and variance of the input symbols and the computation of the output LLR are not investigated since they are common steps among all implementations of the linear turbo equalizers presented in this manuscript. The implementation of the low complexity iterative equalizer can be reduced using low complexity MMSE solutions in a similar way to [TuĹchler and Singer, 2011]. Thus, we will investigate on two low complexity implementations for the non linear channel, namely the No-Apriori (NA) approximation and the Averaged Low Complexity (ALC) MMSE approximation. Both approximations rely on computing a time invariant MMSE solution to lower the complexity of matrix inversions.

3.5.2 No-Apriori (NA) MMSE approximation

In this first low complexity equalizer, the computation of the matrix inverse in the MMSE solution for each estimated symbol is alleviated using a fixed time domain solution using the approximation that no a priori information is available. In this case, the mean and variances of the transmitted symbols are $E[x_n] = 0$ and $v_n = 1$, $\forall n \in \{0, \ldots, N-1\}$, which yields a NA-MMSE solution $\mathbf{a}_{NA}$ as in (2.24):

$$\mathbf{a}_{NA} = \mathbf{u}_n^T \mathbf{H}^H \left(\mathbf{H}\mathbf{H}^H + \left(\sigma_w^2 + \sigma_{\tilde{w}}^2\right) \mathbb{I}_N \right)^{-1} \tag{3.21}$$

It should be noted that the No-Apriori approximation is only used in the computation of the MMSE solution, whereas the soft interference cancellation uses the input a priori information to compute soft symbol estimates. This solution is equivalent to the MMSE solution presented in [Ampeliotis et al., 2008] which has been presented as a non linear turbo equalizer, whereas in our derivation, we clearly show that it is actually a low complexity approximation of the linear MMSE solution.

Soft demapper

Computing the exact error variance is more computationally complex than the exact MMSE since some simplifications are not allowed. As such, the estimation variance writes as:

$$var(e_n) = \mathbf{a}_{NA} Cov(\mathbf{z}_n, \mathbf{z}_n) \mathbf{a}_{NA}^H - |\kappa_n|^2$$

In contrast with the exact covariance computation which will be designated by **implementation-a**, authors in [Ampeliotis et al., 2008] presented a simplified NA-MMSE error-variance which neglects the contribution of third order Volterra kernels. In this thesis, we will make a similar simplification, but instead of neglecting these covariances, the third order Volterra kernels will be considered as a Gaussian noise with variance $\sigma_{\tilde{w}}^2$. This simplification will be referred to as **implementation-b** and the error variance writes then as:

$$var(e_n) = \mathbf{a}_{NA} \left(\mathbf{H} Cov(\mathbf{x}_n, \mathbf{x}_n) \mathbf{H}^H + (\sigma_w^2 + \sigma_{\tilde{w}}^2) \mathbb{I}_N \right) \mathbf{a}_{NA}^H - |\kappa_n|^2 \tag{3.22}$$

Although being less computationally complex than implementation-a, the proposed simplification provides inaccurate LLRs at high SNR values, since at high SNRs non linear interference can no longer be neglected.

Complexity analysis

To compute the NA-MMSE solution, the matrix inverse in $\mathbf{a}_{NA}$ has a Toeplitz structure which yields an inversion complexity equal to $O(N^2)$ using the Levinson-Durbin inversion for L estimated symbols. As far as the computation of the matrix to be inverted, it requires (MN^2) CM and $(M-1)N^2$ CA, which yields a global complexity in $O(MN^2)$ for a block of L estimated symbols. The complexity of computing soft symbols and linear filtering are also taken into account. The two implementations of the NA-MMSE equalizer we proposed differ in the computation of the error variance. More specifically, the complexity of computing the error variance writes as:

- **Implementation-a**: On the one hand the bias κ_n is computed using (M) CM. On the other hand, the covariance of estimated symbols can be computed using the sub-matrices simplification. This yields to the computation of the last line and column which results in

$$\begin{aligned} \text{Real Multiplies} \quad &\approx \quad N^2(L\mathcal{I}(4\mathcal{M}+3)) + 3LM^2 + L(2M+\mathcal{I}) \\ &+ \quad NL\left[\mathcal{I}(2M+1+(M-1)(4\mathcal{M}+3)+(\mathcal{I}-1)(6\mathcal{M}+5))+1\right] \end{aligned} \tag{3.23}$$

- **Implementation-b** : If the third order Volterra covariances are assimilated to a noise, only the covariance of the linear interference is computed leading to a number of real multiplications:

$$\text{Real Multiplies} \quad \approx \quad N^2 + L(2M + N + \mathcal{I}) + 3LM^2 \tag{3.24}$$

3.5.3 Averaged Low Complexity (ALC) MMSE approximation

In this second low complexity implementation, the criterion to be minimised is no longer the instantaneous MMSE, but rather an average MMSE over K symbols. The MMSE solution $\mathbf{a}_{ALC}$ thus minimizes the following MMSE:

$$(\mathbf{a}_{ALC}, b_{n,ALC}) = \arg\min_{\mathbf{a},b} \frac{1}{K} \sum_{k=0}^{K-1} E[|\hat{x}_k - x_k|^2] \tag{3.25}$$

In this case, the MMSE solution writes as:

$$\begin{aligned} \mathbf{a}_{ALC} &= \left(\frac{1}{K} \sum_{k=0}^{K-1} Cov\left(x_k, \mathbf{z}_k\right) \right) \left(\frac{1}{K} \sum_{k=0}^{K-1} Cov\left(\mathbf{z}_k, \mathbf{z}_k\right) \right)^{-1} \\ b_{n,ALC} &= E\left[x_n\right] - \mathbf{a}_{ALC} E\left[\mathbf{z}_n\right] \end{aligned} \tag{3.26}$$

Thus $\frac{1}{K}\sum_{k=0}^{K-1} Cov\left(\mathbf{x}_k, \mathbf{x}_k\right)$ becomes a diagonal matrix and can be further simplified by assuming that side effects are negligible, which results in $\frac{1}{K}\sum_{k=0}^{K-1} Cov\left(\mathbf{x}_k, \mathbf{x}_k\right) = v\mathbb{I}_N$ where $v = \frac{1}{K}\sum_{k=0}^{K-1} var(x_k)$.
As for the third order covariances matrices, it can only be shown that they have a Toeplitz structure. Thus, the matrix inversion in the MMSE solution can be efficiently performed in $O(N^2)$. The soft demapping follows the one derived for the NA-MMSE solution. As far as the computational complexity is concerned similar complexity can be found for the ALC compared to the NA solution.

3.5.4 Frequency domain turbo linear MMSE equalizer

A cyclic prefix is inserted and removed on the sides of the channel as illustrated in Figure 1.19. We are interested in the iterative MMSE solution derived in the frequency domain. To do so, let us consider the **convention 1** presented in Section 2.6.1 where a time varying solution processes a fixed block of N received symbols $\mathbf{z}_0 = [z_0, \ldots, z_{N-1}]^T$. Taking into account the notations in (2.48), the MMSE estimates write as:

$$\hat{x}_n = \mathbf{a}_n \mathbf{z}_0 + b_n \tag{3.27}$$

where the solutions $\mathbf{a}_n$ and b_n follow the expressions of (3.12). The computation of the exact MMSE solution in the frequency domain does not simplify much the computational complexity of the receiver. To illustrate such a limitation let us consider only the linear interference in the studied channel. The MMSE solutions

require then the inversion of matrix $\left(\mathbf{H}Cov(\mathbf{x}_n,\mathbf{x}_n)\mathbf{H}^H+\sigma_w^2\right)$ which does not simplify to a diagonal matrix in the frequency domain unless $Cov(\mathbf{x}_n,\mathbf{x}_n)\propto\mathbb{I}_N$. Thus, there would be only a slight enhancement of the complexity, if we consider general values of $Cov(\mathbf{x}_n,\mathbf{x}_n)$. Authors in [TuĹchler and Singer, 2011] proposed using a low complexity implementation of the MMSE solution in order to alleviate this limitation. In this section we choose to use the NA-MMSE approximation, since the ALC implementation does not allow for a diagonalization of the matrix in the frequency domain. As such, the non linear interference appears as additive white Gaussian noise with variance $\sigma_{\tilde{w}}^2=\sum_{(i,j,k)}|h_{ijk}|^2$ and the covariance of received symbols writes as:

$$C_{ZZ}\triangleq Cov(\mathbf{z}_0,\mathbf{z}_0)=\mathbf{H}\mathbf{H}^H+(\sigma_{\tilde{w}}^2+\sigma_w^2)\mathbb{I}_N \tag{3.28}$$

The NA- MMSE solution can thus be written as:

$$\hat{x}_n=\mathbf{u}_n^T\mathbf{H}^HC_{ZZ}^{-1}\left(\mathbf{z}_0-E\left[\mathbf{z}_0\right]\right)+\mathbf{u}_n^T\mathbf{H}^HC_{ZZ}^{-1}\mathbf{H}\mathbf{u}_nE\left[x_n\right] \tag{3.29}$$

Using the results in Section 1.8.1, the term $C=\mathbf{u}_n^T\mathbf{H}^HC_{ZZ}^{-1}\mathbf{H}\mathbf{u}_n$ is constant $\forall n\in\{0,\ldots,N-1\}$, and thus, the estimated symbols $\hat{\mathbf{x}}=[\hat{x}_0,\ldots,\hat{x}_{N-1}]^T$ can be written in a compacted form as follows:

$$\hat{\mathbf{x}}=\mathbf{H}^HC_{ZZ}^{-1}\left(\mathbf{z}_0-E\left[\mathbf{z}_0\right]\right)+CE\left[\mathbf{x}\right] \tag{3.30}$$

The computation of these filters can be done efficiently in the frequency domain. To do so, C_{ZZ}^{-1} is computed using the useful results on circulant matrices in Section 1.8.1 as follows :

$$\begin{aligned}C_{ZZ}^{-1} &= \left(\mathbf{F}^{-1}\left((\sigma_{\tilde{w}}^2+\sigma_w^2)\mathbb{I}_N+H_dH_d^H\right)\mathbf{F}\right)^{-1}\\ &= \mathbf{F}^{-1}C_{ZZ,d}^{-1}\mathbf{F}\end{aligned} \tag{3.31}$$

where $C_{ZZ,d}=(\sigma_{\tilde{w}}^2+\sigma_w^2)\mathbb{I}_N+H_dH_d^H$ and the inverse is obtained using the results of Section 1.8.1. It follows that the frequency estimated symbols are:

$$\hat{\mathbf{X}}\triangleq\mathbf{F}\hat{\mathbf{x}}=H_d^HC_{ZZ,d}^{-1}\left(\mathbf{Z}-E\left[\mathbf{Z}\right]\right)+CE\left[\mathbf{X}\right] \tag{3.32}$$

where $E[\mathbf{Z}]=\mathbf{F}E[\mathbf{z}]$ and $E[\mathbf{X}]=\mathbf{F}E[\mathbf{x}]$. The i^{th} soft frequency symbol $E\left[Z_i\right]$ is expressed as follows:

$$E\left[Z_i\right] = H_d(i)E\left[X_i\right]+\sqrt{N}\sum_{p=0}^{N-1}\sum_{q=0}^{N-1}\sum_{r=0}^{N-1}H_{p,q,r}^{(3)}E\left[X_pX_q\overline{X}_r\right]\delta_N(p+q+r-i) \tag{3.33}$$

The constant C can be computed using $\mathbf{u}_0=[1,\,\mathbf{0}_{1\times N-1}]^T$:

$$C = \mathbf{u}_0^T\mathbf{H}^HC_{ZZ}^{-1}\mathbf{H}\mathbf{u}_0=\mathbf{u}_0^T\mathbf{F}^{-1}\mathbf{H}_d^HC_{ZZ,d}^{-1}\mathbf{H}_d\mathbf{F}\mathbf{u}_0$$

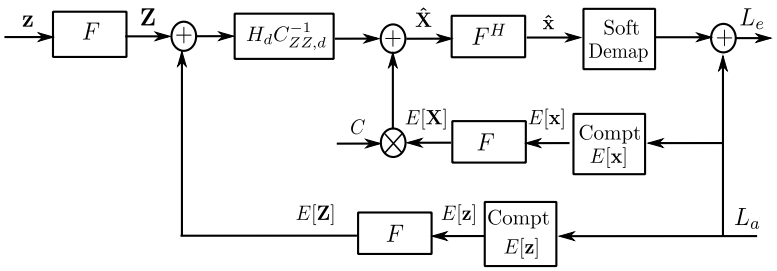

Figure 3.6: SIC MMSE turbo FDE

$$= \frac{1}{N}\sum_{i=0}^{N-1}\frac{|H_d(i)|^2}{\sigma_{\tilde{w}}^2+\sigma_w^2+|H_d(i)|^2} \tag{3.34}$$

where the factor $\frac{1}{N}$ comes from $\mathbf{u}_0^T\mathbf{F}^{-1}=\frac{1}{N}\mathbf{1}_{1\times N}$. Thus, the computation of the frequency domain equalizer yields the following estimates:

$$\begin{aligned}\hat{X}_i &= \frac{H_d^*(i)}{\sigma_{\tilde{w}}^2+|H_d(i)|^2}Z_i+\left(C-\frac{|H_d(i)|^2}{\sigma_{\tilde{w}}^2+\sigma_w^2+|H_d(i)|^2}\right)E[X_i]\\ &- \frac{H_d(i)^*}{\sigma_{\tilde{w}}^2+\sigma_w^2+|H_d(i)|^2}\sum_{p=0}^{N-1}\sum_{q=0}^{N-1}\sum_{r=0}^{N-1}H_{p,q,r}^{(3)}E\left[X_pX_q\overline{X}_r\right]\frac{1}{N^2}\delta_N(p+q+r-i)\end{aligned} \tag{3.35}$$

We recognise in (3.35) and Figure 3.6 the structure of a soft interference canceller where linear ISI $E[X_i]$ and non linear ISI $E\left[X_pX_q\overline{X}_r\right]$ terms appearing in $E\left[Z_i\right]$ are cancelled. The first line of equation (3.35) is similar to a frequency domain turbo MMSE equalizer derived for a linear channel with augmented noise equivalent to the contribution of both the channel noise and the non linear interference. However, the second line equation illustrates how a frequency domain turbo equalizer for non linear third order terms acts as a non linear soft interference canceller. It should be noted, that this soft frequency domain interference cancellation, yields to a large computational complexity, since it consists of summations over N^3 indexes (p,q,r) which clearly dramatically increases the complexity. Fortunately, these heavy computations can be lightened by computing the non linear interference in the time domain and by means of DFT, computing the corresponding non linear frequency soft interference. More specifically, let:

$$\begin{aligned}E[Z^{(3)}] &= \frac{1}{N^2}\sum_{p=0}^{N-1}\sum_{q=0}^{N-1}\sum_{r=0}^{N-1}H_{p,q,r}^{(3)}E\left[X_pX_q\overline{X}_r\right]\Delta_N(p+q+r)\\ &= F\sum_{i=0}^{M-1}\sum_{j=0}^{M-1}\sum_{k=0}^{M-1}H_{ijk}E[\mathbf{x}^{ijk}]\end{aligned} \tag{3.36}$$

where we define $\Delta_N(p+q+r)=[\delta_N(p+q+r-0),\ldots,\delta_N(p+q+r-N-1)]^T$. Computing soft non linear symbols is then less computationally complex provided that $N^3>\mathcal{I}+3N\log 2(N)$.

Soft demapper

In order to map the output of the equalizer to code LLRs, we define the residual equalizer output error $e_n = \hat{x}_n - \kappa_n x_n$. Computing the distribution of the estimation error instead of the distribution of $\hat{x}_n$ given x_n turns out to be a practical choice, since one needs not track occurrences of x_n in third order covariances in Section 3.5.2. For practical considerations, this error is assumed to be Gaussian. More precisely:

$$\begin{aligned}
\kappa_n &= Cov(\hat{x}_n, x_n) \\
&= \mathbf{u}_n^T Cov(\hat{\mathbf{x}}, \mathbf{x})\mathbf{u}_n \\
&= \frac{1}{N}\mathbf{u}_n^T \mathbf{F}^{-1} Cov(\hat{\mathbf{X}}, \mathbf{X})\mathbf{F}\mathbf{u}_n \\
&= \frac{1}{N}\mathbf{u}_n^T \mathbf{F}^{-1} C_{ZZ} Cov(\mathbf{Z}, \mathbf{X})\mathbf{F}\mathbf{u}_n \\
&= \mathbf{u}_n^T \mathbf{F}^{-1} H_d^H C_{ZZ,d}^{-1} \left(H_d \mathbf{F} Cov(\mathbf{x}, \mathbf{x})\right)\mathbf{u}_n \\
&= \mathbf{u}_n^T F^{-1} H_d^H C_{ZZ,d}^{-1} \left(H_d \mathbf{F}\left(V + (1 - v_n)\mathbf{u}_n\mathbf{u}_n^T\right)\right)\mathbf{u}_n \\
&= \mathbf{u}_n^T \mathbf{F}^{-1} H_d^H C_{ZZ,d}^{-1} H_d \mathbf{F}\mathbf{u}_n \\
&= C
\end{aligned} \tag{3.37}$$

It can be shown that the expectation of the residual error is $E[e_n] = 0$. The variance of the residual error writes as follows:

$$\begin{aligned}
var(e_n) &\triangleq Cov(e_n, e_n) = Cov(\hat{x}_n, \hat{x}_n) - |C|^2 \\
&= \mathbf{u}_n^T Cov(\hat{\mathbf{x}}, \hat{\mathbf{x}})\mathbf{u}_n - |C|^2 \\
&= \mathbf{u}_n^T \mathbf{F}^{-1} Cov(\hat{\mathbf{X}}, \hat{\mathbf{X}})\mathbf{F}\mathbf{u}_n - |C|^2 \\
&= \mathbf{u}_n^T \mathbf{F}^{-1} H_d^H C_{ZZ,d}^{-1} Cov(\mathbf{Z}, \mathbf{Z}) C_{ZZ,d}^{-1} H_d \mathbf{F}\mathbf{u}_n - |C|^2 \\
&= \mathbf{u}_n^T \mathbf{F}^{-1} H_d^H C_{ZZ,d}^{-1} \left(H_d \mathbf{F}\left(V + (1 - v_n)\mathbf{u}_n\mathbf{u}_n^T\right)\mathbf{F}^{-1} H_d^H + (\sigma_{\tilde{w}}^2 + \sigma_w^2)\mathbb{I}_N\right) C_{ZZ,d}^{-1} H_d \mathbf{F}\mathbf{u}_n - |C|^2
\end{aligned}$$

where $V = diag(v_0, \ldots, v_{N-1})$ and v_i is the covariance of the i^{th} symbol. The term $(1 - v_n)\mathbf{u}_n\mathbf{u}_n^T$ is added due to the subtraction of the contribution of symbol x_n which translates to $v_n = 1$. In the computation of the covariance of received symbols, the contribution of the non linear ISI terms was approximated by $\sigma_{\tilde{w}}^2$. This approximation was referenced as implementation-b in Section 3.5.2. The equalizer output $\hat{x}_n \sim \mathcal{N}(\kappa_n x_n, v_{e_n})$ and the output extrinsic LLR L_e^E can be computed following (3.19).

Complexity analysis

The computational complexity for a block of L frequency domain equalizer outputs can be decomposed into 4 DFT processing, to respectively compute the frequency domain received symbols $\mathbf{Z}$, the frequency domain soft symbols $E[\mathbf{X}]$ and the frequency domain non linear soft symbols and finally to compute the time domain estimated symbols. There is also need to compute the reconstructed soft interference with a complexity $(\mathcal{I}L)$ CM and $(\mathcal{I}-1)L$ CA. This results in a number of operations:

$$\text{Real Multiplies} \approx 8L\log_2(L) + 3L + \mathcal{I}L \tag{3.38}$$

Throughout this chapter, two different channel codes are considered. On the one hand, we will use rate R convolutional codes in conjunction with $8PSK$ modulations as presented in the test channel 1. On the other hand, we will investigate on the use of block LDPC codes for test channels 2 and 3. In the following, we shall present SISO decoding modules for both convolutional and block codes.

3.6 SISO MAP decoding over a trellis

Let us consider a SISO decoder with input apriori LLRs $L_a^D(c_{n,i})$ which are set from the equalizer. The deinterleaver between the equalizer and the decoder ensures that the a priori input LLRs are independent. Optimal SISO MAP decoding relies on the trellis structure of the code, and the derivations of the decoded bit probabilities can be efficiently implemented using the BCJR algorithm. Yet, since the inner code does not see channel observations, there are some changes in the derivation of the branch transition metrics. To do so, let us consider the trellis of a (L_c, R) code, where L_c designates the constraint length and R is the code rate. For illustration purposes, let us consider a binary $R = 1/N$ convolutional code. Let us also consider, there are $\mathcal{S}$ states in the code trellis. A transition from a state s_{n-1} to a state s_n occurs when $s_n = F_1(s_{n-1}, u_n)$ where F_1 is the transition function. For example for a $L_c = 3$, the memory state consists of the couple $s_{n-1} = \{u_{n-1}, u_{n-2}\}$ and $s_n = F_1(s_{n-1}, u_n) = \{u_n, u_{n-1}\}$. The transition from a state s_{n-1} to a state s_n generates a length N code $\mathbf{c}_n = [c_{n,0}, \ldots, c_{n,N-1}] \triangleq F(s_{n-1}, s_n)$. The MAP SISO decoder computes both the a posteriori probability of information bits for bit detection, and extrinsic LLR of coded bits, which are used by the SISO equalizer in the following iteration. As such, the code can be seen as two different trellises, one where branch metrics are related to transitions corresponding to the input information bits, and a second representation where the branch metrics are related to the values of trellis output coded bits. More specifically,

the MAP detection of one information bit u_n writes as follows:

$$\begin{aligned} L_{ap}(u_n) &= \log \frac{P(u_n = 0|L_a^D(\mathbf{c}))}{P(u_n = 1|L_a^D(\mathbf{c}))} \\ &= \log \frac{\sum_{s,s' \in \mathcal{S}_0^u} P\left(\sigma_{n-1} = s, \sigma_n = s'|L_a^D(\mathbf{c})\right)}{\sum_{s,s' \in \mathcal{S}_1^u} P\left(\sigma_{n-1} = s, \sigma_n = s'|L_a^D(\mathbf{c})\right)} \end{aligned} \tag{3.39}$$

where $\mathcal{S}_b^u$ designates the set of states transition where the input information bit $u = b$. Similarly, the a posteriori probability of a coded bit $c_{n,j}$ writes as:

$$\begin{aligned} L_{ap}(c_{n,j}) &= \log \frac{P(c_{n,j} = 0|L_a^D(\mathbf{c}))}{P(c_{n,j} = 1|L_a^D(\mathbf{c}))} \\ &= \log \frac{\sum_{s,s' \in \mathcal{S}_0^c} P\left(\sigma_{n-1} = s, \sigma_n = s'; L_a^D(\mathbf{c})\right)}{\sum_{s,s' \in \mathcal{S}_1^c} P\left(\sigma_{n-1} = s, \sigma_n = s'; L_a^D(\mathbf{c})\right)} \end{aligned} \tag{3.40}$$

where $\mathcal{S}_b^c$ is the set of states transitions where the j^{th} codeword $j \in \{0, \dots N-1\}$ is equal to b. The probabilities $P\left(\sigma_{n-1} = s, \sigma_n = s'|L_a(\mathbf{c})\right)$ can be efficiently computed using the BCJR algorithm which is modified for an inner code as follows:

$$P\left(\sigma_{n-1} = s, \sigma_n = s'; L_a^D(\mathbf{c})\right) = \sum_{s,s' \in \mathcal{S}_{\tilde{x}}} \alpha_n(s)\gamma_n(s,s')\beta_n(s') \tag{3.41}$$

where α_n and β_n are computed using similar recursions as in the MAP equalizer, and the transition metric γ_n is computed as follows:

$$\gamma_n(s,s') = \prod_{j=0}^{N-1} P(c_{n,j} = F_j(s,s')|L_a^D(\mathbf{c})) \tag{3.42}$$

where $F_j(s,s')$ is the j^{th} coded bit in the codeword $F(s,s')$ in the transition from s to s' codeword .

3.7 SISO LDPC decoder

Low Density Parity Check Codes are linear block codes which were first introduced by [Gallager, 1962]. At the time, LDPC Codes did not get much interest since they were too complex for the implementation. For almost the remaining of the century, successful channel coding was based on algebraic and structured codes. It is only after the advent of turbo codes in early 90's by [Berrou et al., 1993] that the LDPC codes were rediscovered by [MacKay, 1999] and gained a wide interest among the coding community. Both turbo and LDPC code brought new insights on using iterative decoding to approach Shannon limit performance. Since the last decade, numerous studies have been exclusively devoted to designing capacity approaching LDPC codes which allowed LDPC codes to be serious competitors to turbo-codes in the standardization processes.

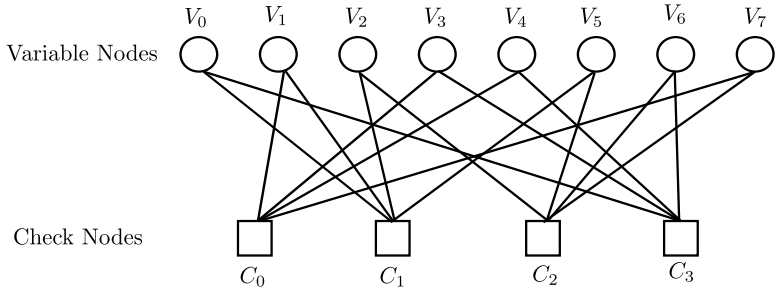

Figure 3.7: Tanner graph representation of the LDPC code matrix H where $(N = 8, d_v = 2, d_c = 4)$

3.7.1 Useful notations and definitions

A LDPC code over $GF(2^p)$ is represented by its sparse matrix H of dimension $(N - K) \times N$ where N is the codeword length and K is the information word length and $N - K$ is the parity length. The code rate $R \geq \frac{K}{N}$ with equality when the matrix is full rank. In this thesis, we are only interested in binary codes over $GF(2)$. As far as the structure of LDPC codes is concerned, the check matrix can be either regular or irregular. A regular LDPC code can be characterised by 3 parameters (N, d_v, d_c) where d_v and d_c represent the number of non zero elements per column and line respectively. The code rate thus writes as $R \geq K/N = 1 - d_v/d_c$ with equality when H is full rank. Alternative representations of LDPC relying on graphical representation have been introduced by [Tanner, 1981] using Tanner graphs and by [Kschischang et al., 2001] using factor graphs. A tanner graph is a bipartite graph consisting of edges relating two types of nodes: Variable Nodes (VN) and Check Nodes (CN). For a $N - K \times N$ parity check matrix, the corresponding tanner graph contains N variable nodes and $N - K$ check nodes. Each variable node is connected by an edge to a check node if the corresponding matrix entry is 1. As such, we can define the variable (check) node degree as the number of edges related to the variable (check) node. To illustrate how a tanner graph is constructed, let us consider the following parity check matrix H:

$$H = \begin{pmatrix} 0 & 1 & 0 & 1 & 1 & 0 & 0 & 1 \\ 1 & 1 & 1 & 0 & 0 & 1 & 0 & 0 \\ 0 & 0 & 1 & 0 & 0 & 1 & 1 & 1 \\ 1 & 0 & 0 & 1 & 1 & 0 & 1 & 0 \end{pmatrix} \tag{3.43}$$

A LDPC code represented by the matrix H is regular and the number of nodes per line and column is constant and belongs to the family of codes parametrised by the triplet $(N = 8, d_v = 2, d_c = 4)$. Figure 3.7 illustrates the Tanner graph obtained by the matrix H. It should be noted that the matrix H is only one instance of the

ensemble of LDPC matrices parametrised by $(N = 8, d_v = 2, d_c = 4)$. As such it can be seen as a realisation of a global interleaver, relating N variable nodes of degree $d_v = 2$ to $N - K$ check nodes of degree d_c. An irregular LDPC code is by definition a non-regular code. It is usually represented by a pair of polynomials:

- Variable node polynomial:
$$\lambda(x) = \sum_{i=1}^{d_v} \lambda_i x^{i-1} \tag{3.44}$$
where λ_i is the proportion of edges connected to a variable node of degree i and d_v is the maximum number of edges connected to a variable node.

- Check node polynomial:
$$\rho(x) = \sum_{j=1}^{d_c} \rho_j x^{j-1} \tag{3.45}$$
where ρ_j is the proportion of edges connected to a check node of degree j and d_c is the maximum number of edges connected to a check node.

Defining these two polynomials allows for writing the design rate of irregular codes as:

$$R = 1 - \frac{\sum_{j=1}^{d_c} \rho_j / j}{\sum_{i=1}^{d_v} \rho_i / i} \tag{3.46}$$

An alternative polynomial representation can be also derived for irregular LDPC codes consisting of the following polynomials:

- Variable nodes polynomial:
$$\tilde{\lambda}(x) = \sum_{i=1}^{d_v} \tilde{\lambda}_i x^{i-1} \tag{3.47}$$
where $\tilde{\lambda}_i$ represented the proportion of variable nodes of degree i.

- Check nodes polynomial:
$$\tilde{\rho}(x) = \sum_{j=1}^{d_c} \tilde{\rho}_j x^{j-1} \tag{3.48}$$
where $\tilde{\rho}_j$ represented the proportion of check nodes of degree j.

The equivalence between the two polynomial representations is given by:

$$\tilde{\lambda_i} = \frac{\lambda_i / i}{\sum_k \lambda_k / k} \quad \tilde{\rho}_j = \frac{\rho_j / j}{\sum_k \rho_k / k} \lambda_i = \frac{i\tilde{\lambda}}{\sum_k k\tilde{\lambda}_k} \quad \rho_j = \frac{j\tilde{\rho}_j}{\sum_k k\tilde{\rho}_k} \tag{3.49}$$

Thus, a family of irregular codes can be either parametrised by the triplet $(N, \lambda(x), \rho(x))$ or by the alternative representation $(N, \tilde{\lambda}(x), \tilde{\rho}(x))$.

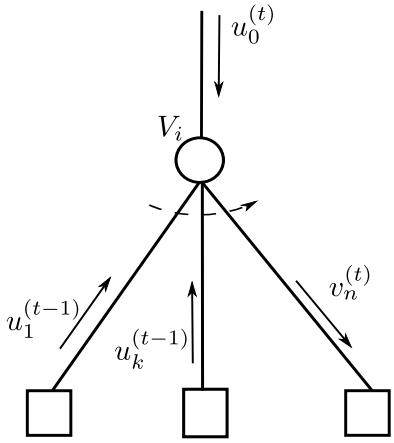

Figure 3.8: Belief propagation for a degree i VN

If the encoding process generally follows that of a block code where coded bits should satisfy the parity check matrix, decoding LDPC codes is a rather challenging issue. The next section presents an iterative decoder for LDPC codes.

3.7.2 Belief Propagation

As presented in [Gallager, 1962], LDPC codes can be decoded using a Maximum Likelihood decoder. However the computational complexity being prohibitively exponential, Gallager also investigated sub-optimal iterative decoding procedures. This iterative decoding has been investigated in [Gallager, 1962],[Tanner, 1981] and lately investigated in [MacKay and Neal, 1997] under different names: Belief Propagation (BP) or Sum Product (SP) [Chung et al., 2001]. The BP algorithm consists of passing messages between the variable and check nodes at each step of the decoding iteration, which propagates information into different parts of the Tanner graph. It can be shown that when the graph contains no cycles, the BP algorithm converges to optimal symbol decoding performance. However, for finite length LDPC codes, which are not cycle-free, the decoding algorithm is sub-optimal. However, thanks to iterative decoding, very good capacity approaching performance could be reached. The messages passed along edges of the LDPC graph, are for binary LDPC codes extrinsic LLRs computed at each variable and check node based on a local MAP criterion. To illustrate the BP decoding let us consider a variable node of degree i and its connected edges as depicted in Figure 3.8.
At iteration (t) the VN of degree i receives 1 message from the channel detector $u_0^{(t)}$ and i messages $u_k^{(t-1)}$ from the check nodes it is connected to. For each connected edge m, the VN sends an updated message v_m^t taking into account all the information it received from edges $k \neq m$. The updated message writes by Bayes

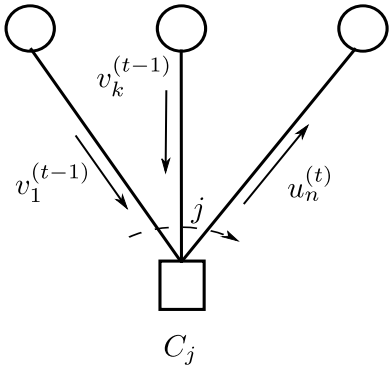

Figure 3.9: Belief propagation for a degree j CN

application $\forall m = 1 \dots i$:

$$v_m^{(t)} = u_0^{(t)} + \sum_{k=1, k\neq m}^{i} u_k^{(t-1)} \tag{3.50}$$

A parity check of degree j receives j messages $v_k^{(t)}$ and computes for each edge n, the updated message $u_m^{(t)}$ without using the incoming message from that edge $v_n(t-1)$ which yields a updating function $\forall n = 1 \dots j$:

$$\tanh \frac{u_n^{(t)}}{2} = \prod_{k=1, k\neq n}^{j} \tanh \frac{v_k^{(t)}}{2} \tag{3.51}$$

The a posteriori LLRs after L iterations are then computed using:

$$v_{app} = u_0 + \sum_{k=0}^{i} u_k^{(L)} \quad \forall n = 0, \dots, N-1 \tag{3.52}$$

3.8 Comparison of iterative equalizers

3.8.1 Complexity comparison

In order to compare the complexity of the iterative receivers derived in the previous section we make use of the following assumptions:

- The expectations of soft linear and non linear interference is available.
- The complexity for computing the Log likelihood ratios in (3.19) is not taken into account since it is a common feature between all equalizers and only depends on the modulation cardinality.

Figure 3.10 illustrates the complexity of different realisations of the turbo equalizer of the test channel 2 in Table 1.7 as a function of the feed-forward filter length N with the following parameters $\mathcal{I} = 7$, $\mathcal{M} = 16$

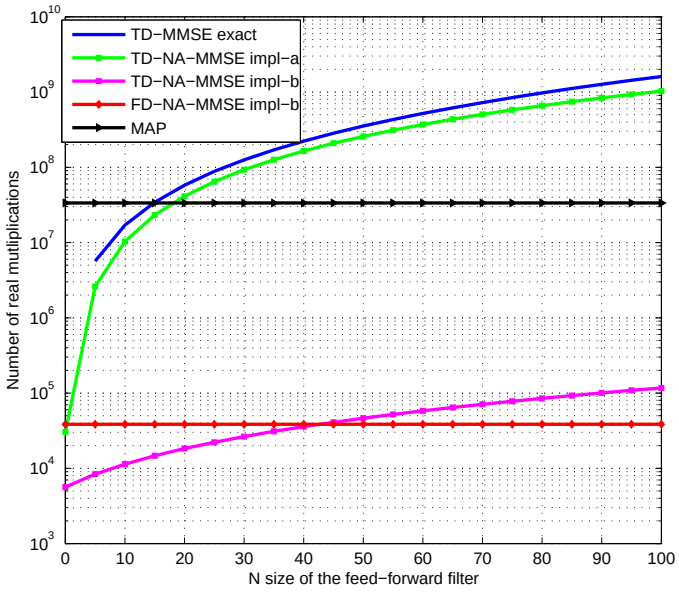

Figure 3.10: Complexity comparison for iterative receivers

(16APSK), $M = 4$ and for a block of $N = 512$ equalizers. It can be first noticed that the MMSE exact time domain equalizer yields a large complexity compared to approximated implementations. Secondly, as expected the implementation-a of the NA-MMSE is more complex than the approximation-b. Finally, the NA-MMSE in the frequency domain becomes interesting when the feed-forward satisfies $N \geq 45$.

3.8.2 Performance comparison

In order to benchmark the proposed equalizers with the literature existing results, we use the channel of the test channel 1 in table 1.7. Blocks of bits are coded using a rate 1/2 convolutional code, interleaved using a random interleaver and mapped into 8PSK symbols. The transmitted symbols are then fed to a Volterra non linear channel and at the receiver we investigated on MAP, MMSE, MMSE-NA , MMSE-ALC and FD-MMSE equalizers. The results are depicted in Figure 3.11. The performance of the iterative equalizers at the first iteration are similar since the NA-MMSE corresponds to the exact MMSE implementation when No-Apriori is available which corresponds to the first iteration. Furthermore it can be noticed that for example at $BER = 10^{-4}$ there are almost $2dBs$ gain in the ratio $\frac{E_b}{N_0}$ after the 4^{th} iteration compared to the first iteration. When comparing the NA-MMSE implementations (a) and (b), it can be noticed that due to the

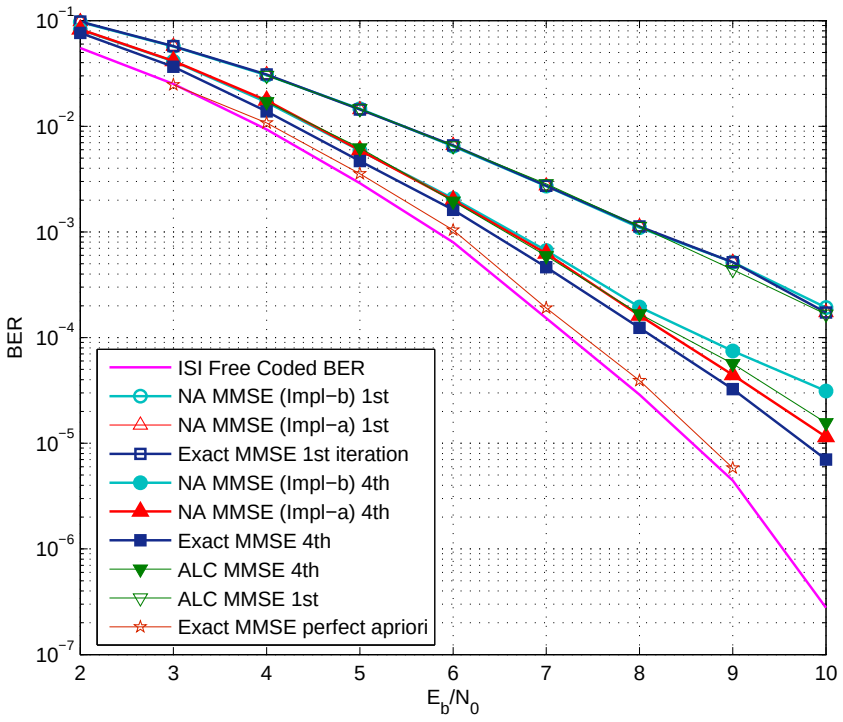

Figure 3.11: Performance comparison of the non linear channel iterative receivers

simplification of the equalizer variance computation, the performance of the implementation-a is superior to that of the implementation-b. The low complexity ALC equalizer has equivalent performance to the NA-MMSE equalizer. Finally, when the exact MMSE is fed *almost perfect* priors, it can be seen that the performance is parallel with a slight difference owing to numerical stability.

3.9 Receiver asymptotic analysis and design

In the analysis of the convergence of Soft Input Soft Output receivers, it is valuable to determine the SNR threshold beyond which the receiver converges to its limiting performance as the number of iterations increases. To do so, it is useful to track the evolution of the extrinsic LLRs exchanged between the SISO modules. Two main techniques have been proposed in the literature to evaluate the progression of the exchanged messages through iterations. The first technique which was originally proposed by [Gallager, 1963] and later by [Richardson et al., 2001], relies on the so-called *density evolution* which tracks the evolution of

the probability density functions of the LLRs at the output of a SISO decoder. This method usually provides accurate results but suffers from high computational cost since tracking the pdf yields an infinite dimensional problem. To cope with this shortcoming, authors in [Chung et al., 2001] have approximated the pdf of exchanged LLRs as Gaussian densities over the binary memoryless AWGN channel, and thus only track the mean of these Gaussian densities. Results showed that in addition to computation savings, the proposed method allows for the design of good irregular codes. A second technique introduced by [Ten Brink, 1999] uses the average mutual information between extrinsic LLRs and the transmitted symbols. The evolution of this mutual information is then represented using a *graphical tool*, the EXtrinsic Information Transfer (EXIT) chart, and allows for a fine characterisation of the decoder behaviour along iterations. In this section, we are interested in the application of EXIT chart to the prediction of convergence of the iterative equalizers for the non linear satellite channel presented in the previous section. The EXIT chart technique is not only a graphical tool for threshold estimation of a SISO module, but it also can be used to design optimised receivers where the outer LDPC code is optimized to better fit the equalizer's output. We will show later how this optimization can be carried out for $\mathcal{M}$-ary modulations and more specifically 16APSK modulations. But let us first introduce some useful notions and results on the mutual information at the output of the SISO equalizers.

3.9.1 Mutual information computation

Let us consider equally likely binary BPSK random variables $X \in \{-1, 1\}$. The mutual information between X and the corresponding LLRs L writes as:

$$I(L, X) = \frac{1}{2} \sum_{x=\pm 1} \int_{-\infty}^{\infty} p(L|x) \log_2 \left(\frac{2p(L|x)}{p(L|x=1) + p(L|x=-1)} \right) dL \tag{3.53}$$

We define two LLRs densities properties:

- Symmetry: A LLR is said to be symmetric when the random variable L satisfies: $P(L|X = 1) = P(-L|X = -1)$.

- Consistency: A LLR L satisfies the consistency condition when $P(-L|x = 1) = \exp(L)P(L|x = 1)$.

Usually, the distribution of the probability $P(L|x = 1)$ is not available, so the mutual information in equation (3.53) can be computed via numerical simulations. However, for some classes of channels interesting properties for the mutual information have bein expressed. Let us investigate these properties on the Gaussian channel.

Parameters for the J function		Parameters for the J^{-1} function	
$a_1 = -0.0421061$	$a_2 = 0.00181491$	$a'_1 = 1.09542$	$a'_2 = 0.706692$
$b_1 = 0.209252$	$b_2 = -0.142675$	$b'_1 = 0.214217$	$b'_2 = 0.386013$
$c_2 = -0.00640081$	$c_2 = -0.0822054$	$c'_1 = 2.33727$	$c'_2 = -1.75017$
$d_2 = 0.0549608$			

Table 3.1: Approximation parameters for the J and J^{-1} function

Mutual information under the Gaussian assumption

Let us consider BPSK messages x drawn form the set $\{-1, 1\}$ transmitted through a noisy Gaussian channel yielding $y = ax + w$ where a is a possible attenuation, and w is a white Gaussian noise with variance σ_w^2. The a posteriori LLRs output by a soft maximum a posteriori detector using a priori input LLR L_a writes as [Hagenauer, 2004]:

$$L_{ap}(x) = \log \frac{p(x=+1|y)}{p(x=-1|y)} = \frac{2a}{\sigma_w^2} y + L_a(x) \tag{3.54}$$

The extrinsic LLR thus are distributed following the distribution of the received symbol $y \sim \mathcal{N}(\pm a, \sigma_w^2)$ which yields $L_e \sim \mathcal{N}(\frac{\sigma^2}{2}, \sigma^2)$ where $\sigma^2 = \frac{4a^2}{\sigma_w^2}$. Additionally, the LLRs satisfy the consistency condition [Hagenauer, 2004] since:

$$p(-y|x) = \exp(-\frac{\sigma^2}{2a} xy) p(y|x) \tag{3.55}$$

Using the symmetry and consistency properties, the mutual information under the Gaussian approximation writes as:

$$I(L_e, X) = 1 - \int_{-\infty}^{\infty} p(L|x=+1) \log_2(1 + \exp(-L)) dL = J(\sigma) \tag{3.56}$$

where the expectation is with respect to L_e with distribution

$$p(L_e|x=+1) = \frac{1}{\sqrt{2\pi\sigma^2}} \exp\left(\frac{-(L_e - \sigma^2/2)^2}{2\sigma^2}\right) \tag{3.57}$$

This yields to the expression of the function J described in [ten Brink et al., 2004] which is computed using polynomial and exponential approximations (obtained by Marquard-Lavenberg algorithm), and writes as:

$$J(\sigma) \approx \begin{cases} \sigma^3 + b_1\sigma^2 + c_1\sigma & 0 \leq \sigma < \sigma^* \\ 1 - \exp(a_2\sigma^3 + b_2\sigma^2 + c_2\sigma + d_2) & \sigma^* < \sigma < 10 \\ 1 & \sigma \geq 10 \end{cases}$$

where $\sigma^* = 1.6363$ is the turning point of the curve and the approximation coefficients can be found in Table 3.1. Moreover, the inverse of the function J can be found using logarithmic and polynomial expansions as in [ten Brink et al., 2004]:

$$J^{-1}(I) \approx \begin{cases} a_1' I^2 + b_1' I + c_1' \sqrt{(I)} & 0 \leq I \leq I^* \\ -a_2' \log(b_2'(1-I)) - c_2' I & I^* < I < 1 \end{cases}$$

where $I^* = 0.3646$ and the approximation coefficients can be found in Table 3.1. It has been observed that due to the non linear processing inside the SISO decoder, the output LLRs could be well approximated using a Gaussian assumption. As such, we can consider that the equalizer input mutual information follows the expression in (3.53). The mutual information at the output of the equalizer can be computed using numerical simulations. Thus, the following scheduling is used for EXIT charts computation: Given input transmitted bits $x \in \{-1, 1\}$ and I_a value

1. Compute $\sigma = J^{-1}(I_a)$
2. Generate consistent symmetric L_a following $L_a \sim \mathcal{N}(x\sigma^2/2, \sigma^2)$
3. Compute the extrinsic equalizer L_e output given the input generated LLR L_a.
4. Numerically compute the mutual information at the output of the equalizer following expression (3.53).

Mutual information for AWGN demapper of BICM DVB-S2 constellations

It has been shown in [Hagenauer, 2004] and [ten Brink et al., 2004] that optimal detection for a gray mapped QAM constellation does not depend on the input a priori information but only depends on the SNR. Thus, there is no use iterating when demapping a gray mapped QAM Bit Interleaved Coded Modulation (BICM) over AWGN channels. In this section, we are interested in the output LLRs of the soft demapper of the coded DVB-S2 modulation constellations namely for QPSK, 8PSK and 16APSK modulations. As far as QPSK is concerned, it can be shown that the output LLRs are equivalent to the ones derived for BPSK modulated symbols. It can actually be shown that $J(\sqrt{\frac{4}{\sigma_w^2}})$ is the exact value of the mutual information where σ_w^2 is the complex noise variance. As far as higher order modulations are concerned, it can be noticed from the output LLRs that their distribution is rather a Gaussian Mixture (GM) writing as $\sum_{m=1}^{M_G} \pi_m \mathcal{N}(\beta_m \frac{\sigma^2}{2}, |\beta_m|\sigma^2)$ where $\sigma^2 = \frac{4}{\sigma_w^2}$ and σ_w^2 is the complex noise variance. In this case, the mutual information can be written as follows:

$$\Psi(\sigma) = \sum_{m=1}^{M_G} \pi_m J(\sqrt{|\beta_m|}\sigma) \tag{3.58}$$

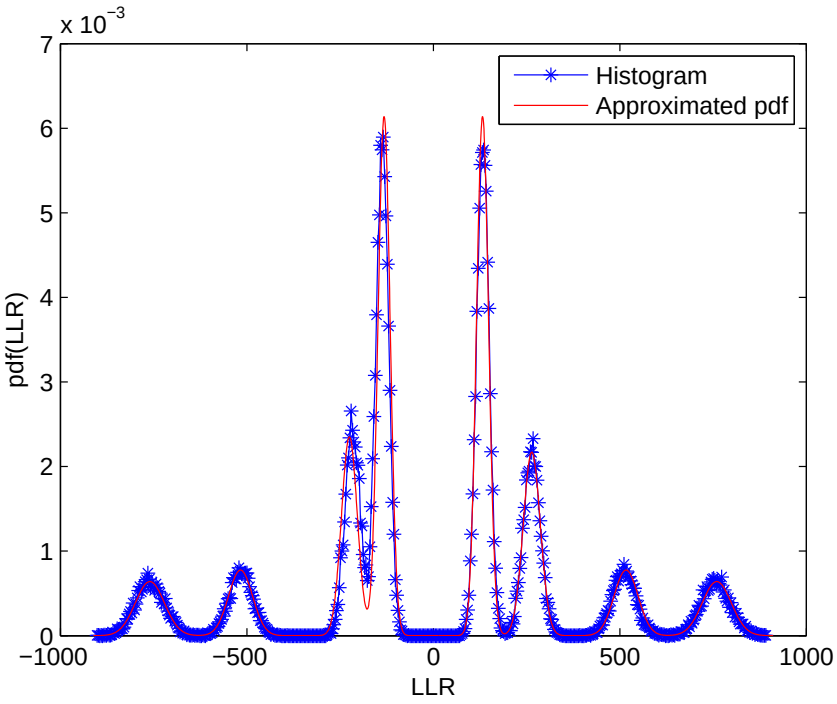

Figure 3.12: Gaussian mixture LLRs for 16APSK rate 3/4 at $E_b/N_0 = 20dB$

In general β_m and π_m depend both on the SNR and the input mutual information. For gray mapped $8PSK$ it can be noticed that the mutual information of the soft BICM demapper does not evolve much as a function of the input mutual information I_a. Moreover, from simulations we noticed that these parameters vary slightly as a function of the SNR, which thus yields to SNR independent parameters β_m and π_m.

As far as 16APSK is concerned, the mutual information depends on the ring ratios γ which was optimised in [De Gaudenzi et al., 2006] with respect to the desired coding rate. Figure 3.13 depicts the evolution of the 16APSK-BICM soft demapper for two selected coding rates $R = 1/2$ and $R = 3/4$. It can be noticed that the EXIT chart of the 3/4-16$APSK$ modulation varies slightly as a function of the input mutual information, whereas the 1/2-16$APSK$ modulation can be can be considered independent from the input mutual information for medium to high SNRs. Figure 3.12 depicts the distribution of the output LLRs of the 3/4 16APSK. Following the same approximation as for a $8PSK$ modulation, we can derive approximated Gaussian mixture parameters for the mutual information of the $16 - APSK$ BICM soft demapper using the 3/4-16$APSK$ mapping scheme. These parameters can also be considered SNR independent.

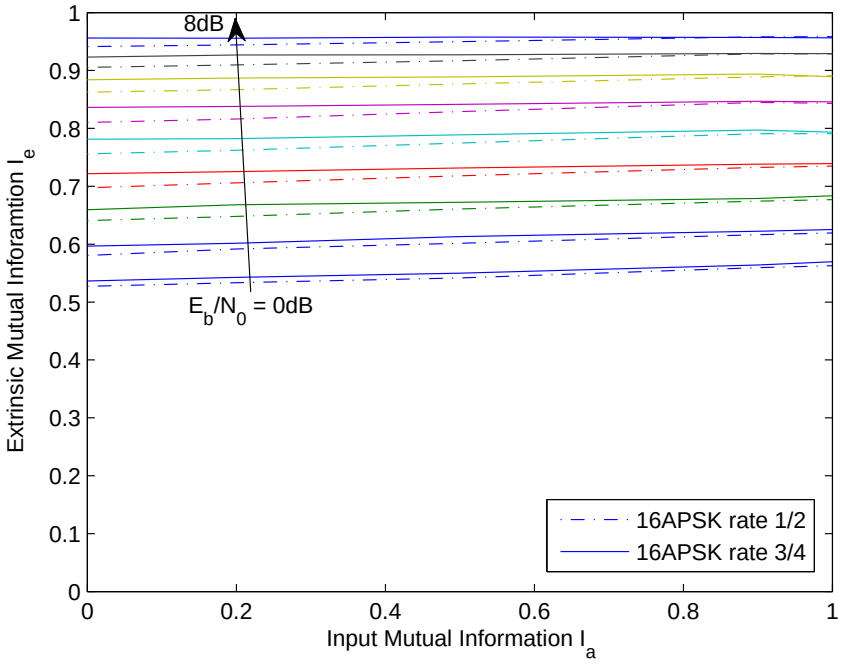

Figure 3.13: EXIT charts for the AWGN 16APSK BICM soft demapper

Table 3.2 presents the parameters π_m and β_m for the 16APSK (rate R=3/4) modulation which are computed using Gaussian Mixture fitting-based Expectation Maximisation.

Figure 3.14 plots the mutual information for the AWGN 16APSK BICM soft demapper using the Gaussian Mixture approximation which parameters are provided in Table 3.2, and different Gaussian approximations. It can be noticed that Gaussian mixture approximation provides more accurate modelling of the mutual information than the tested Gaussian approximations. Similarly we define the inverse function Ψ^{-1} which relates a mutual information to the corresponding LLR variance σ. The approximation is a non linear function of the mutual information follows the derivation of [ten Brink et al., 2004] and coefficient were computed using trust-region-reflective non linear least square fitting, after a coarse estimation of the turning point. Ψ^{-1} writes as follows:

$$\Psi^{-1}(I) = \begin{cases} a_1 I^2 + a_2 I + a_3\sqrt{I} & if\ I < 0.5936 \\ -b_1 \log(-b_2(I-1)) + b_3 I & if I \geq 0.5936 \end{cases} \tag{3.59}$$

where $(b_1, b_2, b_3) = (1.97900.69593.2484)$ and $(a_1, a_2, a_3) = (3.8533 - 0.07384.0560)$. Figure 3.15 depicts the obtained Ψ and Ψ^{-1} functions using the above approximations.

8PSK $M_G = 4$	16 APSK $M_G = 8$	
$-\beta_1 = \beta_4 = 1$	$\beta_5 = -\beta_4 = 0.33$	$\beta_6 = -\beta_3 = 0.66$
$-\beta_2 = \beta_3 = 4sin(\pi/8)^2$	$\beta_7 = -\beta_2 = 1.29221$	$\beta_8 = -\beta_1 = 1.9$
$\pi_1 = \pi_4 = 1/6$	$\pi_5 = \pi_4 = 0.25$	$\pi_6 = \pi_3 = 0.125$
$\pi_2 = \pi_3 = 1/3$	$\pi_7 = \pi_2 = 0.0625$	$\pi_8 = \pi_1 = 0.0625$

Table 3.2: Gaussian Mixture parameters

Mutual information of MAP and MMSE equalizers

The output extrinsic of a SISO detector writes in general as a function of the SNR and the input mutual information as follows:

$$I_e = \mathcal{T}(I_a, SNR) \tag{3.60}$$

Figure 3.16 plots the obtained EXIT charts of the MAP, MMSE and MMSE-NA-implementation-b equalizers. It can be seen, that the MMSE equalizer starts at equivalent performance as the No-Apriori implementation, which is normal since both solutions are equivalent in the first iteration. But, while the MMSE tends assymptotically to almost ISI free performance, the No-Apriori solution suffers from residueal ISI which prevents it from reaching quasi-ISI free performance. At perfect apriori information, the MAP equalizer approaches the mutual information of a 16APSK BICM AWGN soft demapper. The convergence of MAP detection has been proven in [Sellami et al., 2008] where it is demonstrated that at perfect apriori information, the MAP equalizer tends to ISI free performance.

3.10 Asymptotic code design using EXIT charts

Let us consider the following convention: $I_{X,Y}$ and $L_{C,V}$ are the mutual information and LLRs exchanged between X and Y where $X \in \{E, V, C\}$ where E stands for the equalizer, V for variable nodes and C for check nodes. The EXIT curve of the equalizer plots for a given SNR, $I_{E,V} = T(I_{V,E}, SNR)$, where T is a non-decreasing function. For ease of notation this function will be abused to $I_{E,V} = T(I_{V,E})$ and the SNR is assumed to be constant over the optimisation process. These EXIT charts are also exploited in finding an upper bound to the achievable rate of the iterative receiver. The upper bound, is given by the so called *area theorem* [Hagenauer, 2004] which states that for serially concatenated codes in a Binary Erasure Channel (BEC), the achievable rate R of the outer code, is upper-bounded by the integral of the inner code transfer curve T i.e. $R \leq \int_0^1 T(I)dI$ when the latter is a rate 1 code. It is widely observed that this upper bound is a

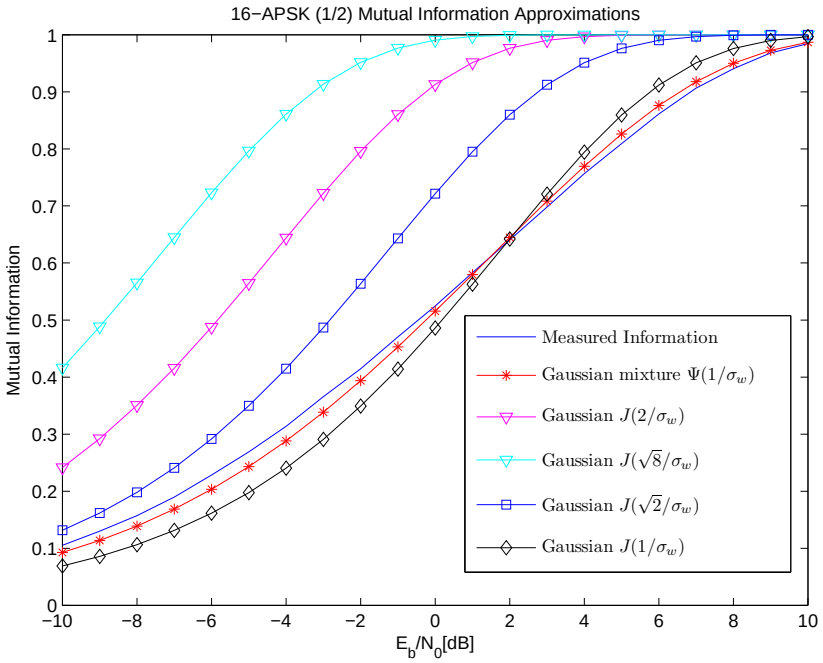

Figure 3.14: Mutual Information for the 16APSK-BICM soft demapper using different approximations

good approximation for other channel models including the Gaussian and ISI channels.

The optimization of the iterative receiver requires tracking the evolution of the variance or equivalently expectation of the exchanged mutual informations. The mutual information at the output of the equalizer consists of a Gaussian mixture which parameters π_m and β_m evolve depending on the input a priori information. Thus for each SNR and each value of the input mutual information, one needs to computed the parameters of the Gaussian mixture, which clearly induces large complexity. A possible solution to this problem is to consider a reference mixture of Gaussians which will serve as a projection law for the equalizer output mutual information. Since optimally and at perfect a priori, the equalizer output joins that of the AWGN-BICM soft demapper, we will take this Gaussian mixture as the reference distribution.

In order to optimize the LDPC code for a given receiver structure, the mutual informations at the input and output of the equalizer, variable and check nodes are evaluated. The objective is to optimize the edge-degree distribution polynomials $\lambda(X)$ and $\rho(X)$ in order to achieve the highest rate under some set of constraints.

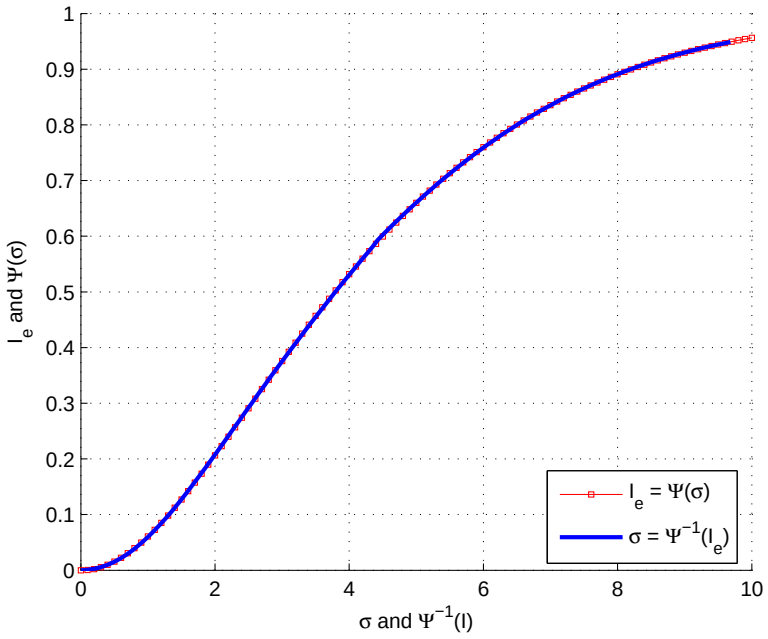

Figure 3.15: The function $\Psi(\sigma)$ and its inverse $\Psi^{-1}(I_e)$ for 16-APSK BICM

3.10.1 Iterative receiver scheduling and interleaver assumptions

We will assume that Belief Propagation (BP)-based LDPC decoding is used. Besides, equalization is assumed to be run independently on each group delimited by a partial interleaver i.e. transition effects are neglected. In order to optimize the iterative receiver, the following scheduling will be used: a global iteration t is composed of one pass in the equalizer followed by one BP iteration (one data-pass plus check-pass update) in the LDPC decoder. We further assume partial interleaving Π_p *between the channel equalizer and the LDPC code* operated degree-wise, i.e. each partial interleaver is associated with the VNs of the same degree. The assumption is similar to [ten Brink et al., 2004] and ensures an efficient linear optimization problem solving. Furthermore, and for independence considerations, a global interleaver Π_{LDPC} is assumed between check and variable nodes as depicted in Figure 3.18 representing the classical code ensemble interleaving.

3.10.2 Code optimization

Let us now compute the average mutual information for the afore-described receiver scheduling.

At iteration t:

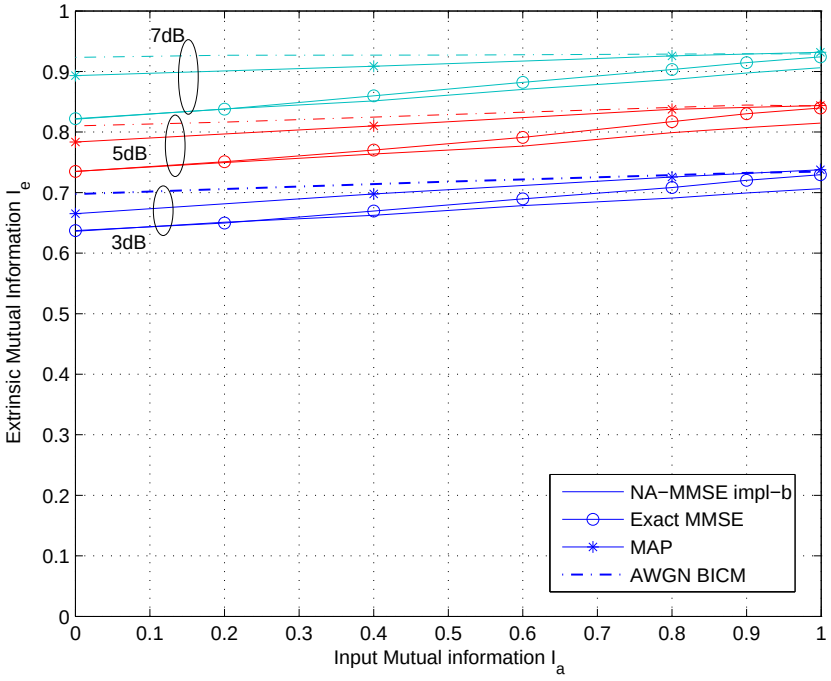

Figure 3.16: Mutual Information for the 16APSK-BICM MAP and MMSE equalizers for test channel 2

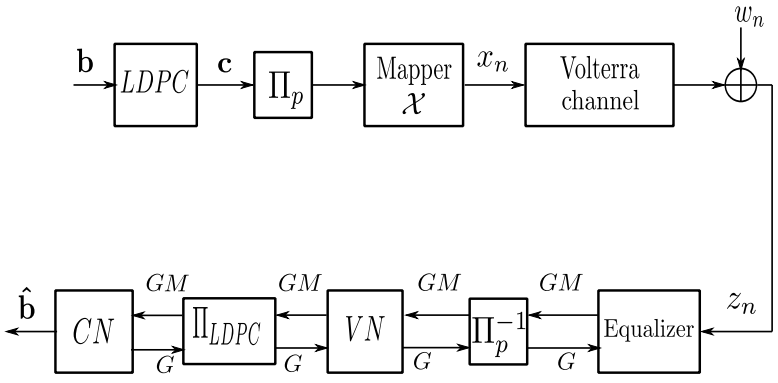

Figure 3.17: Global scheme of a satellite communication channel. GM stands for quantities with a Gaussian Mixture approximation, G for Gaussian approximation

1. A variable node V of degree i receives $(i+1)$ LLR messages namely i check nodes LLRs $L_{C,V}^{t-1}$ following

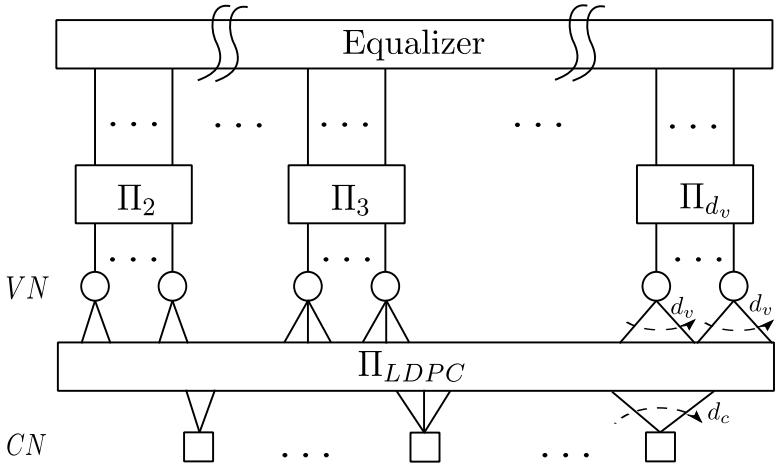

Figure 3.18: Partial and ensemble interleaving

a Gaussian distribution, and the equalizer extrinsic LLR $L^t_{E,V}$ following a GM distribution. It computes then the output LLR $L^t_{V,C}$ on the branch n:

$$L^t_{V,C}(n) = L^t_{E,V} + \sum_{k\neq n, k=1}^{i} L^{t-1}_{C_k,V} \tag{3.61}$$

The resulting LLR follow a GM distribution which is the convolution of a Gaussian and a GM distribution. More specifically,

$$I^t_{V,C}(i) = \sum_{m=1}^{M_G} \pi_m J\left(\sqrt{\beta_m \Psi^{-1}\left(I^t_{E,V(i)}\right)^2 + (i-1)J^{-1}\left(I^{t-1}_{C,V}\right)^2}\right) \tag{3.62}$$

where $I^t_{E,V(i)} = T\left(I^{t-1}_{V,E}(i)\right)$. Thus, the overall variable nodes output mutual information $I^t_{V,C}$ is expressed as follows:

$$I^t_{V,C} = \sum_{i=2}^{d_v} \lambda_i I^t_{V,C}(i) \tag{3.63}$$

It is worth noting that by taking $M_G = 1$, $\beta_m = 1$ and $\pi_m = 1$, equation (3.62) simplifies to the Gaussian approximation in [ten Brink et al., 2004].

2. A check node C of degree j receives j variable nodes LLRs. The output LLR at an edge m is computed by a non linear combination of the input messages as in (3.51):

$$L^t_{C,V}(m) = 2\tanh^{-1}\left(\prod_{k\neq m}^{j} \tanh\left(\frac{L^{t-1}_{V_k,C}}{2}\right)\right) \tag{3.64}$$

The characterisation of the pdf of the output check node LLR is not straightforward. However, by using a consistent Gaussian approximation, one can compute the mean of the output LLR and project it on the right mutual information [Narayanan et al., 2005]. Yet, a simpler efficient approximation named *reciprocal channel* can be used [ten Brink et al., 2004]. Thus, the mutual information of the check node is expressed as:

$$I_{C,V}^{t} = 1 - \sum_{j=2}^{d_c} \rho_j J\left(\sqrt{j-1} J^{-1}\left(1 - I_{V,C}^{t}\right)\right) \tag{3.65}$$

3. A variable node V of degree i computes the extrinsic LLR to be forwarded to the equalizer as apriori information $L_{V,E}$ as follows:

$$L_{V,E}^{t}(i) = \sum_{k=1}^{i} L_{C_k,V}^{t} \tag{3.66}$$

Thus, the associated mutual information for a variable node of degree i writes as:

$$I_{V,E}^{t}(i) = J\left(\sqrt{i} J^{-1}\left(I_{C,V}^{t}\right)\right) \tag{3.67}$$

Combining equations (3.62), and (3.63), and (3.65), and (3.67), the variable to check node information at iteration t, $I_{V,C}^{t}$, writes in a parametric recursive way as:

$$I_{V,C}^{t} = \mathcal{G}\left(\lambda(X), I_{V,C}^{t-1}, \rho(X), T()\right) \tag{3.68}$$

This function is non linear in the mutual information $I_{V,C}$, $\rho(X)$ but linear in the variable node-degree distribution polynomial $\lambda(X)$ for fixed values of the aforementioned parameters. Thus, by fixing a distribution $\rho(X)$, which is generally considered with concentrated degrees, optimization consists of maximizing $\sum_i \lambda_i / i$ subject to the following constraints:

$$\begin{cases} \textit{Convergence} & \mathcal{G}(\tilde{\lambda}, x, \rho, T(.)) \geq x \\ \textit{Proportions} & \sum_{i=2}^{d_v} \lambda_i = 1 \\ \textit{Stability} & \lambda_2 \sum_{m=0}^{M_G} \pi_m e^{\beta_m \Psi^{-1}(T(1))/8} < \frac{1}{\sum_{j=2}^{d_c} \rho_j (j-1)} \end{cases}$$

For 16-APSK, $T(1) = \Psi\left(\sqrt{\frac{4||h||.^2}{\sigma_w^2}}\right)$ where $||h||^2$ is the channel energy.

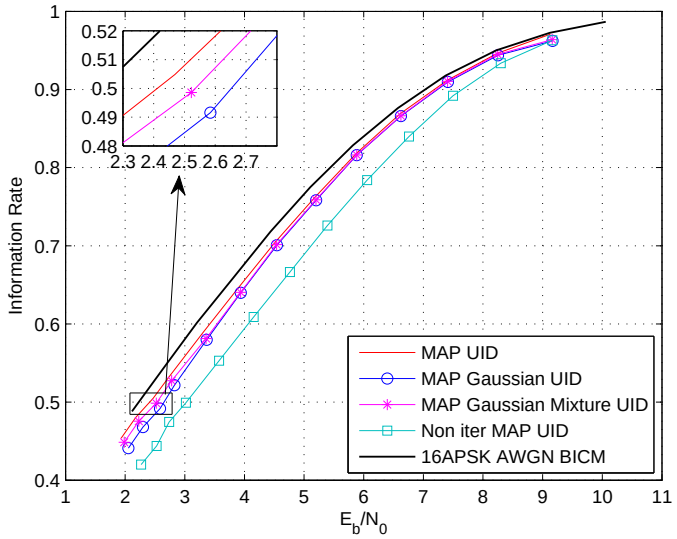

Figure 3.19: Achievable designed rates compared with the MAP optimal equalizer and the 16-APSK ISI-free rates for a maximum $d_v = 10$ over the test channel 2

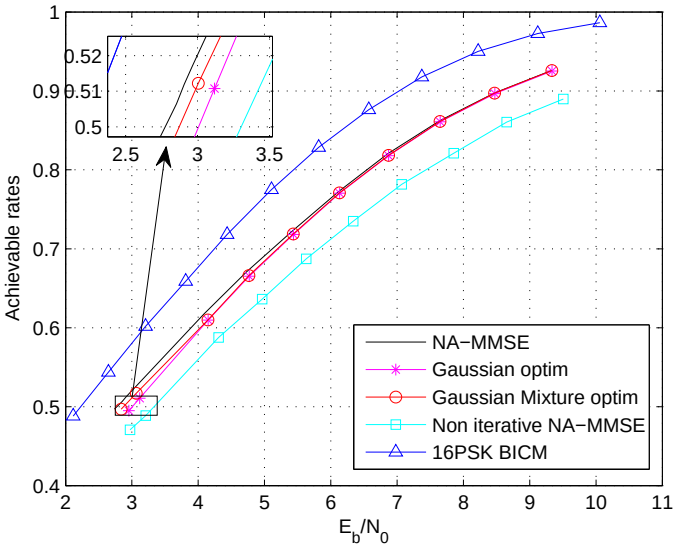

Figure 3.20: Achievable designed rates compared with the NA-MMSE equalizer and the 16-APSK ISI-free rates for a maximum $d_v = 10$ over the test channel 2

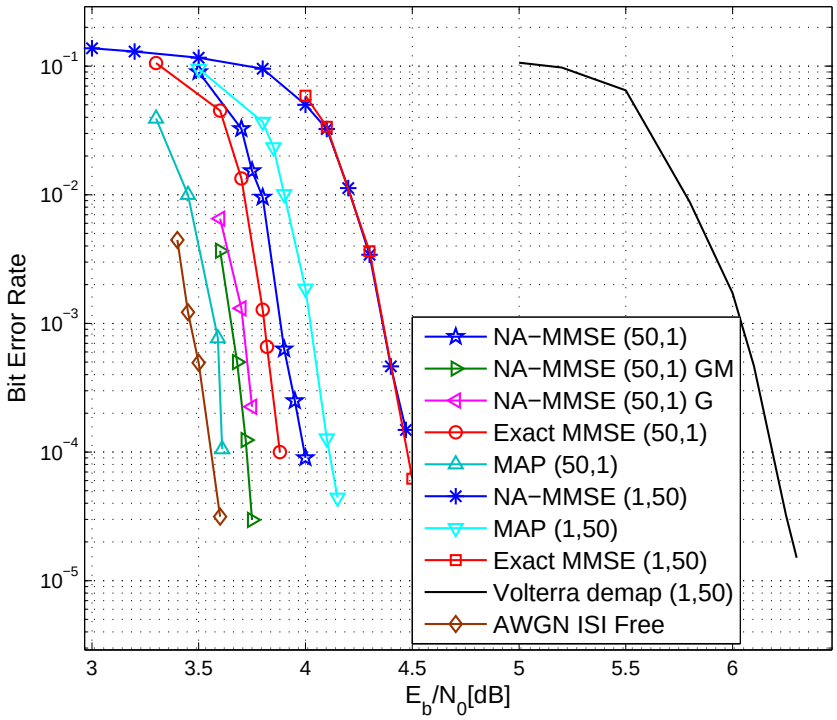

Figure 3.21: Bit error rate for the iterative receivers and the optimized LDPC code

3.10.3 Optimization results

Design rates

In this section, we present optimization results obtained for a MAP turbo equalizer over the channel 2. Figure 3.19 plot the approximation on achievable rates of both the 16-APSK BICM, computed using the EXIT area theorem of a soft demapper over AWGN channel, and the MAP equalizer computed also using the area integral. Figure 3.20 plots the comparison between optimized NA-MMSE rates and the BICM rate. Both figures also plot the optimized rates, using both the Gaussian [ten Brink et al., 2004] and the Gaussian mixture approximations previously derived. On the one hand, it can be noticed that the iterative designed receivers achieve gains of $0.5dB$ over the non iterative MAP equalization for the non linear channel and $0.3dB$ using the NA-MMSE equalizer.

On the other hand, the designed receiver using the Gaussian mixture approximation achieves a theoretical gain of $0.1dB$ over the Gaussian approximation both for the MAP and $0.15dB$ for the NA-MMSE equalizer.

Bit Error Rate performance

For our simulations, we considered the short frame lengths introduced in DVB-S2 where $N_{LDPC} = 16200$. The rate 1/2 DVB-S2 and designed codes was used. Figure 3.21 plots the Bit Error Rate of some of the optimal and sub-optimal receivers, along with the designed No-Apriori optimized codes performance. The following conventions are used for legends:

- The notation (A,B) designates A iterations between the equalizer and the decoder and B internal decoder iterations for each of the turbo-iteration.
- Unless otherwise specified, the channel code used is the DVB-S2. The GM notation designates codes optimized following the Gaussian Mixture approximation and G stands for the Gaussian approximation.

In order to investigate the gain achieved with iterative equalization, we also present the performance of the so-called Soft Volterra demapper. This demapper assimilates the linear and non linear Volterra kernels to additive noise. In other words, the demapped symbols probabilities write as:

$$P(x_n = \tilde{x}) \propto \exp(\frac{|z_n - h_0\tilde{x}|^2}{\sigma_w^2 + \sigma_v^2}) \tag{3.69}$$

where $\sigma_v^2 = \sum_{i=1}^{M-1} |h_i|^2 + \sum_{i,j,k} |h_{i,j,k}|^2$ is the overall Volterra interference power and σ_w^2 is the noise power. Results show that at least a gain of $1.8dB$ is achieved when using non iterative equalization for the Volterra channel. The achieved gain for the $(50, 1)$ MAP turbo equalizer over the Volterra demapper is about $2.8dB$. The comparison between iterative and non iterative implementations of the equalizers shows that equalizing with parameters $(50, 1)$ outperforms for the same equalizer the $(1, 50)$ configuration. It is interesting to note that 50 iterations of linear equalizers with only 1 LDPC pass performs better than the non iterative MAP equalizer (1,50). Furthermore, optimizing the code yields even better performance. Indeed, for a code optimized for the No-Apriori equalizer, a gain of $2.5dB$ is achieved over the Soft Volterra demapper. A slight improvement between the Gaussian and Gaussian mixture approximation designed codes is observed. In a nutshell, code optimization along with low complexity iterative receivers can offer very satisfying performance as well as reasonable complexity.

3.11 Conclusions

In this chapter, we presented iterative receivers for the non linear satellite channels. First, we derived optimal and sub-optimal non linear and linear SISO equalizers in the time and in the frequency domain. We compared their performance and their complexity and showed that the NA-MMSE implementation yields a low

complexity receiver along with interesting error rate performance. In a second part, we analysed the EXIT charts of DVB-S2 constellations for both BICM-AWGN scenario and MAP and MMSE receivers over the non linear channel. We showed that unlike binary modulations, the LLRs at the output of the SISO detector can be efficiently modelled as a Gaussian Mixture instead of the Gaussian approximation. This analysis has enabled the design and optimization of the outer LDPC code, where edge-polynomials were optimised using the Gaussian Mixture approximation. The results show an improvement of error rates when compared to non optimized channel codes.

3.12 Conclusions (French)

Dans ce chapitre, nous avons présenté des récepteurs itératifs pour les canaux non linéaires satellites. Dans un premier temps, nous avons dérivé des expressions optimales et sous-optimales de récepteurs itératifs tant dans le domaine temporel que fréquentiel. Ensuite nous avons comparé les performances de ces récepteurs ainsi que leur complexité et avons montré que l'approximation 'Sans Apriori' donnait lieu à un récepteur moins complexe tout en offrant des performances en taux d'erreurs binaires intéressantes. Dans un second temps, nous avons analysé les courbes dites EXIT de certaines constellations DVB-S2 pour la BICM sur un canal AWGN ainsi que les égaliseurs MAP et MMSE itératifs pour le canal non linéaire. Nous avons montré, que contrairement aux modulations binaires, les sorties LLRs extrinsèques des détecteurs SISO peuvent être modélisées de manières plus précises sous forme de mélange de Gaussiennes au lieu d'une approximation Gaussienne. Ceci nous a permis d'analyser et d'optimiser le code canal externe LDPC dont les polynômes de branches ont été optimisés en utilisant cette approximation en mélange de Gaussiennes. Les résultats démontrent qu'il y a une amélioration des performances en terme de taux d'erreurs en comparaison avec des codes non optimisés.

Chapter 4

SC-OFDM in satellite communications

Contents

4.1 Introduction

In the previous chapters we addressed the issue of mitigating the non linear interference resulting from using high order modulations such as 16APSK with non linear amplifiers. In this chapter, we are interested in an additional aspect of increasing the throughput per bandwidth through occupying as much as possible the IMUX and OMUX bandwidths even in their frequency selective regions. This implies that the IMUX and OMUX responses have longer time impulse responses. A possible way to counteract the complexity of time domain processing of this increased interference is using frequency domain equalizers. In this context, Single Carrier Orthogonal Frequency Division Multiplexing (SC-OFDM) offers interesting low complexity frequency domain equalization abilities along with simple and flexible generation of the transmitted waveforms. To illustrate these features, we will first present a general frequency domain description of the SC-OFDM system and show how it can be expressed as a time domain circular convolution. We will then investigate on the spectrum characteristics of the SC-OFDM waveform and derive analytical expressions of its power spectral density. Then, we will apply linear equalization methods and by means of analytically derived SINR formulas we will assess the theoretical and experimental error rates performance.

4.2 Introduction (French)

Dans les chapitres précédents, nous avons étudié les méthodes de réduction des interférences non linéaires issues de l'utilisation de modulations d'ordre élevé avec des amplificateurs non linéaires. Dans ce chapitre, nous nous intéressons à un aspect supplémentaire de l'augmentation de l'efficacité spectrale au travers de la maximisation de l'utilisation de la bande des filtres multiplexeurs IMUX et OMUX même dans leur zone de forte sélectivité en fréquence. Ceci implique que les réponses impulsionnelles des IMUX et OMUX deviennent très longues. Une manière de palier l'augmentation de la complexité des traitements temporels de cette interférence est l'utilisation de l'égalisation fréquentielle. Dans ce contexte, les formes d'onde de type SC-OFDM offrent une égalisation fréquentielle à faible complexité ainsi qu'une génération plus simple et flexible des signaux transmis. Afin d'illustrer ces avantages, nous présenterons dans un premier temps le système SC-OFDM fréquentiel et démontrerons qu'il est équivalent à une convolution circulaire dans le domaine temporel. Nous nous intéresserons ensuite aux caractéristiques spectrales de la forme d'onde SC-OFDM et dériverons des expressions analytiques de sa densité spectrale de puissance. Finalement, nous appliquerons des méthodes d'égalisation linéaire et, en utilisant des formules dérivées du rapport signal à bruit et interférences, nous prédirons les performances en termes de taux d'erreurs.

4.3 SC-OFDM

To satisfy the increasing demand for high data rates, the Third Generation Partnership Project (3GPP) has proposed using single and multi-carrier transmission schemes in the Long Term Evolution (LTE) namely Orthogonal Frequency Division Multiple Access (OFDMA) and Single Carrier Frequency Division Multiple Access SC-FDMA. As far as the downlink is concerned, high data rates yield increased frequency selectivity of the transmission channel which calls for using multi-carrier transmission schemes such as OFDMA. However, multi-carrier communications suffer from a high Peak to Average Power Ratio (PAPR). Thus using OFDMA in an uplink mobile communication system would yield a low energy efficiency of User Equipments (UE) which are usually constrained in terms of power consumption. Yet, by means of DFT-precoding of OFDMA, SC-FDMA [Myung et al., 2006] has single carrier characteristics in terms of signal dynamics and thus has lower PAPR than OFDMA which made it a better candidate for the uplink transmission scheme for LTE systems. It can be noted that calling a SC-FDMA system as a *DFT-precoded* OFDMA may lead to some misunderstanding towards the nature of the transmitted signal. SC-FDMA is a single carrier transmission scheme, since because of (or thanks to) the DFT precoding, each symbol is transmitted over the whole signal bandwidth which explains why it is not a multi-carrier system.
As far as satellite applications are concerned, authors in [Gallinaro et al., 2012] have investigated the use of SC-FDMA in the return link of a satellite communication scheme, coping with the issue of power limitations of user equipments on the return link. In this chapter, we are interested in using SC-FDMA as a forward link technology for broadcast satellite systems. As such, it is more convenient to use the term Single Carrier-Orthogonal Frequency Division Multiplexing (SC-OFDM), since the broadcast transmission relies rather on multiplexing than multiple access. The ongoing "Enabling Next GeneratIon NEtworks for broadcast Services (ENGINES)" project [ENG,] is investigating on using SC-OFDM in the DVB-Next Generation Handheld (DVB-NGH) [Gomez-Barquero et al., 2014]. The DVB-NGH [Gómez-Barquero, 2013] standard uses both satellite and mobile network infrastructures in order to improve the system coverage. The stakes in the standardisation of the DVB-NGH physical layer lie in two key elements. On the one hand, the proposed waveforms need to have good power efficiency and low envelope fluctuations to meet satellite amplifiers requirements. On the other hand, efficient equalization techniques have to be used to cope with the selectivity of the terrestrial mobile channel.

In our study, the frequency selectivity does not stem from the mobile channel as in the DVB-NGH but rather from the interference due to using the IMUX and OMUX in their frequency selective regions. In order to illustrate this increase in the selectivity, let us consider the IMUX/OMUX frequency responses for

Symbol Rate roll-off α	$\alpha = 0.1$	$\alpha = 0.2$	$\alpha = 0.05$
$R_s = 27.5Mbauds$	18	12	24
$R_s = 30Mbauds$	19	11	30

Table 4.1: Values for the over-all channel number of symbol spaced taps

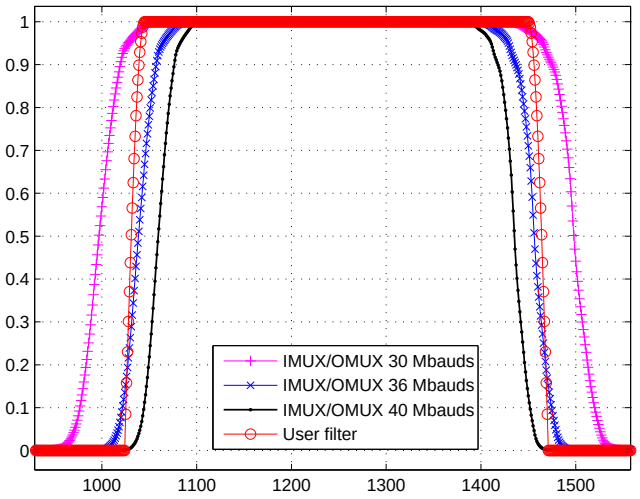

Figure 4.1: IMUX/OMUX responses for different symbol rates

different signal rates. It can be noted that the larger the signal rate, the more selective the IMUX/OMUX response. Table 4.1 presents the number of dominant (90 % of the overall energy) symbol-spaced taps of the overall raised cosine and IMUX and OMUX filter responses for different signal rates (thus shaping roll-offs) at a given bandwidth. It can be noticed that the larger the symbol rate, the longer the overall impulse response.

Notations: In the following, the term A-FFT (resp. B-IFFT) designates a FFT over A points (resp. IFFT over B points). Time domain (resp. frequency domain) variables are represented by lower (resp. upper) case letters. The FFT (resp. IFFT) operator applied to time domain symbols x_n (resp. frequency domain symbols X_k) of length L write as follows:

$$x_n \quad = \quad \text{L-IFFT}(X_k) = \frac{1}{L}\sum_{p=0}^{L-1} X_p \Omega_L^{pn}$$

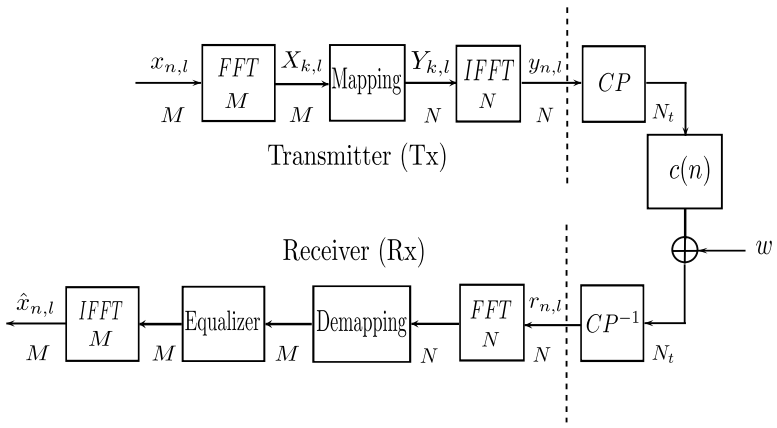

Figure 4.2: SC-FDMA and SC-OFDM frequency based representation

$$X_k \quad = \quad \text{L-FFT}(x_n) = \sum_{p=0}^{L-1} x_p \Omega_L^{-pk}$$

The notation $(.)_{k,l}$ indicates the symbol on the k^{th} sub-carrier for the l^{th} time domain symbol and $\Omega_L^k = \exp(j2\pi k/L)$.

4.3.1 Frequency based SC-OFDM scheme description

Consider the scheme depicted in Figure 4.2. Blocks of M independent zero mean and identically distributed symbols $x_{n,l}$ at a rate R_s are converted to frequency domain symbols $X_{k,l}$ by an M-FFT, then mapped into M out of N sub-carriers before being converted back to the time domain by an N-IFFT. In order to cope with the frequency selectivity of the channel $c(n)$, a Cyclic Prefix (CP) of length N_g is appended to the resulting time domain symbols to build the SC-OFDM symbol of length $N_t = N + N_g$. This results in simplified equalization at the receiver, thanks to the circularity of the channel matrix due to the CP. Even though the CP is a part of the transmitter processing, it is integrated in the channel part in Figure 4.2 since it is used for channel circularity. The signal is then affected by an additional Gaussian circular noise w with variance σ_w^2. At the receiver, after CP removal, symbols are transformed into frequency domain symbols using a N-FFT. The sub-carriers are then demapped in order to extract the corresponding user data symbols. A frequency domain equalizer is then used to cope with channel impairments. The obtained frequency symbols are converted back to the time domain using a M-IFFT. Two principal schemes have been proposed for SC-FDMA to map the M frequency symbols into the N available sub-carriers, namely Localised and Interleaved mappings. In the localised mapping, the user is assigned a group of contiguous sub-carriers, whereas in the Interleaved or

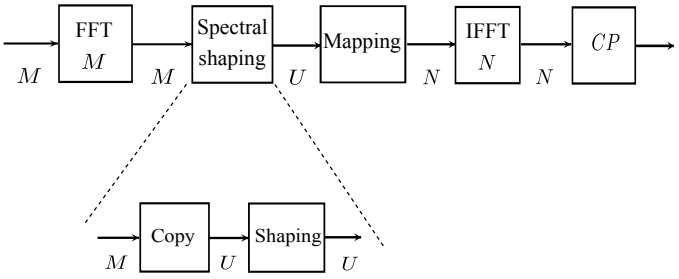

Figure 4.3: EW-SC-OFDM transmission scheme

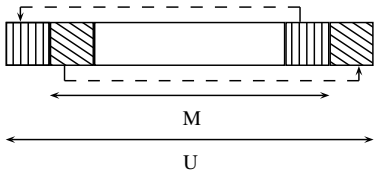

Figure 4.4: Exteding from a length M to $U \leq 2M$

Distributed mapping, the user sub-carriers are evenly spaced. Unlike SC-FDMA, only the localised scheme is used in SC-OFDM since the objective is to map the $M \sim N$ outputs to the N IFFT inputs. Thus, it is assumed that the M-FFT outputs $X_{k,l}$ are directly placed into the middle a block of contiguous N-IFFT inputs.

4.3.2 Extended Weighted SC-OFDM

Many of the OFDMA PAPR reduction techniques can be applied to SC-OFDM and SC-FDMA more generally as a special case of *precoded OFDMA* [Han and Lee, 2005] [Danilo-Lemoine et al., 2007]. Among the family of time domain solutions, authors in [Azurdia-Meza et al., 2008] proposed parametric linear pulse shapes which are Nyquist-shapes having lower PAPR than raised cosine pulse shaping.

The second family relies on frequency domain precoding or spectral shaping [Slimane, 2007], [Falconer, 2011], and [Yuen and Farhang-Boroujeny, 2012]. In [Slimane, 2007], raised cosine frequency shapes were investigated at the cost of decreased spectral efficiency. In [Falconer, 2011], Falconer presented a linear frequency precoding window which (numerically) minimizes the variance of the instantaneous output power but induces a slight noise enhancement. In contrast, authors in [Yuen and Farhang-Boroujeny, 2012] proposed a mathematical model of the PAPR reduction problem and derived new optimized windows using Lagrangian multipliers. These frequency windows optimized with the Compensation of Noise Enhancement Penalty (CNEP) reduce

the PAPR and improve the system performance in terms of Bit Error Rate (BER).
In this section, we are interested in the so-called Spectrum Shaped SC-OFDM [Mauritz and Popovic, 2006] or equivalently known as Extended Weighted SC-OFDM (EW-SC-OFDM). The idea behind EW-SC-OFDM lies in applying a frequency window between the FFT and IFFT in order to lower the side-lobes of the resulting time domain generated waveform. The window length can either be equal to the symbol length or larger e.g. root raised cosine window. If the extended length U of the spectrum shape is not larger than M, then the shaping will only consist of an element wise multiplication with the shaping window. However, if the length of the window shape exceeds the number of M-FFT outputs (i.e. $U > M$), then the number of frequency symbols needs to be increased by the so-called copying block [Kawamura et al., 2006] which is referred to as extension in EW-SC-OFDM. The transmitted symbols are thus *extended* to reach the excess bandwidth characterised by a roll-off and *weighted* by the window values. Figure 4.3 depicts the principle of EW-SC-OFDM. The extension consists of appending both a cyclic prefix and suffix to the M-FFT symbol until the desired length U is reached as depicted in Figure 4.4.
To assess the signal fluctuation of the single carrier SC-OFDM, EW-SC-OFDM and OFDM, the following (but non-exhaustive) metrics can be used:

- the Peak to Average Power Ratio which characterises the excursion of the maximum power with respect to the average power as [Ciochina et al., 2008]:

$$PAPR = \frac{\max\limits_{t}(|x(t)|^2)}{E[|x(t)|^2]} \sim \frac{\max\limits_{n}|x(n)|^2}{\frac{1}{N_s}\sum_{n=0}^{N_s-1}|x(n)|^2} \tag{4.1}$$

  where the second equation is written in discrete time and is valid for a sufficiently up-sampled signal $x(n)$ and N_s is the number of simulation samples.

- INP Instantaneous normalized power [Ciochina, 2009] which is a more refined criterion than PAPR, and gives an insight on the clipping effect for all samples instead of the maximum clipping value PAPR which can only characterise the worst case scenario.

$$INP = \frac{|x(n)|^2}{\frac{1}{N_s}\sum_{n=0}^{N_s-1}|x(n)|^2} \tag{4.2}$$

Figure 4.5 depicts the Complementary Cumulative Distribution Function (CCDF) of the INP for OFDM , SC-OFDM and SC-TDM in comparison with EW-SC-OFDM which we investigated for roll-offs 0.05 and 0.25 with the system parameters provided in [ENGINES, 2011] $N = 512$ and $M = 432$ and an oversampling factor equal to 4 using the 16-APSK modulation. It can be noticed that in comparison with OFDM, SC-OFDM and

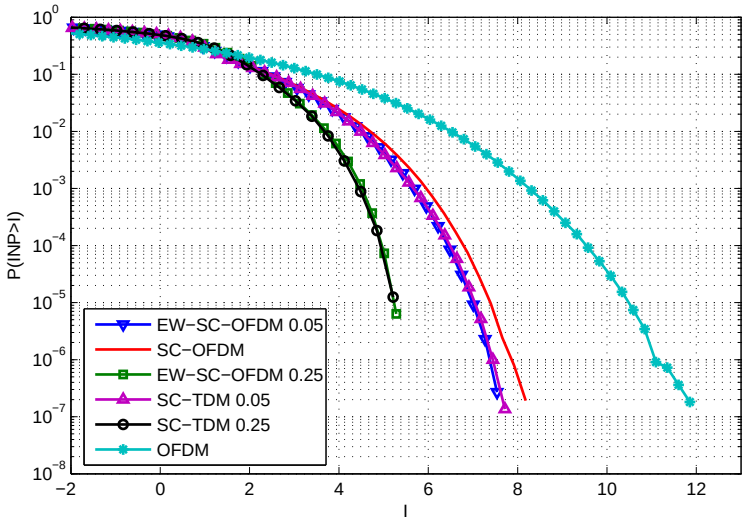

Figure 4.5: CCDF of INP for SC-OFDM, EW-SC-OFDM (roll-offs 0.05 and 0.25) and OFDM using $N = 512$ and $M = 432$ with an oversampling factor 4 for 16APSK

EW-SC-OFM exhibit better INP properties. Moreover, the EW-SC-OFDM is similar in INP to the classical single carrier SC-TDM using the same roll-off. Most of the literature uses the frequency domain representation of SC-OFDM/SC-FDMA to derive system metrics which unfortunately lack of intuition since they are written in matricial form. In this chapter, we will derive a time domain circular convolution based representations of SC-OFDM which helps deriving general metrics such as the PSD and the SINR.

4.4 From frequency to time domain representation

As shown hereafter, the time domain representation of SC-OFDM allows for a simple derivation of PSD and SINR formulas. In the originally proposed SC-FDMA, the IFFT size N needs not be a multiple of M. The LTE fractional case i.e. $N \neq kM,\ k \in \mathbb{N}^*$ was intended for flexible resource allocation among users.
In the DVB-NGH proposal for SC-OFDM, the size $M \sim N$ implies using fractional rates. Unfortunately, few studies have addressed this case since most of the studies relied on an integer ratio N/M. In this section, we derive a time domain model/representation for general (fractional) values of M and N using multi-rate signal processing properties. More precisely, we use FFT and IFFT operations with size equal to the Least Common Multiple (LCM) of M and N. This allows us to derive a simple yet effective system description relying on

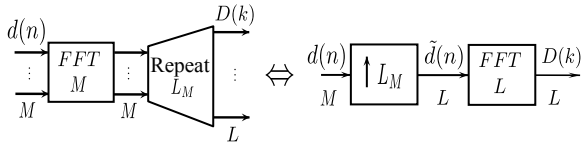

Figure 4.6: Up-sampling identity

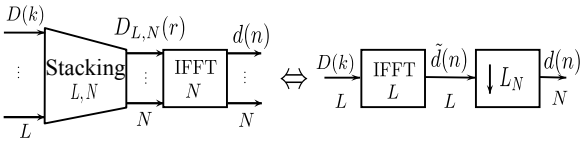

Figure 4.7: Down-sampling identity

circular convolution. To do so, we start by reminding some multi-rate noble FFT/IFFT identities.

4.4.1 Multi-rate FFT/IFFT noble identities

Let L be the LCM of M and N i.e. $L = ML_M = NL_N$ where L_M, $L_N \in \mathbb{N}$. Obviously, if N is a multiple of M then $L = N$ and $L_N = 1$ which means that the following general results can be easily applied for the specific case when N is a multiple of M. Moreover L_M and L_N are co-prime numbers i.e. they do not have any common divider and they satisfy $L_M|N$ and $L_N|M$ where "|" stands for "divides".
Let us consider the multi-rate equivalences [Vaidyanathan, 1988] depicted in Figures 4.6 and 4.7.

- **Up-sampling identity**: The cascade of up-sampling by a factor L_M followed by a FFT of size L is equivalent to a FFT of size M followed by an L_M-fold repetition of the M outputs.
- **Down-sampling identity**: The cascade of IFFT of size L followed by L_N-down-sampling is equivalent to stacking with parameters (L, N) followed by a IFFT of size N. Stacking with parameters (L, N) consists of a summation of L terms at a regular spacing equal to N as depicted in Figure 4.8. This means that for $r \in 0, \ldots, N-1$:

$$D_{L,N}(r) = \frac{1}{L_N} \sum_{s=0}^{L_N-1} D(sN + r) \tag{4.3}$$

  where $L_N = \frac{L}{N}$.

In the following we give equivalent models for different parts of the SC-OFDM system depicted in Figure 4.2 and more specifically the transmitter (Tx), the receiver (Rx), and the selective channel.

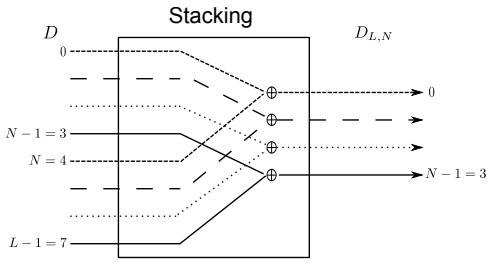

Figure 4.8: An example of stacking with $L = 8$, $N = 4$, and $L_N = 2$

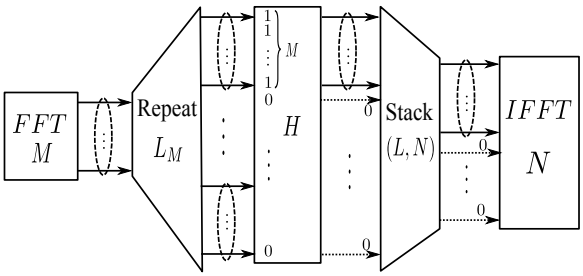

Figure 4.9: Localised mapping modelling

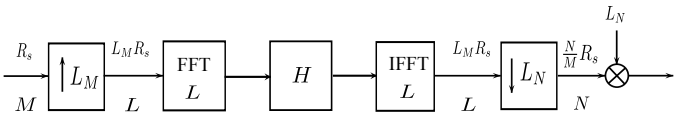

Figure 4.10: Transmitter equivalent model

4.4.2 Transmitter (Tx) equivalent model

Let us consider the transmitter delimited by (Tx) in Figure 4.2. In SC-OFDM, the user's M-FFT outputs are mapped into the first block of M entries in the N-IFFT inputs. This operation can be seen equivalent to the scheme depicted in Figure 4.9. The M inputs are block-repeated L_M times to generate L inputs. The sampling rate is increased from the symbol rate R_s to $L_M R_s$. The L samples are then multiplied with an equivalent transmit shaping window with frequency response H of length L where only M entries are non zero. Finally to obtain the N-IFFT inputs, a stacking operator following (4.3) is used in order to combine the L elements into N IFFT inputs. The resulting sampling frequency is equal to $\frac{N}{M}R_s$. It can be shown that for stacking with parameters (L, N) if the input symbols have less than or equal to N non zero inputs, then the stacking operator is only a multiplication with a factor $\frac{1}{L_N}$ of these N elements. Thus, when H has only M non zero elements $(M \leq N)$, the stacking operator allows bringing the first user's M-FFT outputs to the M

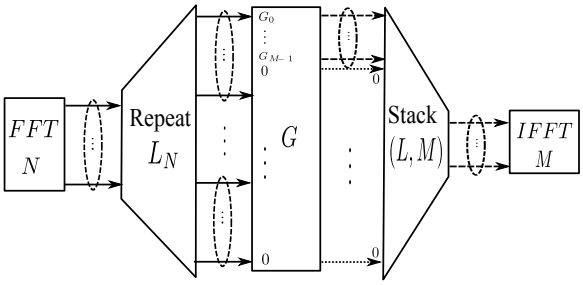

Figure 4.11: Localised demapping and equalization equivalent model

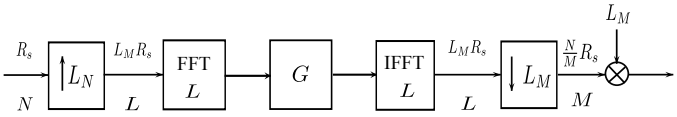

Figure 4.12: Receiver equivalent model

first inputs of the N-IFFT, with the other $N - M$ entries equal to 0, multiplied by $\frac{1}{L_N}$. By using multi-rate identities, the system becomes equivalent to the model depicted in Figure 4.10. Multiplication with L_N after the N-IFFT compensates for the stacking multiplication factor.

4.4.3 Receiver (Rx) modelling

At the receiver, after CP removal, the block of N received samples is processed by an N-FFT. The user's corresponding M frequency bins are extracted out of the N bins by demapping. They are then equalized with a one-tap frequency domain equalizer of length M thanks to the circularity of the channel. An M-IFFT transforms the equalized frequency samples into user's estimated time domain symbols. As with the transmitter modelling, we will use multi-rate identities to define the equivalent receiver model illustrated in Figure 4.11. Indeed, the receiver processing can be decomposed first into an N-FFT followed by a repetition of size L_N leading to L samples. The resulting samples are then jointly demapped and equalized using a frequency response G of length L which is non-null only in the user's allocated frequency bins. A stacking operator of parameters (L, M) is used to combine the L resulting bins into M frequency symbols which are then processed by an M-IFFT block to yield the user's estimated symbols. By using the noble multi-rate identities, the receiver can be modelled as in Figure 4.12.

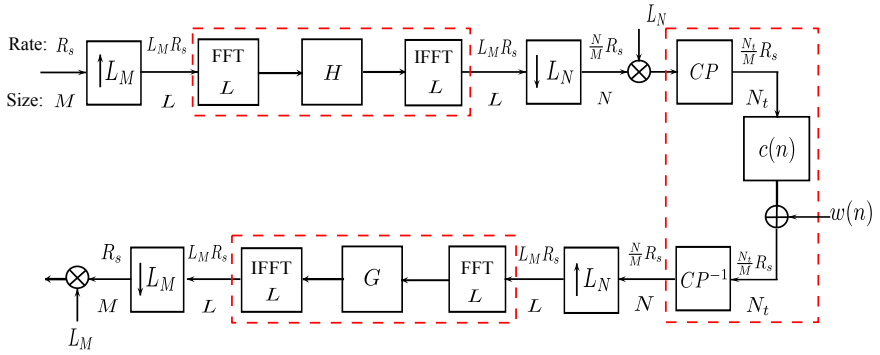

Figure 4.13: SC-OFDM equivalent frequency domain system model

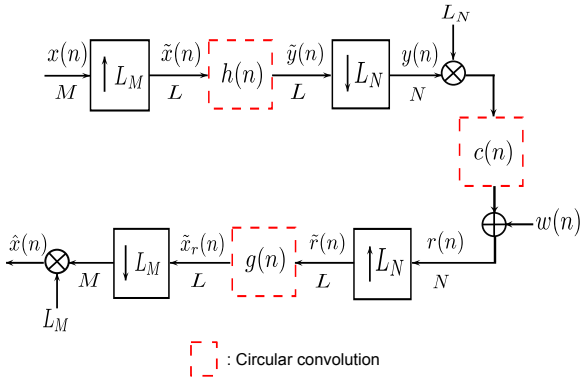

Figure 4.14: SC-OFDM equivalent time domain system model

4.4.4 Global system time domain equivalent model

Let us consider the system representation in Figure 4.13 which is obtained by replacing both the transmitter and receiver by their equivalent models in Figures 4.10 and 4.12. In order to develop the time domain model, we use two important frequency-time equivalences. On the one hand, it is well known that a frequency domain multiplication with a frequency response H of length L translates into circular convolution in the time domain with the time domain filter $h(n) = IFFT_L(H)$ which writes as follows:

$$h(n) = \frac{1}{L} \sum_{p=0}^{L-1} H_p \Omega_L^{pn} \tag{4.4}$$

The output symbols $\tilde{y}(n)$ of the circular convolution of filter $h(n)$ and symbols $\tilde{x}(n)$ can be expressed as follows:

$$\tilde{y}(n) = \sum_{m=0}^{L-1} \tilde{x}(m) h(< n - m >_L) = h(n) \circledast \tilde{x}(n) \tag{4.5}$$

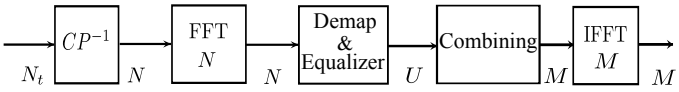

Figure 4.15: Receiver structure of SC-OFDM using spectral shaping of length $U \geq M$

where $< . >_L$ denotes the modulo L operator and $\circledast$ stands for circular convolution.
In a similar way, by defining $g(n) = \frac{1}{L}\sum_{p=0}^{L-1} G_p \Omega_L^{pn}$ The received equalized symbols $\tilde{x}_r(n)$ are expressed as follows:

$$\tilde{x}_r(n) = \sum_{m=0}^{L-1} \tilde{r}(m) g(< n-m >_L) = g(n) \circledast \tilde{r}(n) \tag{4.6}$$

On the other hand, inserting a CP -of length N_g longer than the channel memory- at the output of the transmitter and removing it at the input of the receiver, yields a circular time domain convolution. As a consequence, using the two aforementioned properties, blocks delimited with dashed lines in Figure 4.13 are equivalent to circular convolution in the time domain as represented in Figure 4.14.

4.4.5 EW-SC-OFDM as a circular convolution

Spectral Shaping (SS) or Extension and weighting consists of multiplying the M-FFT outputs by a shaping window which leads to lower side-lobes and thus a reduced PAPR. However, the extensions (or duplication) has been proposed in the case of root raised cosine shaping, the length of which would not exceed $2M$. Yet, this process can be extended to a more general scheme which consists of the aforementioned repetition block illustrated in Figure 4.9 allowing for a length of spectral shaping up to $U \leq L$. As such, the general model depicted in Figure 4.10 also applies for the EW-SC-OFDM of length U up to L. The spectral shaping window can thus be included in the frequency response of the transmit filter H.
An additional difference between EW-SC-OFDM and classical SC-OFDM lies in the receiver processing(see Figure 4.15). Indeed, since some of the M symbols have been duplicated to reach a length $U \geq M$ a "frequency combining" block has to be added before passing through the final M-IFFT in order to combine received symbols issuing from the duplicated transmitted symbols. The frequency combining as presented in [Kawamura et al., 2006] is in fact a special case of the stacking operation in equation (4.3). Note that since the stacking at the receiver has parameters (L, M) and the stacking inputs contain $U \geq M$ non zeros elements, the operation is no longer transparent (i.e. no longer a simple multiplication with $\frac{1}{L_M}$). This impacts channel equalization as will be discussed later. In a nutshell, the EW-SC-OFDM scheme is also covered by the general model proposed in Figure 4.13. Next section presents a summary of different system parameters of the general model depicted in Figure 4.13 allowing to find the classical SC-OFDM and EW-SC-OFDM transmit and

Figure 4.16: Spectral shaping filter with root raised cosine

receive transfer functions.

4.4.6 Special cases of the general scheme: SC-OFDM and EW-SC-OFDM

SC-OFDM

In the SC-OFDM scheme proposed in DVB-NGH, the mapping frequency response H consists of a block of M non-zero frequency bins out of L. It can thus be viewed as a rectangular shaping in the frequency domain with length M which satisfies:

$$H_k = \begin{cases} 1 & if\ 0 \leq k \leq M-1 \\ 0 & if\ M \leq k \leq L-1 \end{cases} \tag{4.7}$$

In an equivalent way, the SC-OFDM equalizer and demapper G consists of a frequency response with only M non zero elements i.e. $|G_p| = 0$ if $p \geq M$ as depicted in Figure 4.11.

Raised cosine EW-SC-OFDM

Let us consider a root raised cosine spectral shaping with a roll-off factor α. Let $M_\alpha = \lfloor \alpha \frac{M}{2} \rfloor$ where $\lfloor . \rfloor$ denotes the floor operator. The length of the root raised cosine window U satisfies $0 \leq U = M + 2M_\alpha \leq 2M$. The data is placed in the 1^{st} block of M resource frequencies which implies that the left hand side interference is reported to the last frequency bins. More precisely, the spectral shaping window depicted in Figure 4.16 writes as follows:

$$H_k \begin{cases} \neq 0 & if\ k = \{0, \ldots, 2M + M_\alpha - 1\} \Cup \{L - M_\alpha, \ldots, L-1\} \\ = 0 & else \end{cases}$$

The equalizer frequency response consists thus of U non zero frequency bins.

Next sections provide analytical expressions of both PSD and SINR for the general SC-OFDM scheme where frequency responses of the transmit window H, the channel C and the equalizer G are assumed general

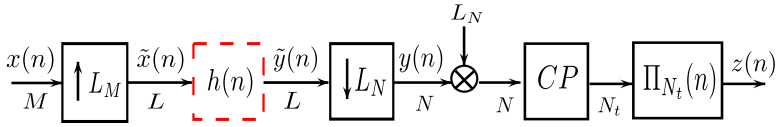

Figure 4.17: Transmitter model of SC-OFDM with pulse shaping

i.e. no restriction on the number of non zero elements is made. Numerical applications are then presented for the two special cases of SC-OFDM and raised cosine EW-SC-OFDM.

4.5 PSD analysis of SC-OFDM

PSD analysis is an essential feature to ensure that the transmit power spectrum is confined within a predefined transmission spectrum mask. In the case of multi-user communications, it is also valuable for resource allocation [Aziz et al., 2011]. Unlike PAPR reduction techniques, OFDM PSD formulas [van Waterschoot et al., 2010] can not be directly applied to SC-OFDM since DFT precoding changes the statistical properties of the OFDM input symbols. In this work, we derive PSD formulas based on the novel time domain representation of SC-OFDM and apply it to both the rectangular SC-OFDM and root raised cosine EW-SC-OFDM.

Let us consider the general scheme depicted in Figure 4.17. A CP is appended to the samples $L_N y(n)$ to form the SC-OFDM symbols of length N_t. A pulse shaping waveform $\Pi_{N_t}(n)$ of length N_t symbols is used at the front end of the transmitter. This pulse shaping function emulates the block nature of the SC-OFDM system and can possibly consist of other pulse shapes that the rectangular shape.

The transmitted SC-OFDM symbols $z(n)$ write as follows:

$$z(n) = L_N \sum_{l=-\infty}^{\infty} y(< n - lN_g >_N)\Pi_{N_t}(n - lN_t)$$

Using the modulo arithmetic equality $< n - lN_g >_N L_N =< (n - lN_g)L_N >_L$, we can write the transmitted symbols as:

$$\begin{aligned} z(n) &= L_N \sum_{l=-\infty}^{\infty} \sum_{p=0}^{L-1} \tilde{x}_{p,l} h(< (n - lN_g)L_N - p >_L)\Pi_{N_t}(n - lN_t) \\ &= L_N \sum_{l=-\infty}^{\infty} \sum_{p=0}^{M-1} x_{p,l} h(< (n - lN_g)L_N - pL_M >_L)\Pi_{N_t}(n - lN_t) \end{aligned} \quad (4.8)$$

The power spectral density of these symbols writes as (detailed derivations can be found in appendix C):

$$\overline{S_z}(f) = \frac{M\sigma_x^2}{N_t N^2} \sum_{r=0}^{M-1} \left| \sum_{s=0}^{L_M-1} H_{sM+r} \Psi_{N_t} \left(f - \frac{sM+r}{N} \right) \right|^2 \tag{4.9}$$

where $\Psi_{N_t}(f)$ is the Energy Spectral Density (ESD) of the time domain shaping filter $\Pi_{N_t}(n)$.
It is interesting to point out that the final PSD expression can be interpreted in a sense that due to the repetition block, each symbol out of the M SC-OFDM input symbols undergoes a global frequency response which is the sum of all M-evenly spaced frequency responses H_{sM+r} where $s \in [0 : L_M - 1]$.

4.5.1 PSD with rectangular shaping : SC-OFDM

As previously explained in Section 4.4, the equivalent transmit window in SC-OFDM implementation is a rectangular window of length M placed in frequency bins $0, \ldots, M-1$. It follows that:

$$\overline{S}_z(f) = \frac{M\sigma_x^2}{N_t N^2} \sum_{r=0}^{M-1} \left| \Psi_{N_t}(f - \frac{r}{N}) \right|^2$$

A (digital) sampled rectangular filter of length N_t has a Dirichlet kernel transfer function described as follows [van Waterschoot et al., 2010]:

$$\Psi_{N_t}(w) = sinc_{N_t}(w) = \begin{cases} -1^{w(N_t-1)} & if \ w \in \mathbb{Z} \\ \frac{sin(N_t w/2)}{N_t sin(w/2)} & otherwise \end{cases} \tag{4.10}$$

Figure 4.18 plots the power spectral density of SC-OFDM obtained by a Welch periodogram with 5% overlapping for the fractional rate ($M = 426$, $N = 512$). The theoretical and estimated PSD are perfectly matched.

4.5.2 PSD with root raised cosine EW-SC-OFDM

For the EW-SC-OFDM with root raised cosine, the transmit window H is expressed in section 4.4.
The power spectral density reads as follows:

$$\overline{S}_z(f) = \frac{M\sigma_x^2}{N_t N^2} \sum_{r=0}^{M-1} \left| \Gamma_{N_t}^{(r)}(f) \right|^2$$

where $\Gamma_{N_t}^{(r)}$ is the equivalent transmit response given in (4.11).

$$\Gamma_{N_t}^{(r)}(f) = \begin{cases} H_{M+r}\Psi_{N_t}(f - \frac{r}{N}) + H_{2M+r}\Psi_{N_t}(f - \frac{M+r}{N}) & if \ r = 0, \ldots, M_\alpha - 1 \\ H_{M+r}\Psi_{N_t}(f - \frac{r}{N}) & if \ r = M_\alpha, \ldots, M - M_\alpha - 1 \\ H_{M+r}\Psi_{N_t}(f - \frac{M+r}{N}) + H_r\Psi_{N_t}(f - \frac{L-r}{N}) & if \ r = M - M_\alpha, \ldots, M-1 \end{cases} \tag{4.11}$$

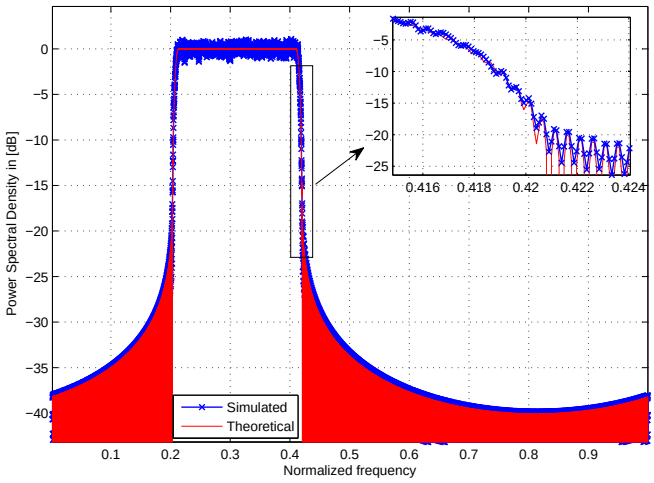

Figure 4.18: PSD EW-SC-OFDM with $M = 426$, $N = 512$, and $\alpha = 0$

Figure 4.19 plots the power spectral density of root raised cosine EW-SC-OFDM obtained by a Welch periodogram with 25% overlapping for the fractional rate ($M = 426$, $N = 512$) with oversampling factor 4. Both simulations and theoretical expressions match.

4.6 Linear equalization and SINR

In this section, we will show that the new derived time domain representation leads to a convenient and simple derivation of the SINR with linear equalizers which can be applied to any SC-OFDM scheme. The advantage of this analytical result is that it applies to a wide range of frequency precoding schemes as well as fractional and non fractional SC-OFDM rates. Knowing the SINR is an essential feature for Bit Error Rate prediction methods based on physical layer abstraction methods and thus for both link and system level analysis.
Let us define $\tilde{c} = L - IFFT\left(\tilde{C}\right)$ as the up-sampled IFFT of the frequency response C_k. This allows for a compact system model as depicted in Figure 4.20 where $p(n)$ is the over-all system time response which writes as:

$$p(n) = h(n) \circledast \tilde{c}(n) \circledast g(n) \qquad 0 \leq n \leq L-1 \tag{4.12}$$

The frequency response of the overall system is $P_k = H_k \tilde{C}_k G_k$ for $k \in [0 : L-1]$. The equivalent noise $\tilde{w}(n)$ is obtained by up-sampling the additive noise $w(n)$ by a factor L_N, circularly convolving with the equalizer

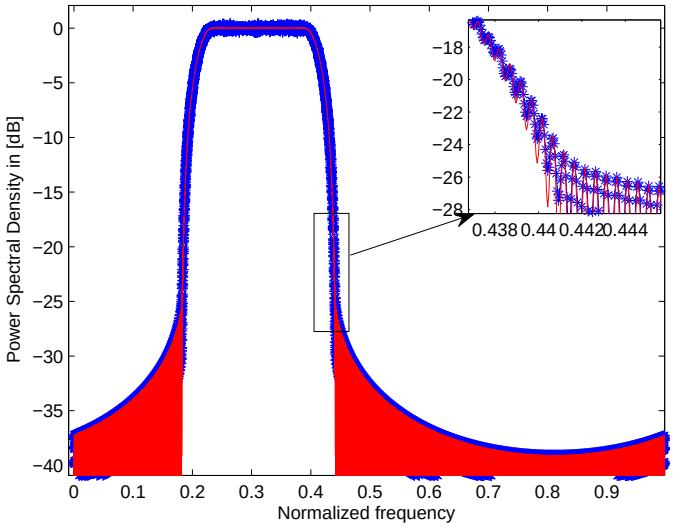

Figure 4.19: PSD EW-SC-OFDM with $M = 426$, $N = 512$, and $\alpha = 0.25$

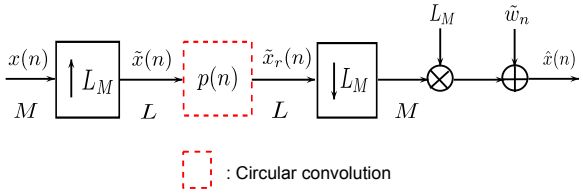

Figure 4.20: SC-OFDM simplified system model

$g(n)$ and down-sampling it by a factor L_M as demonstrated in Figure 4.21. The final multiplication factor in the general scheme arises from the L_M downsampling-stacking inversion. Let us consider the general model depicted in Figure 4.20. For a block of N received symbols, the demapped equalized symbols $\hat{x}(n)$ write as follows, $\forall n \in [0 : M-1]$:

$$\begin{aligned}
\hat{x}(n) &= L_M \tilde{x}_r(nL_M) + \tilde{w}(n) \\
&= L_M \left(\sum_{k=0}^{L-1} p(< nL_M - k >_L) \tilde{x}(k) \right) + \tilde{w}(n) \\
&= L_M \left(\sum_{m=0}^{M-1} p(< (n-m)L_M >_L) \tilde{x}_r(mL_M) \right) + \tilde{w}(n) \\
&= L_M \left(\sum_{m=0}^{M-1} p(< (n-m)L_M >_L) x(m) \right) + \tilde{w}(n)
\end{aligned}$$

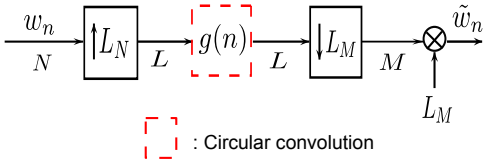

Figure 4.21: Equivalent noise

$$= \quad x_u(n) + x_i(n) + \tilde{w}(n)$$

where we define the:

- useful signal $x_u(n) = L_M p(0) x(n)$
- interfering signal $x_i(n) = L_M \sum_{n \neq m} p(< (n-m) L_M >_L) x(m)$
- equivalent noise $\tilde{w}(n)$.

Given these notations, we can define the SINR as the metric relating the power of the desired signal at the receiver to the amount of interference and noise. More specifically, it is defined as follows:

$$SINR = \frac{P_u}{\sigma_i^2 + \sigma_{\tilde{w}}^2} \tag{4.13}$$

where $P_u = E[|x_u(n)|^2]$, $\sigma_i^2 = E[|x_i(n)|^2]$, $\sigma_{\tilde{w}}^2 = E[|\tilde{w}(n)|^2]$ are the powers of the useful resp. interfering and noise terms. Let us compute the powers involved in the SINR.

4.6.1 The useful term power P_u

The useful term power is $P_u = (L_M)^2 |p(0)|^2 \sigma_x^2$ where σ_x^2 is the variance of the transmitted symbols x_n. From the FFT definition, $p(0) = \frac{1}{L} \sum_{k=0}^{L-1} P_k$.
Thus, the useful power can be written as :

$$P_u = \frac{\sigma_x^2}{M^2} \left| \sum_{k=0}^{L-1} P_k \right|^2 \tag{4.14}$$

4.6.2 The interfering term power σ_i^2

For $n \in [0 : M-1]$ the received symbols $x_r(n) = x_u(n) + x_i(n) = L_M \sum_{m=0}^{M-1} p(< (n-m) L_M >_L) x(m)$.
The power of the received symbols $x_r(n)$ writes as:

$$\sigma_r^2 = E[|x_r(n)|]^2 = (L_M)^2 \sigma_x^2 \sum_{m=0}^{M-1} |p(< (n-m) L_M >_L)|^2 = P_u + \sigma_i^2 \tag{4.15}$$

The received signal results from up-sampling and down-sampling the original stationary symbols with the same factor L_M. Thus, it is a stationary process and its power is not dependent on the time index n. More specifically, for $n \in [0 : M-1]$, let $\tilde{p}(n) = p(nL_M)$, i.e. $\tilde{p}$ is the down-sampled global filter p by a factor L_M. From the previous result of down-sampling in Figure 4.7, the global filter writes as $\tilde{p}(n) = M - IFFT(P_{L,M})$ where $P_{L,M}(r) = \frac{M}{L}\sum_{l=0}^{L_M-1} P_{lM+r}$ is the stacking output for $r \in [0 : M-1]$.
Thus, $p(nL_M)$ can be written as :

$$p(nL_M) = \tilde{p}(n) = \sum_{r=0}^{M-1} P_{L,M}(r)\Omega_M^{kr} \tag{4.16}$$

From Parseval identity, we have:

$$\sum_{n=0}^{M-1} |p(nL_M)|^2 = \frac{1}{M}\sum_{r=0}^{M-1} |P_{L,M}(r)|^2 = \frac{1}{M}\left(\frac{M}{L}\right)^2 \sum_{r=0}^{M-1} \left|\sum_{l=0}^{L_M-1} P_{lM+r}\right|^2 \tag{4.17}$$

It follows that:

$$\sigma_r^2 = \frac{\sigma_x^2}{M}\sum_{r=0}^{M-1} \left|\sum_{l=0}^{L_M-1} P_{lM+r}\right|^2 \tag{4.18}$$

Inserting this result in (4.15), the power of the interfering term is as follows:

$$\sigma_i^2 = \sigma_r^2 - P_u = \frac{\sigma_x^2}{M^2}\left(M\sum_{r=0}^{M-1} \left|\sum_{l=0}^{L_M-1} P_{lM+r}\right|^2 - \left|\sum_{k=0}^{L-1} P_k\right|^2\right) \tag{4.19}$$

4.6.3 The noise power $\sigma_{\tilde{w}}^2$

Let us consider the equivalent noise depicted in Figure 4.21. Due to up-sampling by a factor L_N and down-sampling by a different factor L_M, the noise is not necessarily stationary. It can however be shown that unless special conditions are imposed on the equalizing filter $g(n)$, the noise is cyclo-stationary. This means that the SINR will have instantaneous values depending on the position of the noise sample in the block. However, we can derive a *mean* SINR by stationarizing the noise process leading to a noise variance (detailed calculations can be found in Annex C):

$$\sigma_{\tilde{w}}^2 = E[|\tilde{w}(n)|^2] = \frac{\sigma_w^2 N}{M^2}\sum_{k=0}^{L-1} |G_k|^2 \tag{4.20}$$

Merging the three results of (4.14), (4.19), and (4.20) the mean SINR reads as:

$$SINR = \frac{\left|\sum_{k=0}^{L-1} P_k\right|^2}{M\sum_{r=0}^{M-1}\left|\sum_{l=0}^{L_M-1} P_{lM+r}\right|^2 - \left|\sum_{k=0}^{L-1} P_k\right|^2 + N\frac{\sigma_w^2}{\sigma_x^2}\sum_{k=0}^{L-1}|G_k|^2} \tag{4.21}$$

4.6.4 SINR function of SNR

It is interesting to have a formulation of the SINR in terms of SNR, to have an easy asymptotic interpretation of the system performance function of SNR. The SNR is defined as the ratio of the signal power at the input of the receiver to the noise power.

The signal power computed at the input of the receiver is $P = \sigma_x^2 \frac{M}{N^2} \sum_{k=0}^{L-1} \left| H_k \tilde{C}_k \right|^2$.

The noise power at the input of the receiver is function of the sampling rate and reads: $\sigma_b^2 = N_0 F_s$ where $F_s = \frac{N}{M} R_s$ is the sampling rate at the input of the receiver and R_s is the user sampling rate. It should be noted that to fulfil the Shannon sampling theorem for SC-OFDM ($F_s \geq 2R_s$), N should satisfy $N \geq 2M$. In the case of raised cosine spectral shaping, N should satisfy $N \geq 2(1+\alpha)M$. In practice, to avoid aliasing, an oversampling factor equal to 4 is used for SC-OFDM throughout this chapter.

It follows that:

$$\frac{E_s}{N_0} = \frac{PT_s}{N_0} = \frac{P}{N_0 R_s} = \frac{\sigma_x^2}{\sigma_w^2} \frac{1}{N} \sum_{k=0}^{L-1} \left| H_k \tilde{C}_k \right|^2 \tag{4.22}$$

Thus, using the following result:

$$N \frac{\sigma_w^2}{\sigma_x^2} = \left(\frac{E_s}{N_0} \right)^{-1} \sum_{k=0}^{L-1} \left| H_k \tilde{C}_k \right|^2 \tag{4.23}$$

Equation (4.21) leads to the following SINR:

$$SINR = \frac{\left| \sum_{k=0}^{L-1} P_k \right|^2}{M \sum_{r=0}^{M-1} \left| \sum_{l=0}^{L_M - 1} P_{lM+r} \right|^2 - \left| \sum_{k=0}^{L-1} P_k \right|^2 + \left(\frac{E_s}{N_0} \right)^{-1} \sum_{k=0}^{L-1} \left| H_k \tilde{C}_k \right|^2 \sum_{k=0}^{L-1} |G_k|^2} \tag{4.24}$$

It should be noted that unlike SINR expressions in [3GPP TSG-RAN WG1 Meeting43 051352, 2005], the above SINR analytical expressions apply to the fractional case as well which is more convenient for SC-OFDM.

In the next section we will apply results of the SINR to some SC-OFDM implementations with two linear equalizers, namely the ZF and the MMSE frequency domain equalizer.

4.6.5 Linear equalizers: MMSE and ZF

Let us derive expressions of linear equalizers for SC-OFDM general scheme beginning with linear equalization. The estimated symbols write as follows:

$$\hat{x}_n = L_M \left(\sum_{m=0}^{M-1} \tilde{p}(< n-m >_L) x(m) \right) + \tilde{w}(n)$$

where $\tilde{p}$ is the M-IFFT of the frequency response $\frac{M}{L}\sum_{s=0}^{L_M-1} P_{sM+r}$. This results in M frequency domain estimated symbols:

$$\hat{X}_k = \sum_{s=0}^{L_M-1} P_{k+sM} X_k + \sum_{s=0}^{L_M-1} G_{k+sM} \tilde{W}_{k+sM} \tag{4.25}$$

where X_k are the M transmitted frequency domain symbols and $\tilde{W}_k$ are the L FFT noise symbols obtained by replication of the N FFT noise symbols i.e. $\tilde{W}_k = W_{<k>N}$.

Zero Forcing (ZF) equalizer

The frequency response of a ZF equalizer should satisfy $\sum_{s=0}^{L_M-1} P_{sM+r} = 1$ which yields a solution in the form [Clark, 1998]:

$$G_k^{ZF} = \frac{H_k^* C_k^*}{\sum_{s=0}^{L_M-1} \left| H_{sM+k} \tilde{C}_{sM+k} \right|^2} \tag{4.26}$$

Since $\sum_{s=0}^{L_M-1} P_{sM+r}^{ZF} = 1$, the SINR in (4.24) simplifies as follows:

$$SINR^{ZF} = \frac{E_s}{N_0} \frac{M^2}{\sum_{k=0}^{L-1} \left| H_k \tilde{C}_k \right|^2 \sum_{k=0}^{L-1} \left| G_k^{ZF} \right|^2} \tag{4.27}$$

where it can be shown that :

$$\sum_{k=0}^{L-1} \left| G_k^{ZF} \right|^2 = \sum_{k=0}^{M-1} \frac{1}{\sum_{s=0}^{L_M-1} \left| H_{k+sM} \tilde{C}_{k+sM} \right|^2} \tag{4.28}$$

However, the solution G_k^{ZF} may lead to a large noise enhancement when the channel has zeros in its frequency response.

Minimum Mean Square Error (MMSE) equalizer

As for the MMSE equalizer, the frequency response of the equalizer which minimizes the mean square error $E[|\hat{x}_n - x_n|^2]$ writes as:

$$G_k^{MMSE} = \frac{H_k^* C_k^*}{\sum_{s=0}^{L_M-1} \left| H_{sM+k} \tilde{C}_{sM+k} \right|^2 + \frac{\sigma_W^2}{\sigma_X^2}} \tag{4.29}$$

where $\sigma_W^2 = N\sigma_w^2$ and $\sigma_X^2 = M\sigma_x^2$ are the variances of the noise N-FFT outputs and the symbols M-FFT outputs. It can be noticed that due to the repetition block prior to multiplication with the frequency transmit filter response, some sort of diversity is created, and the MMSE equalizer processed this diversity by combining

Feature	Value
Modulation	16APSK -rate 1/2
IFFT size N	512
FFT size M	428
Oversampling factor	4
CP size	1/16
IMUX OMUX bandwidths	30, 36 and 40 MHz
roll-off factor α	0.05

Table 4.2: Simulation parameters for SC-OFDM and EW-SC-OFDM

the symbols originating from the same input M-FFT symbol.

Using (4.23), the equalizer writes as a function of SNR as follows:

$$G_k^{MMSE} = \frac{H_k^* C_k^*}{\sum_{s=0}^{L_M-1} \left| H_{sM+k} \tilde{C}_{sM+k} \right|^2 + \frac{1}{M} \left(\frac{E_s}{N_0} \right)^{-1} \sum_{k=0}^{L-1} \left| H_k \tilde{C}_k \right|^2} \tag{4.30}$$

4.7 Applications to the SINR of SC-OFDM

To assess the performance of the linear equalizers when the IMUX and OMUX filters are used in their frequency selective region, we will assume the non linear amplifier is operated far from its non linear region with a back-off equal to $10dB$. Table 4.2 summarizes the simulation parameters used.

4.7.1 SINR of SC-OFDM

As previously discussed, the transmitter frequency response H is a rectangular window of length M in the classical SC-OFDM, leading to a global filter in the form:

$$P_k = \begin{cases} C_k G_k & 0 \leq k \leq M-1 \\ 0 & M \leq k \leq L-1 \end{cases} \tag{4.31}$$

The Zero Forcing equalizer for SC-OFDM writes for $k \in \{0, \ldots, M-1\}$ as follows:

$$G_k^{ZF} = \frac{C_k^*}{|C_k|^2} \tag{4.32}$$

Thus, $P_k^{ZF} = 1$ for $0 \leq k \leq M-1$.

As a consequence, the SINR of SC-OFDM when zero forcing is used becomes:

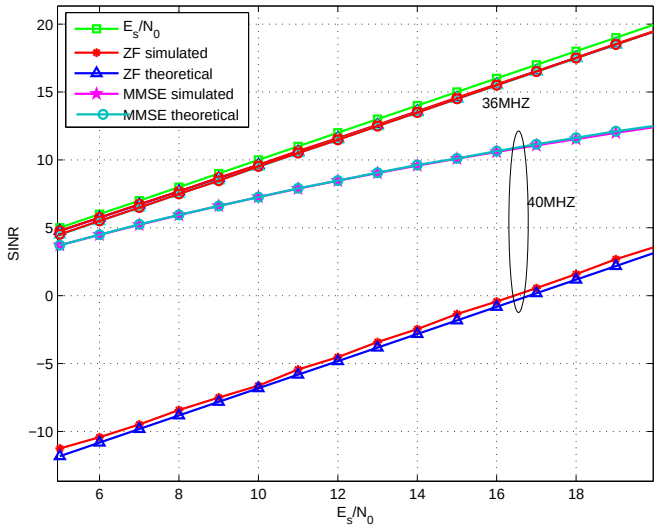

Figure 4.22: MMSE and ZF SINR for EW-SC-OFDM $N = 512$, $M = 426$, and $\alpha = 0.05$

$$SINR^{ZF}_{SC-OFDM} = \frac{E_s}{N_0} \frac{M^2}{\sum_{k=0}^{M-1} |C_k|^2 \sum_{k=0}^{M-1} \left|\frac{1}{C_k}\right|^2} \tag{4.33}$$

The MMSE equalizer writes as:

$$G_k^{MMSE} = \frac{C_k^*}{|C_k|^2 + \frac{1}{M}\left(\frac{E_s}{N_0}\right)^{-1} \sum_{k=0}^{M-1} |C_k|^2} \tag{4.34}$$

4.7.2 SINR of EW-SC-OFDM

Let us consider the Root Raised Cosine filter in (4.11). In this case, the overall system frequency response is expressed as follows:

$$\begin{aligned} \sum_{k=0}^{L-1} \left|G_k^{ZF}\right|^2 &= \sum_{r=0}^{M_\alpha - 1} \frac{1}{\left|H_r \tilde{C}_r\right|^2 + \left|H_{M+r} \tilde{C}_{M+r}\right|^2} + \sum_{r=M_\alpha}^{M-M_\alpha-1} \frac{1}{\left|H_r \tilde{C}_r\right|^2} \\ &+ \sum_{r=M-M_\alpha}^{M-1} \frac{1}{\left|H_r \tilde{C}_r\right|^2 + \left|H_{L-1-r} \tilde{C}_{L-1-r}\right|^2} \end{aligned}$$

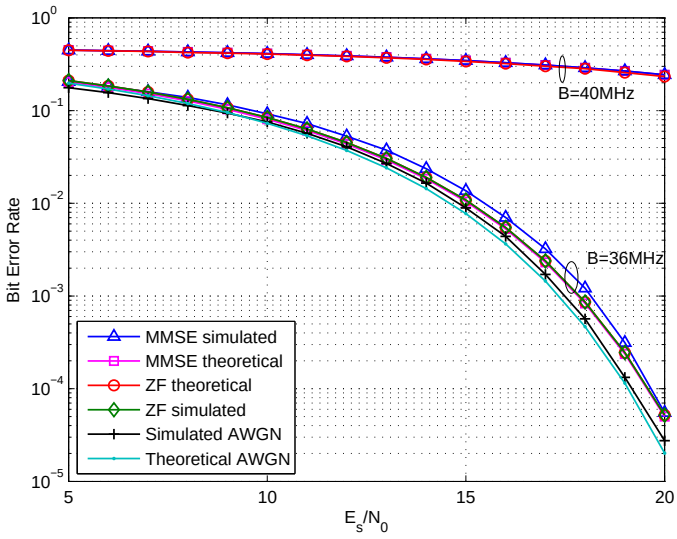

Figure 4.23: MMSE and ZF BER for EW-SC-OFDM $N = 512$, $M = 426$, and $\alpha = 0.05$

Figure 4.22 plots the theoretical and estimated SINR for the EW-SC-OFDM $N = 512$, $M = 426$, and $\alpha = 0.05$. The results show a good match between the theoretial and simulated SINRs which are compared with the SNR E_s/N_0. Based on the SINR values and using the approximated BER expression given in [Sung et al., 2009]:

$$BER(E_s/N_0) = \frac{1}{4}Q\left(\sqrt{\frac{(\gamma^2-\gamma+1)E_s}{2\alpha_0 N_0}}\right)+\frac{1}{4}Q\left(\sqrt{\frac{(\gamma-1)^2E_s}{2\alpha_0 N_0}}\right)+\frac{1}{8}Q\left(\sqrt{\frac{E_s}{\alpha_0 N_0}}\right)+\frac{3}{8}Q\left(\sqrt{\frac{2\gamma^2 sin(\frac{\pi}{12})^2E_s}{\alpha_0 N_0}}\right) \tag{4.35}$$

Figure 4.23 plots the SINR for MMSE and ZF equalization. It can be noticed that the bigger the signal bandwidth, the more degraded the performance is. The approximated expression for 16APSK BER yield good fit with simulated results for both SINR and ZF equalizers.

4.8 Conclusion

In this chapter, an analysis of SC-OFDM waveform and its extended weighted version EW-SC-OFDM were presented. It has been shown that compared to Single Carrier TDM waveforms, the obtained waveforms have similar PAPR properties. Furthermore, we have shown that the FFT precoding in the frequency domain model of SC-OFDM yields a circular convolution in the time domain. Such an equivalence confirms that although called a DFT-precoded OFDM, SC-OFDM is a single rather than multi-carrier transmission scheme. Based

on the time domain representation of SC-OFDM, we have derived expressions of the Power Spectral Density and SINR for linear equalizers. Indeed, the considered communication scenario consists of an AWGN channel with frequency selective on-board satellite multiplexers IMUX and OMUX. Results show that the obtained bit error rate performance could be well approximated using the estimated and theoretical SINR values.

4.9 Conclusion (French)

Dans ce chapitre, nous avons présenté une analyse théorique de la forme d'onde SC-OFDM ainsi que sa version étendue et pondérée EW-SC-OFDM. Nous avons démontré, que comparé à un schéma de transmission mono-porteuse en multiplexage par division de temps, EW-SC-OFDM a les mêmes caractéristiques de rapport entre puissance crête et puissance moyenne. Nous avons démontré dans un second temps que le précodage par FFT dans le domain fréquentiel donnait lieu à une convolution circulaire dans le domaine temporel. Cette équivalence confirme donc que le SC-OFDM est une transmission mono-porteuse. En nous basant sur la représentation dans le domaine temporel du SC-OFDM, nous avons dérivé les expressions de densité spectrale de puissance ainsi que le rapport signal à bruit plus interférences pour des égaliseurs linéaires. En effet, nous considérons que le canal de transmission est un canal à bruit blanc Gaussien, avec des filtres multiplexeurs sélectifs en fréquence. Les résultats montrent que nous pouvons bien approximer le taux d'erreurs binaire en nous basant les rapports signal à bruit théoriques et simulés.

Chapter 5

Conclusions and future work

5.1 Conclusions

Dans cette thèse nous nous sommes intéressés aux techniques permettant d'augmenter le débit sur un lien de diffusion par satellite. L'amélioration du débit est souvent accompagnée d'une apparition voire d'une augmentation de l'interférence entre symboles au niveau des signaux reçus démodulés. L'objectif de cette thèse fut donc de modéliser l'interférence entre symboles qui résulte des techniques étudiées et de proposer des méthodes ainsi que des formes d'ondes adéquates pour une meilleure résistance aux interférences du canal satellite.
La première méthode d'augmentation de débit se base sur l'introduction de nouvelles modulations qui offrent un bon compromis entre efficacité spectrale et efficacité en puissance telles que les modulations APSK proposées dans le standard DVB-S2. Cependant, les amplificateurs de puissance à bord des satellites sont souvent opérés proches de la saturation, ce qui en raison de la forte fluctuation des signaux APSK donne lieu à de l'interférence entre symboles.
Le premier chapitre s'est donc intéressé à la modélisation de l'interférence résultant de l'utilisation de modulation de phase (PSK) et de modulations d'amplitude et de phase (APSK). Nous avons étudié l'influence des différents paramètres des composants du transpondeur. Les résultats ont montré que l'interférence résultante pouvait être exprimée d'une manière approchée sous forme de série de termes non linéaires dite série de Volterra dont nous avons dérivé les modèles temporels et fréquentiels.
Le deuxième chapitre a présenté les méthodes non itératives d'égalisation du modèle de Volterra au niveau temporel et fréquentiel. S'agissant d'égalisation temporelle optimale, le canal de Volterra peut être représenté comme une machine à état, ce qui permet la dérivation d'égaliseurs optimaux symboles et séquence. Quant aux égaliseurs sous optimaux temporels, nous avons dérivé les expressions d'égaliseurs de type Minimum de l'Erreur Quadratique Moyenne (MEQM). Nous avons démontré que l'égaliseur MEQM linéaire pour le canal non linéaire de Volterra considérait l'interférence non linéaire comme étant un bruit additif Gaussien (moyennant certaines approximations concernant les modulations choisies). Cette limitation de l'égaliseur MEQM linéaire peut être contrecarrée en utilisant un égaliseur à retour de décisions qui permet de régénérer une

estimation dure de l'interférence et de la soustraire. Nous avons notamment comparé les performances d'un égaliseur à retour de décision linéaire (afin de soustraire uniquement l'interférence linéaire) à un égaliseur à retour de décision non linéaire tenant compte de l'intégralité de l'interférence linéaire et non linéaire. Enfin, afin de réduire la complexité de l'égalisation temporelle, nous avons étudié l'égaliseur linéaire ainsi que l'égaliseur à retour de décisions dans le domaine fréquentiel en présentant l'égaliseur hybride temporel-fréquentiel. Nous avons comparé les différentes complexités calculatoires de ces égaliseurs et leur évolution en fonction de la taille des symboles traités par ces égaliseurs.

Dans le troisième chapitre, nous avons étudié les récepteurs itératifs pour le canal non linéaire satellite. Les récepteurs itératifs optimaux symboles et séquence ont été présentés et sont similaires aux égaliseurs optimaux pour les canaux sélectifs en fréquence linéaires. Dans un second temps, nous avons dérivé les expressions de l'égaliseur MEQM à réponse variable dans le temps ainsi que deux implémentations à faible complexité invariantes dans le temps. Plus particulièrement, l'approximation 'Sans Apriori' apportait une égalisation de moindre complexité que la solution exacte, tout en offrant des performances acceptables comparées à l'implémentation exacte. Nous avons ensuite optimisé le récepteur itératif comprenant le turbo-égaliseur ainsi que le décodeur LDPC à entrées et sorties souples. La méthode d'optimisation retenue est celle de l'ajustement de la courbe (*curve fitting*) qui se base sur l'optimisation de la courbe EXIT combinée de l'égaliseur et des noeuds de variables avec celle des noeuds de parité. Contrairement aux modulations binaires, les messages issus de l'égaliseur suivent une distribution en mélange de Gaussiennes. Ainsi, en utilisant cette approximation au lieu de l'approximation Gaussienne souvent utilisée dans la littérature, nous avons montré que nous pouvions améliorer les performances du récepteur itératif.

Dans le quatrième chapitre, nous avons étudié une seconde technique permettant d'augmenter les débits au travers de l'élargissement de la bande du signal. Cette augmentation des débits peut entrainer le dépassement de la bande de non sélectivité des filtres de multiplexage à bord du transpondeur. Ainsi, les réponses impulsionnelles obtenues sont plus longues et des techniques d'égalisation sont requises à la réception. Pour pallier à l'augmentation de la complexité des égaliseurs temporels, le standard DVB-NGH a proposé une nouvelle forme d'onde dénommée SC-OFDM et sa version étendue et pondérée EW-SC-OFDM afin d'égaliser plus simplement la sélectivité du canal terrestre mobile dans le domaine fréquentiel. Nous avons donc étudié l'utilisation de cette nouvelle forme d'onde afin d'égaliser la sélectivité des filtres multiplexeurs. Nous nous sommes intéressés dans un premier temps au calcul de la densité spectrale de puissance dont nous avons développé des formules théoriques. Ensuite, nous avons dérivé les formules du rapport signal à bruit plus interférences et avons montré que les formules théoriques et approchées étaient assimilables.

5.2 Perspectives

Plusieurs perspectives peuvent être envisagées comme ouverture de ces travaux sur de futurs axes de recherche. Nous les résumons comme suit :

5.2.1 Estimation canal

Dans cette thèse, nous avons supposé que la réponse des filtres du satellite et celle de la non linéarité étaient fixes et connues du récepteur. En réalité, la réponse de ces éléments varie mais d'une manière assez lente. Il serait donc intéressant de vérifier le comportement des égaliseurs définis précédemment quant à une erreur d'estimation de modèle non linéaire. Un autre axe de recherche consisterait à associer au récepteur un bloc d'estimation de canal et d'en étudier les performances pour une faible voire large variabilité du canal.

5.2.2 Synchronisation horloge et porteuse

Une des hypothèses utilisées dans cette thèse était que l'on avait bien récupéré l'horloge et la fréquence porteuse du signal. En pratique, il existe toujours des écarts en fréquence et en temps qu'il est intéressant d'étudier en présence de non-linéarités ainsi que leur impact sur l'expression du modèle de Volterra. Des versions fractionnées des égaliseurs pourraient aussi être étudiées afin de permettre une récupération plus efficace des erreurs de synchronisation.

5.2.3 Bourrage de zéros ou bien cyclique préfixe ?

Lorsqu'il s'agit de circulariser un canal sélectif en fréquence, deux types de préfixes peuvent être utilisés: le préfixe cyclique, le bourrage à zéros. Le bourrage de zéros [Muquet et al., 2002] consiste à utiliser un préfixe constitué uniquement de zéros. Dans le cadre d'un modèle d'interférences non linéaires, il serait intéressant d'étudier l'applicabilité de cette méthode. Premièrement, au niveau système il faudrait vérifier l'impact d'une suite de zéros sur le contrôleur de gain automatique. Ensuite, au niveau modèle, il est nécessaire de vérifier si l'ajout de zéros permettait d'utiliser les convolutions circulaires de 3ème ordre, et si le modèle fréquentiel du canal de Volterra était toujours valable.

5.2.4 Comparaison avec d'autres techniques

Il serait intéressant de comparer d'une manière plus détaillée nos algorithmes itératifs avec des techniques de pré-distorsion voire d'égalisation. En ce qui concerne les techniques d'égalisation, nous pourrions comparer nos

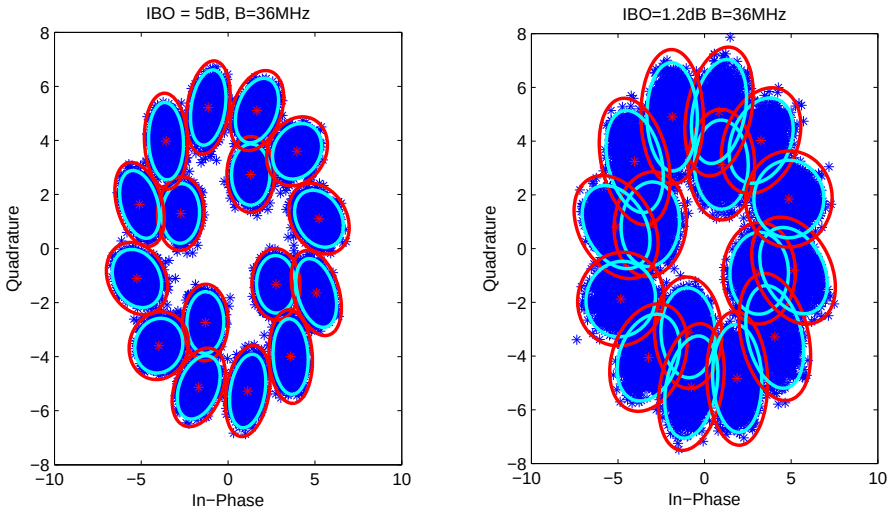

Figure 5.1: EW-SC-OFDM with roll-off $\alpha = 0.05$, $N = 512$ and $M = 426$

travaux aux résultats de [Colavolpe and Piemontese, 2012] pour de l'égalisation en utilisant un graphe de facteurs, avec [Colavolpe et al., 2012] pour la technique dite de raccourcissement de canal, [Abdulkader et al., 2014] pour l'égalisation itérative basée sur les réseaux de neurones. En ce qui concerne les techniques de pré-compensation, nos algorithmes pourraient être comparés aux travaux récents de [Deleu et al., 2014] qui traite un pré-compensateur MEQM itératif.

5.2.5 Égalisation au sens large

Afin de préserver une égalisation à faible complexité pour le EW-SC-OFDM, nous pouvons utiliser un modèle linéaire approché du canal de Volterra. Ce modèle prendrait en compte la corrélation du bruit d'interférences ainsi que démontré dans le chapitre 1. Pour ce faire, nous pourrions estimer la variance et la pseudo-variance de l'interférence que nous supposerons non circulaire. La corrélation entre les deux voies du bruit est caractérisée par la pseudo-variance qui s'écrit:

$$E[Z^2] = \sigma_r^2 - \sigma_i^2 + j2E[Z_r Z_i] \tag{5.1}$$

où σ_r^2 et σ_i^2 sont les covariances des parties réélles et imaginaires de Z et $E[Z_r Z_i]$ est la corrélation entre voies réelle et imaginaire. Comme présenté dans le chapitre 1, le modèle Gaussien linéaire présenté par [Burnet and Cowley, 2005] ne prenait pas en compte cette corrélation, de ce fait, il serait intéressant d'évaluer l'amélioration apportée par cette nouvelle approche. La Figure 5.1 présente la forme de l'interférence générée

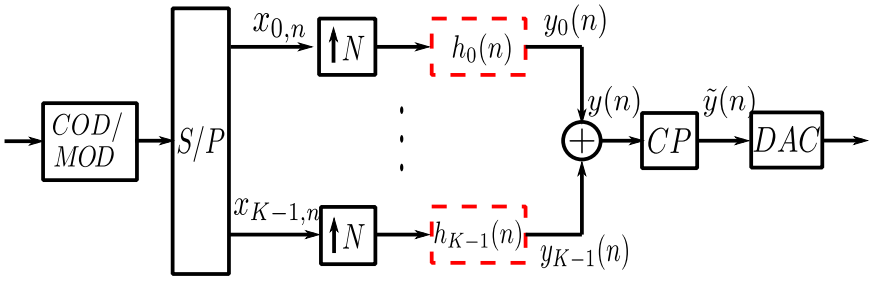

Figure 5.2: Time domain GFDM system

sans bruit pour une modulation SC-OFDM avec les paramètres $N = 512$, $M = 426$, un roll-off $\alpha = 0.05$ et un facteur de sur-échantillonnage égal à 4. Il est clair que l'interférence n'est pas isotrope, et pour le démontrer, nous avons utilisé la relation entre les paramètres de grand axe d'une ellipse avec la variance et pseudo-variance de l'interférence suivant la méthode expliquée en annexe C.

Il a été démontré par [Picinbono and Chevalier, 1995], que pour des variables complexes non circulaires, le détecteur MEQM *au sens large* présentait de meilleures performances que le détecteur MEQM classique. Ainsi, en filtrant le signal et son conjugué, toute l'information sur les moments de second ordre est utilisée, ce qui entraine une amélioration des performances. Nous pourrions donc dériver un égaliseur MEQM au sens large pour le SC-OFDM en nous basant sur ce modèle linéaire.

5.2.6 Generalised Frequency division multiplexing

Concernant les formes d'ondes mieux adaptées à un traitement fréquentiel à la réception, nous pourrions aussi étudier l'applicabilité de la forme d'onde Generalised Frequency Division Multiplexing (GFDM). Le GFDM est un schéma de modulation généralisant les modulations SC-OFDM, EW-SC-OFDM et OFDM au travers d'une division en fréquence non orthogonale. Cette technologie a été proposée pour les réseaux secondaires de la radio cognitive afin d'occuper les trous spectraux. Dans le cadre des applications satellite cette technologie pourrait aussi bien être envisagée dans les liaisons descendantes ou dans des applications de radio cognitive pour les satellites. Le modèle du GFDM est présenté en Figure 5.2. Le modèle de la modulation SC-OFDM sous forme de convolution circulaire présenté dans le quatrième chapitre permet de mieux comprendre en quelle mesure le GFDM généralise la forme d'onde SC-OFDM. Cette technologie consiste à rapprocher les sous porteuses des différents K flux ce qui entraine de l'interférence entre porteuses intrinsèque qu'il est nécessaire d'égaliser à la réception.

5.3 Conclusions

In this thesis, we were interested in the challenges related to increasing the throughput in a broadcast satellite link. Indeed, increasing the throughput is usually tied with the rise or the increase of Inter Symbol Interference in the received demodulated signals. The objective of this thesis was to model this resulting ISI and to suggest adequate waveforms and mitigation techniques to cope with the satellite channel interference.

The first investigated techniques for increasing the throughput is based on the DVB-S2 new modulations schemes namely APSK which offers a good trade-off between power and spectral efficiency. However, the on-board power amplifiers are usually preferred to operate near or at saturation, which yields non linear interference due to the increased envelope fluctuation of APSK signals.

The first chapter investigated on the modelling of the interference originating from using APSK modulations. We studied the influence of different components parameters in the transponder. Results have shown that the resulting interference could be well approached by a Volterra series decomposition which we presented both in the time and frequency domain.

The second chapter presented non iterative equalization techniques to mitigate the time domain Volterra non linear channel. On the one hand, since the Volterra series expansion can be represented by a finite state machine, optimal symbol and sequence based detection could be derived. On the other hand, linear and non linear sub-optimal MMSE detectors have also been presented. We demonstrated that the linear MMSE equalizer could only treat the interference as additive Gaussian noise. This limitation inherent to the linear MMSE equalizer could be alleviated using non linear decision feedback equalizers. More specifically we presented a hard linear DFE which only cancelled the linear ISI, and a hard non linear DFE which cancelled both the linear and nonlinear interference. Last but not least, we studied linear and DFE hybrid time frequency domain equalizers in order to reduce the complexity of time domain equalization. The complexity of these implementations as well as their performance were compared.

In the third chapter, we studied iterative receivers for the non linear satellite channel. Iterative receivers similar to linear ISI channels optimal symbol and sequence based detection were presented using the trellis representation of the Volterra channel. Secondly, we derived expressions of the time varying MMSE iterative equalizer along with two time-invariant low complexity implementations. Particularly, the No-Apriori approximation allows for a low complexity equalization while offering interesting error rate performance. In a second part of the chapter, we designed and optimised an iterative receiver for the satellite channel using an outer LDPC channel code. We used the EXIT curve fitting optimisation technique which consists of optimizing the code degree polynomials in order to best fit the equalizer output messages. Unlike binary modulations, the

equalizer outputs are distributed following a Gaussian Mixture distribution. Thus, by suitably defining the Gaussian mixture parameters, we are able to slightly improved the system performance.
In chapter 4, we studied an other aspect of increasing the throughput over a satellite link, which is carried out by increasing the symbol rate. Indeed the multiplexing filters become frequency selective when the signal bandwidth increases, which yields longer impulse responses and augmented interference. Adequate mitigation techniques are then required. In order to cope with the increased complexity related to the large number of taps, the DVB-NGH has proposed a novel waveform SC-OFDM and its extended version to allow for simpler frequency domain processing. We have shown that the proposed single carrier waveform has similar signal fluctuations to classical single carrier TDM waveforms. Furthermore, derived a novel time domain representation, which is based on circular convolution. This model allows us to derive analytical expressions for the power spectral density and the SINR. Simulations have shown that the obtained SINR allow for a good system performance prediction.

5.4 Future work

Many perspectives can be suggested for the future work as enumerated in the following non exhaustive propositions.

5.4.1 Channel estimation

In this thesis, we have assumed that the channel response characterised by the filters and non-linearity function was fixed and known to the receiver. In practice, these elements responses are not fixed due to variation in temperature and distortions incurred in the propagation link. It would be thus interesting to evaluate the impact of these variations on the channel non linear model and on the behavior of the afore-derived equalizers. Furthermore, it would be interesting to append an estimation block to the receiver and assess the performance in presence of slow to high variations of the channel model.

5.4.2 Frequency and clock synchronisation

On of the main assumptions used in this thesis was perfect time and frequency synchronisation. In reality, there are usually residual synchronisation errors, which it will be interesting to include in our Volterra channel model. It would also be interesting to derive fractional spaced equalizers and evaluate their ability to account for timing synchronisation.

5.4.3 Zero padding or cyclic prefixing?

When it comes to circularising the response of a frequency selective channel, two types of prefixes can be used, the cyclic prefix and zero padding. Zero padding [Muquet et al., 2002] consists of using an all-zero prefix. In the case of a non linear channel, it would be interesting to study the feasibility of this method, first, from a system point of view. and more precisely for Automatic Gain Controllers. Secondly, it is interesting the see the impact of zeros on the Volterra model and more specifically if the third order circular convolution remains unchanged and thus the previously derived frequency domain Volterra representation.

5.4.4 Comparison with alternative techniques

A thorough comparison with equalization and pre-distortion techniques could be envisaged. As far as equalization techniques are concerned, we could compare our work to other equalizers in the literature as for example [Colavolpe and Piemontese, 2012] for factor graph based equalization, [Colavolpe et al., 2012] for channel shortening, [Abdulkader et al., 2014] for neural networks based equalization. As for pre-compensation techniques, the derived equalizers can be compared to the results of [Deleu et al., 2014] who investigated on iterative MMSE pre-distortion.

5.4.5 Widely linear equalization

In order to preserve a low complexity equalization for EW-SC-OFDM when used in a non linear channel, we can derive a linear time domain model, which is more accurate than the linear Gaussian additive noise model of [Burnet and Cowley, 2005]. To do so, we estimate both the covariance and the pseudo-variance of the interference which is considered as an additive non-circular noise. A non circular complex random variable exhibits correlation between its real and imaginary part. This correlation is usually characterised by the so-called pseudo-variance which writes for a random variable Z as

$$E[Z^2] = \sigma_r^2 - \sigma_i^2 + j2E[Z_r Z_i] \tag{5.2}$$

where σ_r^2 and σ_i^2 are the covariances of the real and imaginary parts of Z and $E[Z_r Z_i]$ is the correlation between the real and imaginary parts. As discussed in Chapter 1, the Gaussian linear model provided by [Burnet and Cowley, 2005] does not take into account the apparent correlation in the scatter-plots of the received symbols. Figure 5.1 depicts this correlation along with a graphical representation of the ellipse containing respectively 90% and 95% of realisations of the interference (the ellipse parameters are described in [Ollila, 2008] and detailed in Appendix 2).

It has been shown in [Picinbono and Chevalier, 1995], that the optimum MMSE linear equalizer is the so-called widely linear equalizer which processes both the received signal and its conjugate. We could thus explore on the time and frequency domain widely linear equalization for EW-SC-OFDM over the non linear channel.

5.4.6 Generalised Frequency division multiplexing

As far as advanced waveforms better adapted to frequency domain equalization, we could also investigate on a novel waveform called Generalised Frequency Division Multiplexing (GFDM). GFDM is a transmission scheme generalising both OFDM, SC-OFDM and EW-SC-OFDM. This technology has been proposed for secondary users in a cognitive radio to occupy spectral holes. It can also be envisaged as a downlink technology or in applications of cognitive radio for satellites. The GFDM transmitter is depicted in Figure 5.2. The circular time domain representation provided in Chapter 4, explains why GFDM is a generalisation if SC-OFDM. GFDM consists of overlapping K sub-carriers each containing a SC-OFDM modulation with parameters M and N. Overlapping leads to non-orthogonal frequency division Multiplexing which implies intrinsic inter-carrier interference which needs to be mitigated at the receiver. It is thus interesting to derive equalizers for GFDM over a linear and Volterra channel respectively.

Appendices

Appendix A

Analytical expressions of the power spectral density of SC-OFDM

The autocorrelation $R_z(n,m)$ of symbols $z(n)$ in (4.8) can be derived as follows :

$$\begin{aligned}
R_z(n,m) &= E\left[z(n)z^*(n-m)\right] \\
&= L_N^2 \sum_{l=-\infty}^{\infty} \sum_{p=0}^{M-1} \sum_{l'=-\infty}^{\infty} \sum_{p'=0}^{M-1} E\left[x_{p,l}x^*_{p',l'}\right] h^*(< (n-m-lN_g)L_N - p'L_M >_L) \\
&\quad h(< (n-lN_g)L_N - pL_M >_L)\Pi_{N_t}(n-lN_t)\Pi_{N_t}(n-m-l'N_t) \\
&= L_N^2\sigma_x^2 \sum_{l=-\infty}^{\infty} \sum_{p=0}^{M-1} h(< (n-lN_g)L_N - pL_M >_L)h^*(< (n-m-lN_g)L_N - pL_M >_L) \\
&= \Pi_{N_t}(n-lN_t)\Pi_{N_t}(n-m-lN_t) \qquad \text{(A.1)}
\end{aligned}$$

In order to further simplify the above expression one needs to compute $\sum_{p=0}^{M-1} h(< nL_N - pL_M >_L)h^*(< (n-m)L_N - pL_M >_L)$. When writing the filter $h(n)$ in the frequency domain, the expression nicely simplifies as shown in the following:

$$\begin{aligned}
&\sum_{p=0}^{M-1} h(< nL_N - pL_M >_L)h^*(< (n-m)L_N - pL_M >_L) \\
&= \frac{1}{L^2} \sum_{k=0}^{L-1}\sum_{k'=0}^{L-1} H_k H^*_{k'} \left(\sum_{p=0}^{M-1} \Omega_M^{p(k'-k)}\right) \Omega_L^{(kn-k'(n-m))L_N} \\
&= \frac{1}{L^2} \sum_{s=0}^{L_M-1}\sum_{s'=0}^{L_M-1}\sum_{r=0}^{M-1}\sum_{r'=0}^{M-1} H_{sM+r}H^*_{s'M+r'} \left(\sum_{p=0}^{M-1} \Omega_M^{p(r'-r)}\right) \Omega_L^{(n(sM+r)-(n-m)(s'M+r'))L_N} \\
&= \frac{M}{L^2} \sum_{r=0}^{M-1}\sum_{s=0}^{L_M-1} H_{sM+r}\Omega_{L_M}^{snL_N} \sum_{s'=0}^{L_M-1} H^*_{s'M+r}\Omega_{L_M}^{s'(n-m)L_N}\Omega_N^{rm} \\
&= \frac{M}{L^2} \sum_{r=0}^{M-1} h_r(< n >_{L_M})h_r^*(< n-m >_{L_M})\Omega_N^{rm}
\end{aligned} \qquad \text{(A.2)}$$

where $h_r(< n >_{L_M}) = \sum_{s=0}^{L_M-1} H_{sM+r}\Omega_{L_M}^{snL_N}$. It should be noted that this function $h_r(< n >_{L_M})$ is L_M periodic and satisfies $h_r(< n+N >_{L_M}) = h_r(< n >_{L_M})$ since N is a multiple of L_M.

The transition from the second to the third equality is based on the euclidean division of k and k' over M leading to $k = sM + r$ and $k' = s'M + r'$ where r, $r' \in 0, \ldots, M-1$ and s, $s' \in 0, \ldots, L_M - 1$. The following exponential identity has also been used:

$$\sum_{p=0}^{M-1} \Omega_M^{pr} = \begin{cases} M & if\ r = kM \\ 0 & else \end{cases} \tag{A.3}$$

Equation (A.1) can be finally written as follows:

$$R_z(n,m) = \frac{M\sigma_x^2}{N^2} \sum_{l=-\infty}^{\infty} \sum_{r=0}^{M-1} h_r(< n - lN_g >_{L_M}) \Omega_N^{rm} h_r^*(< n - m - lN_g >_{L_M}) \Pi_{N_t}(n - lN_t) \Pi_{N_t}(n - m - lN_t) \tag{A.4}$$

It can be noticed that $R_z(n,m) = R_z(n+N_t, m)$, thus R_z is N_t-periodic in time. This allows to derive a stationary autocorrelation of symbols $z(n)$ by averaging over the time domain dimension n as follows:

$$\begin{aligned}
\overline{R}_z(m) &= \frac{1}{N_t} \sum_{n=0}^{N_t-1} R_z(n,m) \\
&= \frac{M\sigma_x^2}{N_t N^2} \sum_{r=0}^{M-1} \sum_{n=0}^{N_t-1} \sum_{l=-\infty}^{\infty} h_r^*(< n - m - lN_g >_{L_M}) h_r(< n - lN_g >_{L_M}) \Omega_N^{rm} \Pi_{N_t}(n - lN_t) \Pi_{N_t}(n - m - lN_t) \\
&= \frac{M\sigma_x^2}{N_t N^2} \sum_{r=0}^{M-1} \sum_{n=-\infty}^{\infty} h_r(< n >_{L_M}) h_r^*(< n - m >_{L_M}) \Pi_{N_t}(n) \Pi_{N_t}(n-m) \Omega_N^{rm} \\
&= \frac{M\sigma_x^2}{N_t N^2} \sum_{r=0}^{M-1} \sum_{n=-\infty}^{\infty} \tilde{h}_r(n) \tilde{h}_r^*(n-m) \Omega_N^{rm} \\
&= \frac{M\sigma_x^2}{N_t N^2} \sum_{r=0}^{M-1} R_{\tilde{h}_r}(m) \Omega_N^{rm}
\end{aligned}$$

where we define the equivalent transmit filter $\tilde{h}_r$ as:

$$\tilde{h}_r(n) = h_r(< n >_{L_M}) \Pi_{N_t}(n) = \sum_{s=0}^{L_M-1} H_{sM+r} \Omega_{L_M}^{snL_N} \Pi_{N_t}(n)$$

and the autocorrelation function of $\tilde{h}_r$ is defined by: $R_{\tilde{h}_r}(m) = \sum_{n=-\infty}^{\infty} \tilde{h}_r(n) \tilde{h}_r^*(n-m)$.

As a consequence, the power spectral density of SC-OFDMf can be written as follows:

$$\overline{S_z}(f) = \sum_{m=-\infty}^{\infty} \overline{R}_z(m) e^{-2j\pi mf}$$

$$
\begin{aligned}
&= \frac{M\sigma_x^2}{N_t N^2} \sum_{r=0}^{M-1} \sum_{m=-\infty}^{\infty} R_{\tilde{h}_r}(m) \Omega_N^{rm} e^{-2j\pi mf} \\
&= \frac{M\sigma_x^2}{N_t N^2} \sum_{r=0}^{M-1} \left| \tilde{H}_r(f - \frac{r}{N}) \right|^2 \\
&= \frac{M\sigma_x^2}{N_t N^2} \sum_{r=0}^{M-1} \left| \sum_{s=0}^{L_M-1} H_{sM+r} \Psi_{N_t}(f - \frac{sM+r}{N}) \right|^2
\end{aligned} \tag{A.5}
$$

where $\Psi_{N_t}(f)$ is the Energy Spectral Density (ESD) of the time domain shaping filter $\Pi_{N_t}(n)$.

Appendix B

Equivalent noise variance

The equivalent noise issues from up-sampling by a factor L_N equalizing then down-sampling by a factor L_M. This results in a cyclo-stationary equivalent noise, the autocorrelation of which reads as:

$$R_{\tilde{w}}(k,n) = E[\tilde{w}_k \tilde{w}^*_{k-n}] = L_M^2 \sigma_w^2 \sum_{m=0}^{N-1} g(< kL_M - mL_N >_L) g^*(< (k-n)L_M - mL_N >_L)$$

We can show that this autocorrelation function is L_N-periodic in time by expressing it in the frequency domain as follows:

$$\begin{aligned}
R_{\tilde{w}}(k,n) &= \frac{\sigma_w^2}{M^2} \sum_{m=0}^{N-1} \sum_{i=0}^{L-1} \sum_{i'=0}^{L-1} G_i G^*_{i'} \Omega_L^{i(kL_M - mL_N)} \Omega_L^{-i'((k-n)L_M - mL_N)} \\
&= \frac{\sigma_w^2}{M^2} \sum_{i=0}^{L-1} \sum_{i'=0}^{L-1} G_i G^*_{i'} \Omega_L^{k(i-i')L_M} \Omega_L^{i' n L_M} \sum_{m=0}^{N-1} \Omega_N^{m(i-i')} \\
&= \frac{\sigma_w^2 N}{M^2} \sum_{r=0}^{N-1} \sum_{s=0}^{L_N-1} \sum_{s'=0}^{L_N-1} G_{sM+r} G^*_{s'M+r} \Omega_L^{k(s-s')L_M N} \Omega_L^{(s'N+r)nL_M} \\
&= \frac{\sigma_w^2 N}{M^2} \sum_{r=0}^{N-1} \sum_{s=0}^{L_N-1} \sum_{s'=0}^{L_N-1} G_{sM+r} G^*_{s'M+r} \Omega_L^{k(s-s')L_M N} \Omega_L^{(s'N+r)nL_M}
\end{aligned}$$

We used the fact that L_N is the least integer A such that $AN = BM$ since it is obtained from the least common multiple of M and N.

Thus we compute the stationary power spectral density of the noise, by averaging over the period L_N as follows:

$$\begin{aligned}
\overline{R}_{\tilde{w}}(n) = \frac{1}{L_N} \sum_{k=0}^{L_N-1} R_{\tilde{w}}(k,n) &= \frac{\sigma_w^2 N}{M^2 L_N} \sum_{r=0}^{N-1} \sum_{s=0}^{L_N-1} \sum_{s'=0}^{L_N-1} G_{sM+r} G^*_{s'M+r} \sum_{k=0}^{L_N-1} \Omega_{L_N}^{k(s-s')L_M} \Omega_L^{(s'N+r)nL_M} \\
&= \frac{\sigma_w^2 N}{M^2} \sum_{r=0}^{N-1} \sum_{s=0}^{L_N-1} G_{sM+r} G^*_{sM+r} \Omega_L^{(sN+r)nL_M} \\
&= \frac{\sigma_w^2 N}{M^2} \sum_{r=0}^{L-1} |G_r|^2 \, \Omega_M^{kn} \qquad \text{(B.1)}
\end{aligned}$$

where the transition from the 1^{st} to the 2^{nd} equality results from the fact that L_M and L_N are coprime. As a result, the stationarized noise variance is:

$$\sigma_{\tilde{w}}^2 = \frac{\sigma_w^2 N}{M^2} \sum_{k=0}^{L-1} |G_k|^2 \tag{B.2}$$

It can be noticed that stationarizing the noise would not be necessary if the equalization function G had only N non zero values i.e. $G_r = 0 \, if \, r \geq N$. This would result in a stationary noise which covariance is similar to (B.2).

Appendix C

On How to estimate the ellipse parameters of a non-circular noise

C.0.7 Ellipse characteristics

Let $Z = Z_r + jZ_i$ be a gaussian noncircular noise i.e. $E[Z_r Z_i] \neq 0$. The variance of Z which is $\sigma_z^2 = \sigma_i^2 + \sigma_r^2$ is no longer sufficient to record all second order information. Additional statistics can be captured in the pseudo variance of Z defined as :

$$\tau_Z = E[Z^2] = \sigma_r^2 - \sigma_i^2 + j2E[Z_r Z_i] \tag{C.1}$$

When Z_r and Z_i are independent and identically distributed, the pseudo variance $\tau_Z = 0$ and the noise is circular. In a more general case, the noise is non circular, and its improperness can be characterized by a circularity quotient defined as :

$$\rho_Z = \frac{E[Z^2]}{E[|Z|^2]} = \frac{\tau_Z}{\sigma_Z^2} = r_Z e^{j\theta} \tag{C.2}$$

It has been shown in [Ollila, 2008] that if a random process Z is distributed following $\mathcal{N}(0, \sigma_Z^2, \tau_Z)$ then $p\%$ of its realisation lie inside an ellipse $\mathcal{E}_{\sum}(c^2)$ defined by $c^2 = \chi^2_{2,p}$ and $\sqrt{\lambda_1}c$ and $\sqrt{\lambda_2}c$ are the positive end points of the major and minor axes respectively.

$$\begin{aligned} \lambda_1 &= \frac{\sigma_Z^2 + |\tau_Z|}{2} \\ \lambda_2 &= \frac{\sigma_Z^2 - |\tau_Z|}{2} \end{aligned}$$

The phase of the circularity quotient θ defines the rotation angle of the ellipse α. It has been shown that $\alpha = \frac{arg[\rho_Z]}{2} = \frac{arg[\tau_Z]}{2}$.

C.0.8 Application to a correlated noise

In order to asses the accuracy of this graphical representation, we generate a correlated noise Z as follows:

$$Z = Z_r - Z_i + jZ_r \tag{C.3}$$

where Z_r and Z_i are independent random Gaussian processes identically distributed following $\mathcal{N}(0,1)$. Thus, the variance and pseudo variance of Z are equal to :

$$\begin{aligned} \sigma_Z &= 2\sigma_r^2 + \sigma_i^2 = 3 \\ \tau_Z &= \sigma_i^2 + 2j\sigma_r^2 = 1 + 2j \end{aligned} \tag{C.4}$$

It follows that :

$$\begin{aligned} \lambda_1 &= \frac{3+\sqrt{5}}{2} = 2.618 \\ \lambda_2 &= \frac{3-\sqrt{5}}{2} = 0.382 \end{aligned} \tag{C.5}$$

We approximate the noise by an ellipse which contains 99% and 90% of the points of z; it follows that

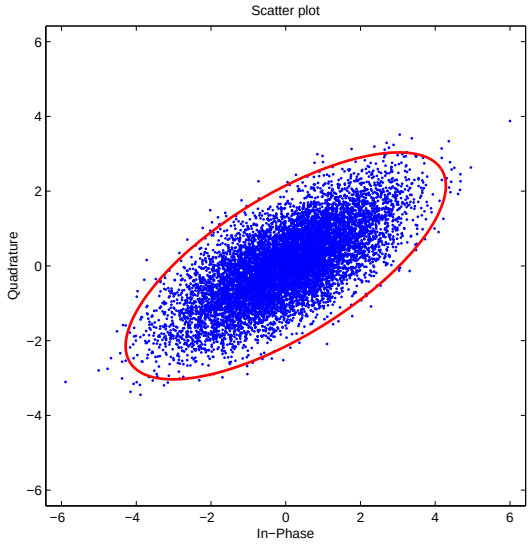

Figure C.1: Approximations to the .99th quantile

$c^2_{.99} = 9.213$ resp $c^2_{.9} = 4.6052$. Figures C.1 and C.2 plot the two approximating ellipses for the improper noise.

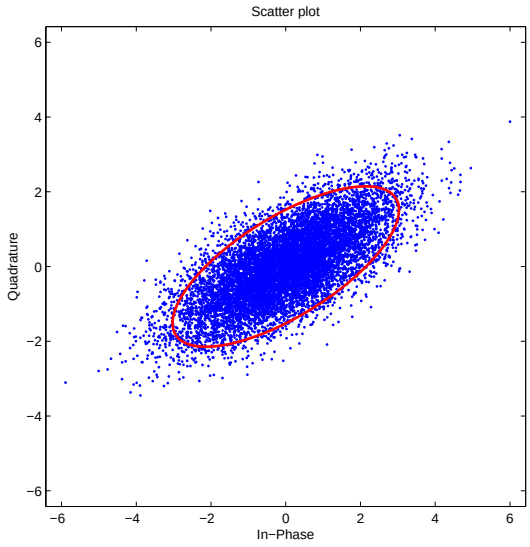

Figure C.2: Approximations to the .90th quantile

Bibliography

[ENG,] http://celticplus.eu/projects/celtic-projects/call7/engines/engines-default.asp.

[3GPP TSG-RAN WG1 Meeting43 051352, 2005] 3GPP TSG-RAN WG1 Meeting43 051352 (2005). Simulation methodology for EUTRA uplink: SC-FDMA and OFDMA.

[Abdulkader et al., 2014] Abdulkader, H., Benammar, B., Poulliat, C., Thomas, N., and Boucheret, M.-L. (2014). Neural Networks-Based Turbo Equalization of a Satellite Communication Channel (regular paper). In *IEEE Workshop on Signal Processing Advances in Wireless Communications (SPAWC), Toronto, 22/06/2014-25/06/2014*, pages 0–0, http://www.ieee.org/. IEEE.

[Al-Dhahir and Cioffi, 1995] Al-Dhahir, N. and Cioffi, J. (1995). MMSE decision-feedback equalizers: finite-length results. *IEEE Transactions on Information Theory,*, 41(4):961–975.

[Ampeliotis et al., 2008] Ampeliotis, D., Rontogiannis, A., Berberidis, K., Papaleo, M., and Corazza, G. (2008). Turbo equalization of non-linear satellite channels using soft interference cancellation. In *Advanced Satellite Mobile Systems, 2008. ASMS 2008. 4th*, pages 289 –292.

[Aziz et al., 2011] Aziz, B., Fijalkow, I., and Ariaudo, M. (2011). Trade off between Frequency Diversity and Robustness to Carrier Frequency Offset in Uplink OFDMA System. In *Global Telecommunications Conference (GLOBECOM 2011), 2011 IEEE*, pages 1–5.

[Azurdia-Meza et al., 2008] Azurdia-Meza, C., Lee, K., and Lee, K. (2008). PAPR Reduction in SC-FDMA by Pulse Shaping Using Parametric Linear Combination Pulses. *IEEE Communications Letters*, 16(12):2008–2011.

[Bahl et al., 1974] Bahl, L., Cocke, J., Jelinek, F., and Raviv, J. (1974). Optimal decoding of linear codes for minimizing symbol error rate (corresp.). *IEEE Transactions on Information Theory*, 20(2):284–287.

[Belfiore and Park, 1979] Belfiore, C. and Park, J.H., J. (1979). Decision feedback equalization. *Proceedings of the IEEE*, 67(8):1143–1156.

[Benammar et al., 2013a] Benammar, B., Thomas, N., Boucheret, M.-L., Poulliat, C., and Dervin, M. (2013a). Analytical expressions of Power Spectral Density for general spectrally shaped SC-FDMA systems. In *2013 Proceedings of the 21st European Signal Processing Conference (EUSIPCO)*, pages 1–5.

[Benammar et al., 2013b] Benammar, B., Thomas, N., Poulliat, C., Boucheret, M.-L., and Dervin, M. (2013b). On linear MMSE based turbo-equalization of nonlinear volterra channels. In *2013 IEEE International Conference on Acoustics, Speech and Signal Processing (ICASSP),*, pages 4703–4707.

[Benammar et al., 2014a] Benammar, B., Thomas, N., Poulliat, C., Boucheret, M.-L., and Dervin, M. (2014a). Asymptotic Analysis and Design of Iterative Receivers for Non Linear ISI Channels. In *The 8th International Symposium on Turbo Codes & Iterative Information Processing*.

[Benammar et al., 2014b] Benammar, B., Thomas, N., Poulliat, C., Boucheret, M.-L., and Dervin, M. (2014b). On Linear Frequency Domain Turbo-Equalization of Non Linear Volterra Channels. In *The 8th International Symposium on Turbo Codes & Iterative Information Processing*.

[Benedetto and Biglieri, 1983] Benedetto, S. and Biglieri, E. (1983). Nonlinear equalization of digital satellite channels. *IEEE Journal on Selected Areas in Communications,*, 1(1):57–62.

[Benedetto and Biglieri, 1999] Benedetto, S. and Biglieri, E. (1999). *Principles of Digital Transmission: With Wireless Applications*. Information Technology Series. Springer US.

[Benedetto et al., 1979] Benedetto, S., Biglieri, E., and Daffara, R. (1979). Modeling and performance evaluation of nonlinear satellite links-a volterra series approach. *IEEE Transactions on Aerospace and Electronic Systems*, AES-15(4):494 –507.

[Benvenuto et al., 2010] Benvenuto, N., Dinis, R., Falconer, D., and Tomasin, S. (2010). Single carrier modulation with nonlinear frequency domain equalization: An idea whose time has come x2014;again. *Proceedings of the IEEE*, 98(1):69–96.

[Benvenuto and Tomasin, 2002] Benvenuto, N. and Tomasin, S. (2002). On the comparison between ofdm and single carrier modulation with a dfe using a frequency-domain feedforward filter. *IEEE Transactions on Communications,*, 50(6):947–955.

[Berrou et al., 1993] Berrou, C., Glavieux, A., and Thitimajshima, P. (1993). Near shannon limit error-correcting coding and decoding: Turbo-codes. 1. In *IEEE International Conference on Communications, 1993. ICC '93 Geneva. Technical Program, Conference Record*, volume 2, pages 1064–1070 vol.2.

[Biglieri et al., 1984] Biglieri, E., Gersho, A., Gitlin, R., and Lim, T. (1984). Adaptive cancellation of nonlinear intersymbol interference for voiceband data transmission. *IEEE Journal on Selected Areas in Communications,*, 2(5):765–777.

[Blachman, 1968] Blachman, N. M. (1968). The uncorrelated output components of a nonlinearity. *IEEE Transactions on Information Theory,*, 14(2):250–255.

[Burnet and Cowley, 2005] Burnet, C. and Cowley, W. (2005). Performance analysis of turbo equalization for nonlinear channels. In *International Symposium on Information Theory, 2005. ISIT 2005. Proceedings.*, pages 2026 –2030.

[Chung et al., 2001] Chung, S.-Y., Richardson, T., and Urbanke, R. (2001). Analysis of sum-product decoding of low-density parity-check codes using a Gaussian approximation. *IEEE Transactions on Information Theory*, 47(2):657–670.

[Ciochina et al., 2008] Ciochina, C., Castelain, D., Mottier, D., and Sari, H. (2008). A Novel Quasi-Orthogonal Space-Frequency Block Code for Single-Carrier FDMA. In *IEEE Vehicular Technology Conference,VTC Spring 2008.*, pages 1137 –1141.

[Ciochina, 2009] Ciochina, I. C. (2009). Conception d une couche physique pour la liaison montante dans des systemes de radiocommunications mobiles cellulaires.

[Clark, 1998] Clark, M. (1998). Adaptive frequency-domain equalization and diversity combining for broadband wireless communications. In *48th IEEE Vehicular Technology Conference, 1998. VTC 98.*, volume 1, pages 409–413 vol.1.

[Colavolpe et al., 2001] Colavolpe, G., Ferrari, G., and Raheli, R. (2001). Reduced-state BCJR-type algorithms. *IEEE Journal on Selected Areas in Communications*, 19(5):848–859.

[Colavolpe et al., 2012] Colavolpe, G., Modenini, A., and Rusek, F. (2012). Channel shortening for nonlinear satellite channels. *IEEE Communications Letters,*, 16(12):1929–1932.

[Colavolpe and Piemontese, 2012] Colavolpe, G. and Piemontese, A. (2012). Novel SISO detection algorithms for nonlinear satellite channels. *IEEE Wireless Communications Letters*, 1(1):22 –25.

[Costa and Pupolin, 2002] Costa, E. and Pupolin, S. (2002). M-QAM-OFDM system performance in the presence of a nonlinear amplifier and phase noise. *IEEE Transactions on Communications*, 50(3):462–472.

[Danilo-Lemoine et al., 2007] Danilo-Lemoine, F., Falconer, D., C-T, L., Sabbaghian, M., Wesołowski, K., et al. (2007). Power backoff reduction techniques for generalized multicarrier waveforms. *EURASIP Journal on wireless communications and Networking*, 2008.

[De Gaudenzi et al., 2006] De Gaudenzi, R., Guillén i Fàbregas, A., and Martinez, A. (2006). Turbo-coded APSK modulations design for satellite broadband communications. *International Journal of Satellite Communications and Networking*, 24(4):261–281.

[Deleu et al., 2014] Deleu, T., Dervin, M., Kasai, K., and Horlin, F. (2014). Iterative predistortion of the nonlinear satellite channel. *IEEE Transactions on Communications*, 62(8):2916–2926.

[Douillard et al., 1995] Douillard, C., Jezequel, M., and Berrou, C. (1995). Iterative correction of intersymbol interference: Turbo equalization. *European Transactions on Telecommunications*, 6(5):507 a ĂŞ511.

[DVB-S2X, 2014] DVB-S2X, D. D. A.-. (2014). Digital video broadcasting (dvb); second generation framing structure, channel coding and modulation systems for broadcasting, interactive services, news gathering and other broadband satellite applications part ii: S2-extensions (dvb-s2x) - (optional).

[EN, 1997] EN, E. (1997). 300 421 DVB-S. *Framing structure, channel coding and modulation for 11/12 GHz satellite services*, 11:12.

[EN, 2009] EN, V. .-. . . E. (2009). Digital video broadcasting (DVB); second generation framing structure, channel coding and modulation systems for broadcasting, interactive services, news gathering and other broadband satellite applications (DVB-S2). *European Standard (Telecommunications series)*.

[ENGINES, 2011] ENGINES (2011). Technical report tr 1.1 intermediate report on dvb-ngh concept studies. Technical report.

[Falconer, 2011] Falconer, D. (2011). Linear Precoding of OFDMA Signals to Minimize Their Instantaneous Power Variance. *IEEE Transactions on Communications*, 59(4):1154–1162.

[Falconer and Ariyavisitakul, 2002] Falconer, D. and Ariyavisitakul, S. (2002). Broadband wireless using single carrier and frequency domain equalization. In *The 5th International Symposium on Wireless Personal Multimedia Communications*, volume 1, pages 27–36 vol.1.

[Fisher et al., 1991] Fisher, K. D., Cioffi, J., Abbott, W., Bednarz, P., and Melas, C. (1991). An adaptive RAM-DFE for storage channels. *IEEE Transactions on Communications*, 39(11):1559–1568.

[Gallager, 1962] Gallager, R. (1962). Low-density parity-check codes. *IRE Transactions on Information Theory,*, 8(1):21–28.

[Gallager, 1963] Gallager, R. G. (1963). *Low Density Parity Check Codes*. Cambridge, MA.

[Gallinaro et al., 2012] Gallinaro, G., Di Cecca, F., and Alagha, N. (2012). SC-FDMA for the Return-Link of Interactive Broadband Systems. In *2012 IEEE First AESS European Conference on Satellite Telecommunications (ESTEL),*, pages 1–7.

[Ghorbani and Sheikhan, 1991] Ghorbani, A. and Sheikhan, M. (1991). The effect of solid state power amplifiers (SSPAs) nonlinearities on MPSK and M-QAM signal transmission. In *Sixth International Conference on Digital Processing of Signals in Communications, 1991.*,, pages 193–197. IET.

[Gilmour, 2011] Gilmour, A. (2011). *Klystrons, Traveling Wave Tubes, Magnetrons, Crossed-Field Amplifiers, and Gyrotrons*. Artech House microwave library. Artech House, Incorporated.

[Glavieux et al., 1997] Glavieux, A., Laot, C., and Labat, J. (1997). Turbo equalization over a frequency selective channel. In *Proc. 1st Symp. Turbo Codes*, pages 96–102.

[Gómez-Barquero, 2013] Gómez-Barquero, D. (2013). *Next generation mobile broadcasting*. CRC press.

[Gomez-Barquero et al., 2014] Gomez-Barquero, D., Douillard, C., Moss, P., and Mignone, V. (2014). DVB-NGH: The Next Generation of Digital Broadcast Services to Handheld Devices. *IEEE Transactions on Broadcasting*, 60(2):246–257.

[Gutierrez and Ryan, 2000] Gutierrez, A. and Ryan, W. (2000). Performance of volterra and MLSD receivers for nonlinear band-limited satellite systems. *IEEE Transactions on Communications*, 48(7):1171 –1177.

[Hagenauer, 2004] Hagenauer, J. (2004). The EXIT Chart - Introduction to Extrinsic Information Transfer. In *in Iterative Processing, Ť In Proc. 12th Europ. Signal Proc. Conf (EUSIPCO*, pages 1541–1548.

[Hagenauer and Hoeher, 1989] Hagenauer, J. and Hoeher, P. (1989). A viterbi algorithm with soft-decision outputs and its applications. In *IEEE Global Telecommunications Conference and Exhibition 'Communications Technology for the 1990s and Beyond' (GLOBECOM), 1989.*, pages 1680–1686 vol.3.

[Han and Lee, 2005] Han, S. H. and Lee, J. H. (2005). An overview of peak-to-average power ratio reduction techniques for multicarrier transmission. *IEEE Wireless Communications*, 12(2):56–65.

[Haykin, 2008] Haykin, S. S. (2008). *Adaptive filter theory*. Pearson Education India.

[Im and Powers, 1996] Im, S. and Powers, E. J. (1996). A fast method of discrete third-order volterra filtering. *IEEE transactions on signal processing*, 44(9):2195–2208.

[J. C. Fuenzalida, 1973] J. C. Fuenzalida, 0. Shimbo, W. L. C. (1973). Time Ůdomain analysis of intermodulation effects caused by nonlinear amplifiers. Technical report.

[Kawamura et al., 2006] Kawamura, T., Kishiyama, Y., Higuchi, K., and Sawahashi, M. (2006). Investigations on Optimum Roll-off Factor for DFT-Spread OFDM Based SC-FDMA Radio Access in Evolved UTRA Uplink. In *3rd International Symposium on Wireless Communication Systems, ISWCS '06.*, pages 383 –387.

[Krall et al., 2008] Krall, C., Witrisal, K., Leus, G., and Koeppl, H. (2008). Minimum mean-square error equalization for second-order volterra systems. *IEEE Transactions on Signal Processing*, 56(10):4729–4737.

[Kschischang et al., 2001] Kschischang, F., Frey, B., and Loeliger, H.-A. (2001). Factor graphs and the sum-product algorithm. *IEEE Transactions on Information Theory*, 47(2):498–519.

[Laot et al., 2001] Laot, C., Glavieux, A., and Labat, J. (2001). Turbo equalization: adaptive equalization and channel decoding jointly optimized. *IEEE Journal on Selected Areas in Communications*, 19(9):1744 –1752.

[Laot et al., 2005] Laot, C., Le Bidan, R., and Leroux, D. (2005). Low-complexity mmse turbo equalization: a possible solution for edge. *IEEE Transactions on Wireless Communications*, 4(3):965–974.

[Liu and Fitz, 2012] Liu, D. and Fitz, M. (2012). Iterative equalization in non-linear satellite channels. In *7th International Symposium on Turbo Codes and Iterative Information Processing (ISTC), 2012*, pages 220 –224.

[Lusicus et al., 1984] Lusicus, B. R., Musicus, B. R., and Musicus, B. R. (1984). Levinson and fast choleski algorithms for toeplitz and almost toeplitz matrices. In *Internal Report, Lab of Elec., MIT*.

[MacKay, 1999] MacKay, D. J. C. (1999). Good error-correcting codes based on very sparse matrices. *IEEE Transactions on Information Theory*, 45(2):399–431.

[MacKay and Neal, 1997] MacKay, D. J. C. and Neal, R. M. (1997). Near shannon limit performance of low density parity check codes. *Electronics Letters*, 33(6):457–458.

[Maral and Bousquet, 2002] Maral, G. and Bousquet, M. (2002). *Satellite Communications Systems: Systems, Techniques and Technology*. Novartis Foundation Symposium. Wiley.

[Mauritz and Popovic, 2006] Mauritz, O. and Popovic, B. (2006). Optimum Family of Spectrum-Shaping Functions for PAPR Reduction of DFT-Spread OFDM Signals. In *IEEE 64th Vehicular Technology Conference, VTC-2006*, pages 1–5.

[Muquet et al., 2002] Muquet, B., Wang, Z., Giannakis, G., de Courville, M., and Duhamel, P. (2002). Cyclic prefixing or zero padding for wireless multicarrier transmissions? *Communications, IEEE Transactions on*, 50(12):2136–2148.

[Myung et al., 2006] Myung, H. G., Lim, J., and Goodman, D. J. (2006). Single carrier FDMA for uplink wireless transmission. *IEEE Vehicular Technology Magazine*, 1(3):30 –38.

[Narayanan et al., 2005] Narayanan, K., Wang, X., and Yue, G. (2005). Estimating the PDF of the SIC-MMSE equalizer output and its applications in designing LDPC codes with turbo equalization. *IEEE Transactions on Wireless Communications*, 4(1):278–287.

[Ollila, 2008] Ollila, E. (2008). On the circularity of a complex random variable. *IEEE Signal Processing Letters,*, 15:841–844.

[Picinbono and Chevalier, 1995] Picinbono, B. and Chevalier, P. (1995). Widely linear estimation with complex data. *IEEE Transactions on Signal Processing*, 43(8):2030–2033.

[Poor, 1994] Poor, H. V. (1994). *An introduction to signal detection and estimation (2nd ed.)*. Springer-Verlag New York, Inc., New York, NY, USA.

[Rapp, 1991] Rapp, C. (1991). Effects of HPA-nonlinearity on a 4-DPSK/OFDM-signal for a digital sound broadcasting signal. In *In ESA, Second European Conference on Satellite Communications (ECSC-2) p 179-184 (SEE N92-15210 06-32)*, volume 1, pages 179–184.

[Richardson et al., 2001] Richardson, T., Shokrollahi, M., and Urbanke, R. (2001). Design of capacity-approaching irregular low-density parity-check codes. *IEEE Transactions on Information Theory*, 47(2):619–637.

[Roumy, 2000] Roumy, A. (2000). *A. Roumy. Egalisation et décodage conjoints : méthodes Turbo.*

[Saleh, 1981] Saleh, A. (1981). Frequency-independent and frequency-dependent nonlinear models of TWT amplifiers. *IEEE Transactions on Communications*, 29(11):1715 –1720.

[Sands and Cioffi, 1994] Sands, N. and Cioffi, J. (1994). An improved detector for channels with nonlinear intersymbol interference. In *IEEE International Conference on Communications, 1994. ICC '94, SUPERCOMM/ICC '94, Conference Record, 'Serving Humanity Through Communications.'*, pages 1226–1230 vol.2.

[Schetzen, 1976] Schetzen, M. (1976). Theory of pth-order inverses of nonlinear systems. *IEEE Transactions on Circuits and Systems*, 23(5):285–291.

[Schetzen, 1980] Schetzen, M. (1980). The volterra and wiener theories of nonlinear systems.

[Sellami et al., 2008] Sellami, N., Roumy, A., and Fijalkow, I. (2008). A proof of convergence of the map turbo-detector to the awgn case. *Signal Processing, IEEE Transactions on*, 56(4):1548–1561.

[Slimane, 2007] Slimane, S. (2007). Reducing the Peak-to-Average Power Ratio of OFDM Signals Through Precoding. *IEEE Transactions on Vehicular Technology*, 56(2):686–695.

[Su et al., 2002] Su, Y., Chiu, M.-C., and Chen, Y.-C. (2002). Turbo equalization of nonlinear TDMA satellite signals. In *Global Telecommunications Conference, 2002. GLOBECOM '02. IEEE*, volume 3, pages 2860 – 2864 vol.3.

[Sung et al., 2009] Sung, W., Kang, S., Kim, P., Chang, D.-I., and Shin, D.-J. (2009). Performance analysis of apsk modulation for dvb-s2 transmission over nonlinear channels. *International Journal of Satellite Communications and Networking*, 27(6):295–311.

[Tanner, 1981] Tanner, R. (1981). A recursive approach to low complexity codes. *IEEE Transactions on Information Theory*, 27(5):533–547.

[Ten Brink, 1999] Ten Brink, S. (1999). Convergence of iterative decoding. *Electronics Letters*, 35(10):806–808.

[ten Brink et al., 2004] ten Brink, S., Kramer, G., and Ashikhmin, A. (2004). Design of low-density parity-check codes for modulation and detection. *IEEE Transactions on Communications*, 52(4):670–678.

[Tuchler, 2000] Tuchler, M. (2000). Iterative equalization using priors.

[TuĹchler and Singer, 2011] TuĹchler, M. and Singer, A. (2011). Turbo equalization: An overview. *IEEE Transactions on Information Theory*, 57(2):920 –952.

[Tuchler et al., 2002] Tuchler, M., Singer, A., and Koetter, R. (2002). Minimum mean squared error equalization using a priori information. *IEEE Transactions on Signal Processing*, 50(3):673 –683.

[Uncini et al., 1999] Uncini, A., Vecci, L., Campolucci, P., and Piazza, F. (1999). Complex-valued neural networks with adaptive spline activation function for digital-radio-links nonlinear equalization. *IEEE Transactions on Signal Processing*, 47(2):505–514.

[Vaidyanathan, 1988] Vaidyanathan, P. (1988). A tutorial on multirate digital filter banks. In *Circuits and Systems, 1988., IEEE International Symposium on*, pages 2241–2248 vol.3.

[van Waterschoot et al., 2010] van Waterschoot, T., Le Nir, V., Duplicy, J., and Moonen, M. (2010). Analytical Expressions for the Power Spectral Density of CP-OFDM and ZP-OFDM Signals. *IEEE Signal Processing Letters*, 17(4):371–374.

[Viterbi, 1967] Viterbi, A. (1967). Error bounds for convolutional codes and an asymptotically optimum decoding algorithm. *IEEE Transactions on Information Theory,*, 13(2):260–269.

[Yee et al., 2003] Yee, M.-S., Yeap, B., and Hanzo, L. (2003). Radial basis function-assisted turbo equalization. *IEEE Transactions on Communications*, 51(4):664–675.

[Yuen and Farhang-Boroujeny, 2012] Yuen, C. and Farhang-Boroujeny, B. (2012). Analysis of the Optimum Precoder in SC-FDMA. *IEEE Transactions on Wireless Communications*, 11(11):4096–4107.